Report 4, 1991

INTERPRETATION OF SCHLUMBERGER SOUNDINGS FROM MT. CAGUA, PHILIPPINES AND TEM SOUNDINGS FROM SVARTSENGI-ELDVORP, SW-ICELAND

Francisco A. Benito,
UNU Geothermal Training Programme,
Orkustofnun - National Energy Authority,
Grensásvegur 9,
108 Reykjavik,
ICELAND

Permanent Address:
Office of Energy Affairs,
Energy Development Services,
Geothermal Division,
Merritt Road, Fort Bonifacio,
Makati, Metro Manila 1201,
PHILIPPINES,

ABSTRACT

An overview is given of the DC-Schlumberger sounding method and different methods of interpretation. The results of an extensive Schlumberger sounding survey from the Mt. Cagua geothermal prospect in the Philippines are presented. Using both one-dimensional and two-dimensional modelling, the interpretation of the Schlumberger soundings delineated a conductive body that covers most of the prospect area. Two geothermal centers are postulated. One is connected to the geothermal system of Cagua Volcano to the west and the other to Baua Volcano in the eastern part of the prospect area.

The basic principles of the central-loop transient electromagnetic (TEM) method are presented. A TEM survey was conducted in the Svartsengi-Eldvorp geothermal field, SW-Iceland, for the purpose of locating the best site for a proposed reinjection well. The results are compared to older Schlumberger sounding data, and confirm the better vertical resolution of the TEM soundings than the Schlumberger in a terrain with a highly resistive surface but low resistivities at deeper levels. A site for the planned reinjection well is proposed, based on the results of the TEM soundings.

TABLE OF CONTENTS

LIST OF FIGURES

LIST OF APPENDICES PUBLISHED SEPARATELY (Benito, 1991)

1. INTRODUCTION

This report is intended to present the results of the work of the author at Orkustofnun (National Energy Authority of Iceland) where he was awarded a United Nations University Fellowship to attend the 1991 UNU Geothermal Training Programme. It deals with methods and techniques of interpretation of Schlumberger and central-loop transient electromagnetic (TEM) soundings from the geothermal fields of Mt. Cagua, Philippines and Svartsengi-Eldvörp, SW-Iceland, respectively.

Schlumberger sounding measurements of the Mt. Cagua geothermal prospect were made by the Philippine National Oil Company - Energy Development Corporation (PNOC-EDC) between 1988-1989. The result, which is presented in a report by Bayrante et al. (1989) delineated a low resistivity anomaly which encloses the main thermal manifestations in the vicinity of Cagua Volcano. Subsequent drilling of two exploratory wells revealed the presence of an active heat source with recorded temperatures above 300°C. However, due to poor permeability the wells were unproductive which led to the decision to expand coverage of the survey area. Additional Schlumberger measurements were then made in early 1991 to study, in detail, the open end of the resistivity anomaly in the northeastern part of the geothermal prospect.

The results of one- and two-dimensional interpretations of Schlumberger soundings from the 1991 survey and of those taken in 1988-1989 in the vicinity of the then-inferred upflow zone are presented. It is an attempt to locate the center of the geothermal field and to delineate the lateral limits of the low resistivity body associated with the field.

The author also partly joined in during the conducting of central-loop TEM soundings in the Svartsengi-Eldvörp area in southwest Iceland. The Svartsengi geothermal power plant in the Reykjanes Peninsula has been in production for the past 15 years. Monitoring of the reservoir has shown extensive pressure drawdown associated with, among other things, calcite scaling in the wells and inflow of colder geothermal fluids. The drawdown has also reduced pressure in the Eldvörp geothermal area located a few kilometers to the west. In order to maintain pressure in the Svartsengi reservoir, reinjection of at least 50% of the produced fluids at a site between Eldvörp and Svartsengi has been recommended. The central-loop TEM survey was conducted to locate the best site for the planned reinjection well for the Svartsengi geothermal power plant. The TEM sounding data was interpreted and correlated with Schlumberger soundings previously carried out in the area to determine the recommended site for the reinjection well.

Three appendices to this report are published as a separate volume (Benito, 1991).

2. RESISTIVITY METHODS IN GEOTHERMAL EXPLORATION

2.1 Introduction

Almost all geophysical methods have been applied in prospecting for geothermal resources. Depending on the type of the geothermal resource, however, some methods have been found to be "simple" and "proven" (Hochstein, 1982) in the sense that the methods can be readily executed in developing countries, like the Philippines, where most of the world's geothermal resources are located. Taking into consideration the physical properties related to geothermal systems, methods which measure parameters related to these properties, e.g. high temperature, alteration, etc., have been found the most useful (Hersir and Bjornsson, 1991). Of these methods, electrical resistivity surveys are used routinely and successfully to prospect for geothermal reservoirs. They map regions of thermal fluids and/or wall rock alteration resulting from interaction of the thermal fluids with the reservoir rocks which may cause resistivity anomalies.

In the Philippines where young, rugged volcanic terrain characterizes most of the geothermal prospects, the conduct of resistivity surveys as an investigative method have been found to be well suited for providing largely definitive data together with rapid areal coverage and cost effectiveness (Barnett et al., 1984). Among the different methods of electrical surveying, the dipole-dipole array is well suited to combined sounding and profiling where it provides modest lateral and vertical resolution. The direct current (DC) Schlumberger method, on the other hand, is commonly used as it provides improved vertical resolution in sounding. Other arrays have been used but are not preferred by practitioners (Ward and Sill, 1983).

In Iceland, however, where the use of DC methods was found to be difficult and time consuming to implement due to conditions at the surface, the central-loop transient electromagnetic (TEM) method has been found advantageous. It is replacing the conventional Schlumberger sounding in geothermal exploration in areas where large parts of the surface are covered with lava, making current injection into the ground almost impossible.

2.2 Electrical resistivity of rocks

The electrical resistivity of rocks depends on the porosity and pore structure of the rock, amount of water (saturation), salinity of the water, temperature, pressure, water-rock interaction and alteration and steam content in the fluid (Hersir and Bjornsson, 1991). The most important factors are the porosity, temperature and water-rock interaction. Conduction is dominantly electrolytic in most of the rocks at the earth's surface as the rock matrix is almost non-conductive. Ionic conduction in the saturating fluid is dependent on the temperature, the concentration and mobility of ions and the presence of connected flow paths through the rock matrix. In geothermal areas the rocks are often altered due to water-rock interaction and conduction is frequently dominated by alteration minerals.

Porosity is defined as the ratio between the pore volume and the total volume of a material. There are three types: intergranular (sediments, volcanic ash), joint-fissures (igneous rocks, lava), and vugular (volcanic rocks, limestone). Pore spaces must be interconnected and filled with water in order for a rock to conduct electricity and, since the rock matrix itself is an insulator, most of the conduction takes place in the connecting pores. The resistivity of water-saturated rocks often varies as approximately the inverse square of the porosity. This empirical relationship, known as Archie's law, is given by the equation:

$$\rho = \rho_w a \phi_t^{-n} \quad (1)$$

where ρ is the bulk (measured) resistivity, ρ_w is the resistivity of the pore fluid, ϕ_t is porosity in proportion to the total volume, a is an empirical parameter that varies from less than 1 for intergranular porosity to over 1 for joint porosity (usually ≈ 1), and n is the cementing factor that varies from 1.2 for unconsolidated sediments to 3.5 for crystalline rocks. According to Archie's law the ratio ρ/ρ_w is constant for a given porosity and should not depend on the resistivity of the water in the rocks, assuming constant temperature. This constant is called the **formation factor,** F:

$$F = a \phi_t^{-n} = \frac{\rho}{\rho_w} \quad (2)$$

The empirical relationship between porosity ϕ_t , and permeability k (in darcies) in crystalline fractured rocks (i.e. for joint porosity) is given by:

$$k = \frac{d^2}{12 F} = constant . d^2 . \phi_t^n \quad (3)$$

where d is the geometric mean fracture width in microns. In the case where conduction is dominated by pore fluid, there is, therefore, a close relationship between electrical resistivity and permeability.

The fluid resistivity is strongly dependent on temperature (T). An empirical relationship between the resistivity of the saturating fluid and temperature of up to 200°C has been given by Dahknov (1962):

$$\rho_f = \frac{\rho_{f^\circ}}{1 + \alpha (T - 18)} \quad (4)$$

where ρ_{f° is the resistivity of the fluid at 18°C and α is the temperature coefficient of resistivity which is $\approx 0.025°C^{-1}$ for most electrolytes. A relationship is established by combining Equations 1 and 4 which allows an estimation of the temperature as a function of bulk resistivity, fluid resistivity and porosity:

$$\rho = \frac{a \rho_{f^\circ} \phi^{-n}}{1 + 0.025 (T - 18)} \quad (5)$$

This relationship has been used by Georgsson (1984) in the Reykjanes Peninsula, southwest Iceland to convert the resistivity to make a map of the temperature distribution at 600 m depth below sea level.

Water rock interaction: Archie's law is usually found to be only valid for conductive solutions ($\rho_w \leq 2$ Ωm). The bulk resistivity is decreased by surface conduction along the interface between rock and water as expressed in the formula,

$$\sigma = \frac{1}{F} \sigma_w + \sigma_s \quad (6)$$

The interface conductivity σ_s , is caused by water-rock interaction. The two main reasons for

interface conductivity are conduction in clay minerals (alteration) and surface double-layer conduction. In Icelandic high temperature areas, the interface conductivity is caused by alteration of the rock matrix. Results from Nesjavellir in SW-Iceland show correlation between temperature, alteration and resistivity. It is common to have high-resistivity below low resistivity in the center of high temperature systems in Iceland. It is believed that the change in alteration minerals from the more conductive clay minerals to the more resistive chlorite and epidote is the reason for the high-resistivity below low-resistivity layer (Arnason and Hersir, 1990).

3. THE DC-SCHLUMBERGER SOUNDING METHOD

3.1 Theoretical overview

In the Schlumberger array two potential and two current electrodes are placed symmetrically around a midpoint and along a straight line (Figure 1). A current I is injected into the ground through the current electrodes A and B. The resulting potential difference between M and N, ΔV is measured. The measured values I and ΔV together with the geometrical constants S and P are used to calculate the apparent resistivity ρ_a according to the formula,

$$\rho_a = \frac{\Delta V}{I} \frac{\pi(S^2-P^2)}{2P} \tag{7}$$

where S is half the current electrode spacing (AB/2) and P is half the potential electrode spacing (MN/2).

In order to relate the measured values with actual resistivity stratification at the subsurface and, thus, obtain a qualitative interpretation of the measurement, it is necessary to derive the relationships for the potential field set up by a single point source of current at the surface of a horizontally layered earth. This is done by considering the relationships of current density, the electric field and resistivity. If we assume isotropic horizontal layering with the last layer N of infinite thickness, the general solution for the potential at any given layer is defined in cylindrical coordinates by,

$$V_i(r,z) = \frac{\rho_1 I}{2\pi} \int_0^\infty (C_i(\lambda)\cosh[\lambda(z-h_i)] + D_i(\lambda)\sinh[\lambda(z-h_i)])\ J_0(\lambda r)\ d\lambda \tag{8}$$

where C_i and D_i are determined recursively in terms of resistivity and thickness of the layers,
J_0 is the Bessel function of order zero
λ is a variable of integration
ρ_1 is the resistivity of the first layer
h_i is the depth to the i^{th} layer
r is the radial distance from the current source
z is the depth below the surface.

The functions C_i and D_i are determined by imposing the following boundary conditions:

(a) The potential $V \to 0$ as $r \to 0$ and $z \to \infty$

(b) The potential is continous at each of the boundary planes between layers, i.e: $V_i = V_{i+1}$.

(c) The vertical component of the current density is continous at the boundary of the layers, i.e. at $z = h_i$,

$$\frac{1}{\rho_i}\frac{\partial V_i}{\partial z} = \frac{1}{\rho_{i+1}}\frac{\partial V_{i+1}}{\partial z} \tag{9}$$

(d) The vertical current density is $J_z = 0$ at the surface layer, except at the current source.

Considering the above boundary conditions it can be shown that $D_N = -C_N$ at the N^{th} layer. By

defining the kernel function $K_i = -C_i / D_i$ we have $K_N = 1$ and K_i is given by the Pekeris recurrence relationship,

$$K_i = \frac{K_{i+1} + \frac{\rho_i}{\rho_{i+1}} \tanh(\lambda d_i)}{\frac{\rho_i}{\rho_{i+1}} + K_{i+1} \tanh(\lambda d_i)} \tag{10}$$

For the uppermost layer, it can be shown that $D_i = -1$ and hence,

$$V_1(r,z) = \frac{\rho_1 I}{2\pi} \int_0^\infty [K_1 \cosh(\lambda z) - \sinh(\lambda z)] \, J_0(\lambda r) \, d\lambda \tag{11}$$

At the surface where $z = 0$, we have

$$V_1(r) = \frac{\rho_1 I}{2\pi} \int_0^\infty K_1 J_0(\lambda r) \, d\lambda \tag{12}$$

Equations 10 and 12 form the basis for one-dimensional interpretation of Schlumberger soundings.

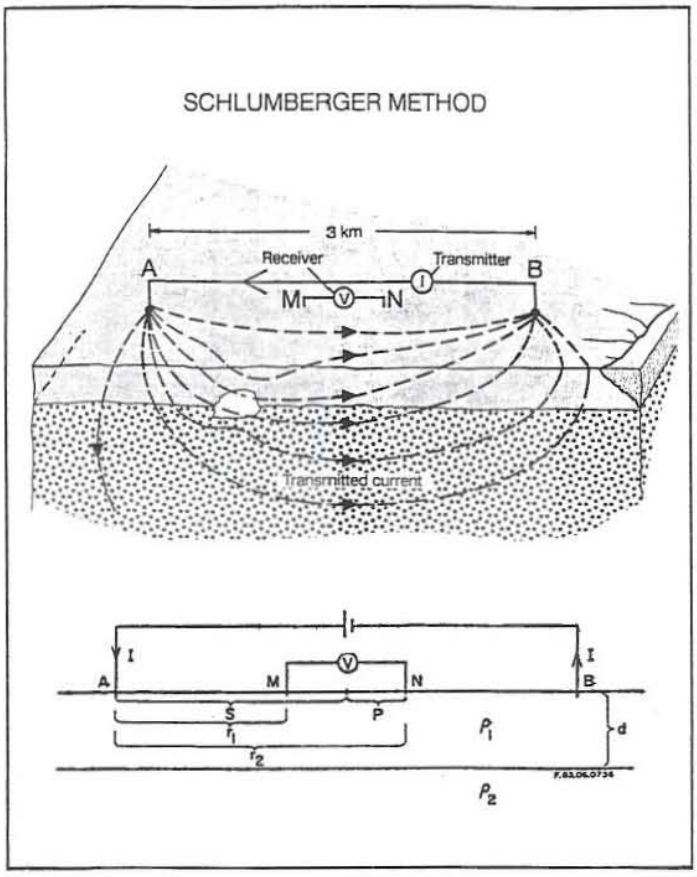

FIGURE 1: The Schlumberger method

3.2 Methods of interpretation

The object of sounding is to determine the variation of electric conductivity with depth. As discussed in the preceeding section, the idea behind vertical electrical sounding is meaningful only for an earth in which the conductivity varies merely with depth without any lateral variation. It has been shown that knowledge of the surface potential due to a point electrode should suffice to determine the thicknesses and resistivities of the various layers. Some interpretation methods based on this approach have been developed (e.g. Pekeris-Koefoed and auxillary point methods), while other methods based on a trial-and-error or optimization approach (e.g. Gosh, Inman and Johansen methods) have been found to be more efficient.

3.2.1 Factors affecting the sounding curves

There are a lot of factors that may cause a distortion of the sounding curves and scattering of ρ_a data. The distortions or errors may be related to the conduct of the survey and usually it is too late for these errors to be corrected once the fieldwork has been completed. Detection of the distortions requires knowledge of the possible causes. They can be caused by instrumental and data acquisition errors (e.g. misreading of instrument settings, contact resistance, etc.) or disturbance of the electrical field at the centre (e.g. leakage current, buried conductors, noise, etc.).

The "errors" mentioned above can be corrected by conducting repeat measurements. However, some "jumps" in some segments of the curve may be mistaken for erroneous data. They may actually be the result of the departure from the boundary conditions of the idealized earth mentioned in Section 3.1 and the "distortions" may reflect the true condition beneath the surface. These "distortions" in the sounding curve are commonly encountered in geothermal areas and should be taken into consideration in the interpretations:

Inhomegeneity and anisotropy: The one-dimensional interpretation of soundings is based on the assumption that the subsurface consists of a sequence of distinct layers of finite thickness separated by horizontal boundary planes, with the deepest layer extending to infinite depth. Each of these layers is assumed to be electrically homogeneous and isotropic. In practice, the assumption of homogeneity holds true if the contrast of resistivities of the geological structures within the layer is not too large. The magnitude of the electric anomalies on a non-homogeneous earth depends upon the resistivity differences between different rocks. Also, in reality geological formations may be electrically anisotropic. In formations rich in clay or shale, for example, the electrical resistivity is the same in all directions along a layer but different perpendicular to the stratification.

Topographic effect: High-temperature geothermal areas are mostly located in mountainous terrains (e.g. Nesjavellir, Krafla, Philippine geothermal fields, the Geysers, etc.). Since topographic effect is inherent to the relative locations of the current and potential electrodes and the nature of the terrain itself, this should be taken into account in the interpretation.

Higher ΔV values would be observed when the potential electrodes are placed perpendicular to the axis of a steep valley compared to what one would observe over a horizontal free surface. This is caused by the "focusing" effect of the valley or the convergence of equipotential lines. On the other hand, the opposite effect is observed over high-angle ridges where a zone of current dispersion and a corresponding divergence of equipotential surfaces normal to the current flow are created (Figure 2). Thus, topographic effect can cause higher ρ_a values over valleys and lower ρ_a values over ridges.

Fox et al. (1978) have studied the nature and significance of topographic effect using finite element computer techniques. Arnason and Hersir (1990) used a program that utilizes a finite element algorithm for modelling arbitrarily shaped two-dimensional resistivity structures with surface topography in their study of the Nesjavellir geothermal field in Iceland. The program, which was developed and written by Ragnar Sigurdsson at Orkustofnun, is discussed in Section 3.2.3.

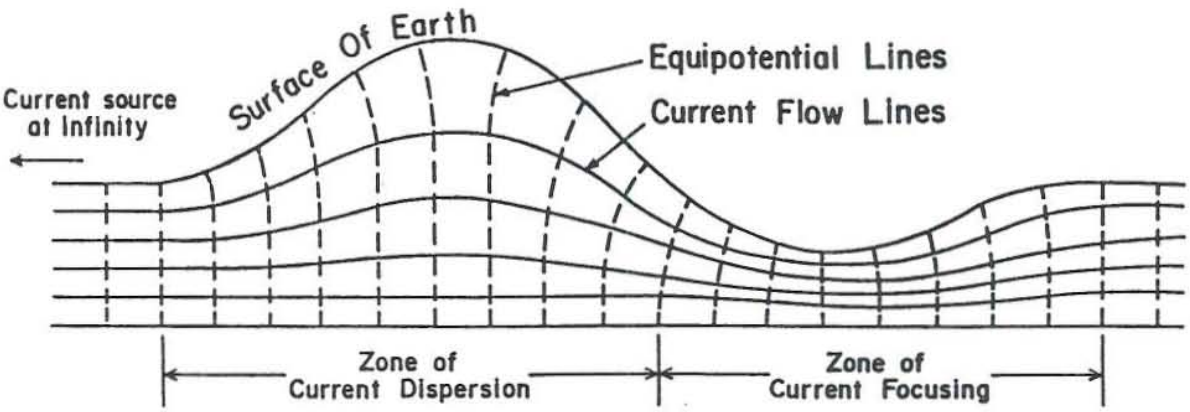

FIGURE 2: The effect of topography on current flow and equipotential lines (Fox et al., 1978)

Near-surface inhomogeneities: In increasing the depth of investigation in the Schlumberger sounding, the current electrodes *A* and *B* are moved symmetrically outwards from the center (Figure 1), while simultaneously keeping the distance between the potential electrodes *M* and *N* fixed. However, when the ratio *AB/MN* becomes so large that the potential drop across *MN* becomes too small to be measured with reasonable accuracy, then the curve may be displaced due to "eccentricity" and it becomes necessary to increase the distance between *MN*. Changing the *MN* distance involves the taking of potential at two or more potential electrode spacings at the same current electrode separation. The resulting apparent resistivity curve thus obtained will show that, in most practical cases, the segments for different *MN* spacings fail to tie in with other parts of the curve.

These "shifts" in the apparent resistivity curves of Schlumberger soundings have been analysed by Arnason (1984). They are found to be of two categories: shifts that converge and shifts that stay constant when electrode spacing is increased (Figure 3). Converging shifts are caused by large resistivity contrasts between layers in horizontally stratified earth. The converging shifts contain information about horizontally stratified resistivity structures. Nonconverging shifts are caused by lateral resistivity variations at the center of the Schlumberger array and, in such a case, the apparent resistivity values measured with the largest potential electrode separation are, in general, most reliable. The segments measured with shorter potential electrode spacings should be shifted so that they tie in with the segment measured with the largest potential electrode spacing. A one-dimensional inversion program with automatic shift conversion has been developed at Orkustofnun and is discussed in the following section.

3.2.2 One-dimensional interpretation and the program ELLIPSE

In the process of interpretation, the raw data or the data obtained from the field is first transformed into apparent resistivity values by use of Equation 7. The data is plotted in a graph, either manually or on a computer terminal screen, depending on the method of interpretation used.

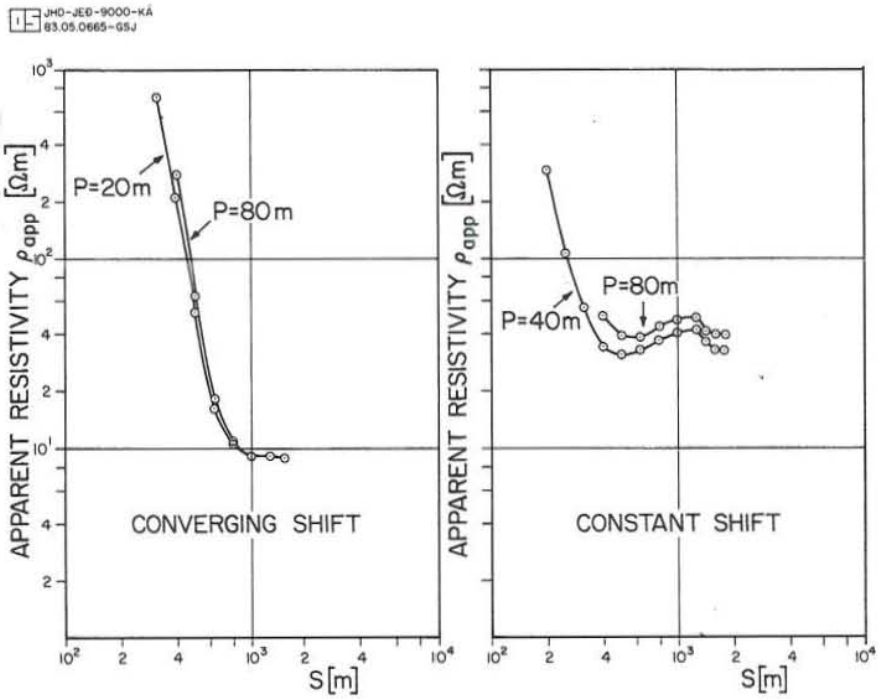

FIGURE 3: Shifts in apparent resistivity curves

In the early years, interpretation of soundings was made by curve matching with the use of master diagrams. This approximate interpretation method involves a comparison of the measured curve with a set of theoretically calculated master curves (Parasnis, 1986). The limitation of this method has been that except for the two-layer case, master curves cannot be presented in a single diagram covering all possible combinations of thickness and resistivity parameters. As a result, extensive catalogues are needed which can only be used for the electrode configuration in question. Furthermore, it is only practical to use the method for up to four (4) layers due to the number of permutations of different resistivity and thickness combinations. With the abovementioned limitations, the method has now become obsolete.

The impractical use of complete curve matching for more than four layers led to the development of the auxillary point method of interpretation. The method is based on the use of auxillary graphs in conjunction with two-layer apparent resistivity model curves to decompose a graph of any number of layers into a set of sequential two-layers. The use of three-layer apparent resistivity model curves has also been found useful. The method is discussed by Orellana and Mooney (1966), Koefoed (1979), Parasnis (1986) and in other publications.

The advent of computers set the stage for iterative interpretation methods relegating the use of approximate interpretation methods to providing initial solutions for subsequent optimization. In forward modelling the field data are compared with the data derived from a layer model obtained by approximate interpretation methods. If the two sets of data are not satisfactorily in agreement, then the parameters of the layer model are adjusted. The iteration is then continued until sufficient agreement between the model data and the field data is obtained. This method is also termed as "comparison in the apparent resistivity domain" (Koefoed, 1979). The other method is called inverse modelling or "comparison in the resistivity transform domain" and it provides direct information on the relative difference (or the sum of squares of difference) between the model data and the field data in terms of the quantity actually determined in the field measurements. Some details of this method can be found in a paper by Johansen (1977).

The one-dimensional interpretation of Schlumberger soundings was done by inverse modelling with the use of the program ELLIPSE developed and written at Orkustofnun. ELLIPSE is a

non-linear least square inversion program using a Levenberg-Marquadt type iteration algorithm. The program does not use the gradient approximation but simulates the actual electrode configuration used in the field by computing the potential at each potential electrode. The forward calculations of the potential and the partial derivatives use a 436 point digital filter. In addition to the resistivities and thicknesses of the layers, the model parameters contain one multiplication coefficient (shift on log scale) for each overlapping transition between segments measured with different potential electrode spacings. By this method, each shift is resolved into converging and nonconverging parts discussed in the preceeding section. Thus, all shifts caused by lateral inhomogeneities close to the centre of the sounding are automatically removed and all segments tied in with the longest potential electrode spacing.

3.2.3 Two-dimensional interpretation and the program FELIX

In one-dimensional modelling, non-horizontal contact anomalies like dipping beds and surface inhomogeneities are assumed non-existent in a horizontally layered earth. In two-dimensional modelling the resistivity can vary in two directions, i.e. in vertical and one lateral direction, but is constant in the other lateral (strike) direction. It is, therefore, useful in the delineation of vertical boundaries of different resistivities of the earth.

The sounding stations to be considered in the two-dimensional modelling should be located along a cross-section nearly perpendicular to resistivity boundaries, and in such a way that the current electrodes are oriented parallel or less than 10° from the direction of the cross-section. The soundings should also be chosen such that the neighboring current electrode spacings overlap and orient in the same direction as that of the profile line. The overlap is necessary as it helps to identify and locate the strong lateral resistivity variations that may cause distortion in the curves during modelling.

Two-dimensional modelling of Schlumberger soundings along cross-section A-A' was done using the program FELIX developed and written at Orkustofnun. The program uses a finite element algorithm for modelling arbitrarily shaped two-dimensional resistivity structures with surface topography. It is composed of two separate programs LIKAN and TULKUN and can model cross-sections with up to ten sounding stations.

The LIKAN program facilitates the construction of two-dimensional resistivity models. Results of the one-dimensional interpretations from ELLIPSE are used as the basis for a starting model. Vertical boundaries are introduced at the positions of suspected vertical boundaries from the result of the one-dimensional model and structural geology. The layers in the model are usually assumed near-horizontal but the thicknesses can be varied accordingly at different sections based on the one-dimensional model. The model is represented in the form of a grid (Figure 4) consisting of blocks defined by their lateral and vertical position including their resistivity values. An efficient grid generator further subdivides the resistivity model into a triangular grid (Figure 5). The grid dimensions increase quadratically with depth and laterally outside the traversed area in a simple and controllable way in order to optimize computational speed against accuracy. The triangular net is then stored in an output file for further processing with the program TULKUN.

In the TULKUN program the potential at the edges of the triangles is calculated by the finite element method, taking into consideration the resistivity and relative position of each triangle. The program computes the apparent resistivity values by simulating the actual electrode configuration. The computed response of the model is then compared with the field data. All points from the computed response of the model should tally with the measured resistivity plot to get a good fit.

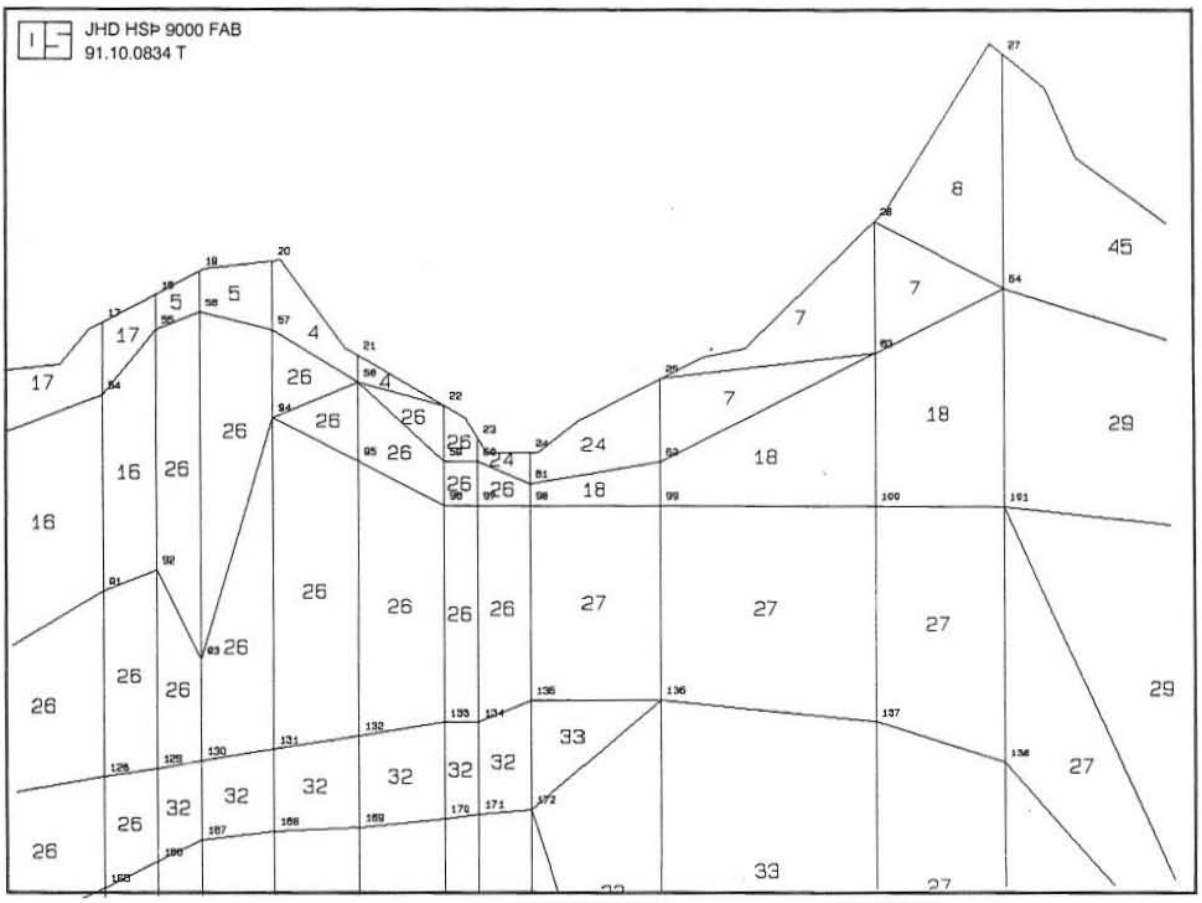

FIGURE 4: Grid model from the program LIKAN

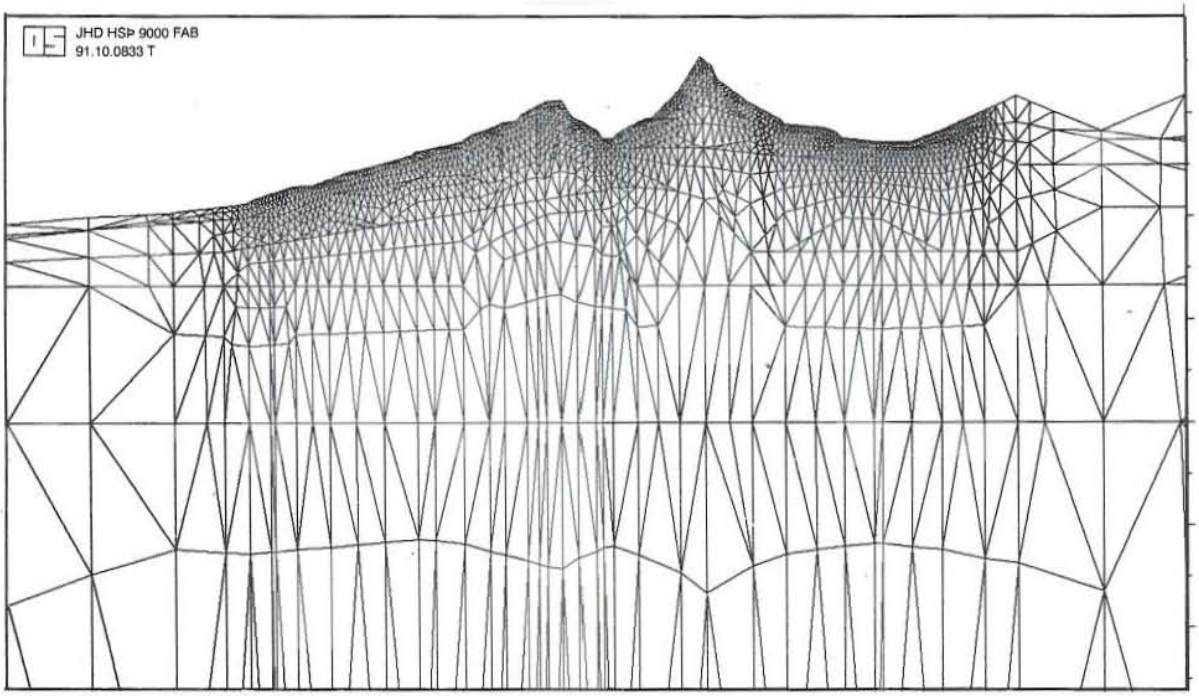

FIGURE 5: Triangular net model from the program TULKUN

3.3 Schlumberger sounding survey in Mt. Cagua, Philippines

3.3.1 Introduction

The Mt. Cagua geothermal prospect is located within the municipality of Gonzaga, Cagayan Province at the northeasternmost tip of Luzon Island, Philippines (Figure 6). The Philippine National Oil Company - Energy Development Corporation (PNOC-EDC) conducted a multi-disciplinary surface exploration survey involving semi-detailed geological mapping, geochemical sampling and electrical resistivity measurements covering mainly the western part of the prospect area in late 1988 up to early 1989. The assessment on the potential of the prospect led to the drilling of two exploratory wells in 1989. The bottomhole temperature recorded from the first well, CG-1D, is greater than 300°C but encountered poor permeability. The second well, CG-2D reached only a maximum of 114°C temperature. Based on the first well, PNOC-EDC decided to expand the exploration northeast of Mt. Cagua towards Mt. Baua.

Two electrical methods were used in the geophysical study of the prospect area: traversing to determine the lateral variation in resistivity of rocks, and vertical sounding to define the resistivity formations at depths (Bayrante et al., 1989). In both methods, the Schlumberger array was used. Maximum sounding arm (AB/2) of 1000 to 1250 m was used for the vertical soundings, while in the traversing measurements, fixed AB/2 spacings of 250 and 500 m and constant MN spacing of 25 m were used. Forty-one (41) Schlumberger sounding stations and 117 Schlumberger traversing measurements were completed in the 1988-1989 survey and an additional 33 Schlumberger soundings were made early this year, 1991. Only the Schlumberger vertical soundings located in the vicinity of Mt. Cagua from the 1988-1989 survey and those measured this year were interpreted by the author. The sounding curves and calculated one-dimensional model curves are presented in Appendix A (Benito, 1991).

3.3.2 General geology

The geological mapping conducted in 1988-1989 in Mt. Cagua was concentrated in the vicinity of Cagua Volcano and only semi-detailed mapping was conducted to the northeast towards Mt. Baua. No detailed description, therefore, of the geology to the northeast (and only the geologic map provided by PNOC-EDC in this part of the prospect area) was available for use by the author during the interpretation.

The geology of the western part of the prospect is described in a report by Bayrante et al. (1989). It is broadly overlain by Pleistocene-Recent volcanic products deposited during the semi-explosive cone building episode of Mt. Cagua. The underlying Quaternary rock units within the prospect area are comprised of a thin pile of andesitic volcanics, lahars and tephras associated with Mts. Cagua and Baua. Sedimentary rocks are found beneath Quaternary deposits and overlap with Tertiary basalts and andesites (i.e. Tabungon Volcanics). The local basement (Palawig Formation) of clastics and mafic lava flows is separated by uncomformities and overlies regionally metamorphosed sediments and volcanics. These are intruded by the predominantly dioritic intrusive Sierra Madre Pluton which, in turn, is cut by basaltic dyke swarms (Figure 2). Fault structures trend NW-SE and ENE-WSW with strike-slips as the predominant features, particularly in the underlying basement rocks.

The distribution of springs in Mt. Cagua is typical for geothermal systems associated with andesitic strato-volcanoes (Bayrante et al., 1989). Neutral chloride springs are observed at low elevations where the hot water table intersects the topography. At higher elevations, the acidic, sulfate springs and fumarolic discharges are common surface features like those at Magrafil and Maasok

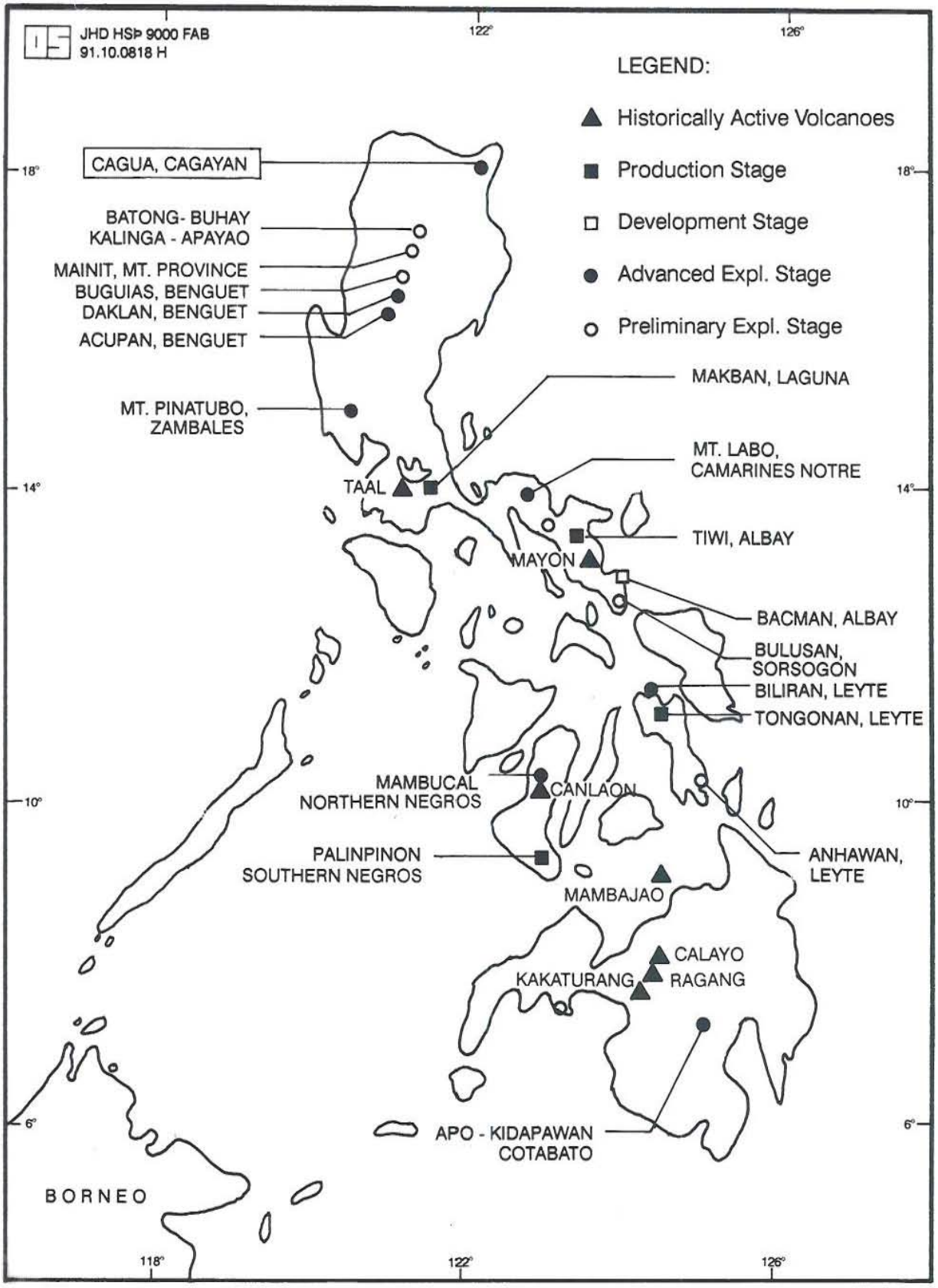

FIGURE 6: Location map of Mt. Cagua geothermal prospect

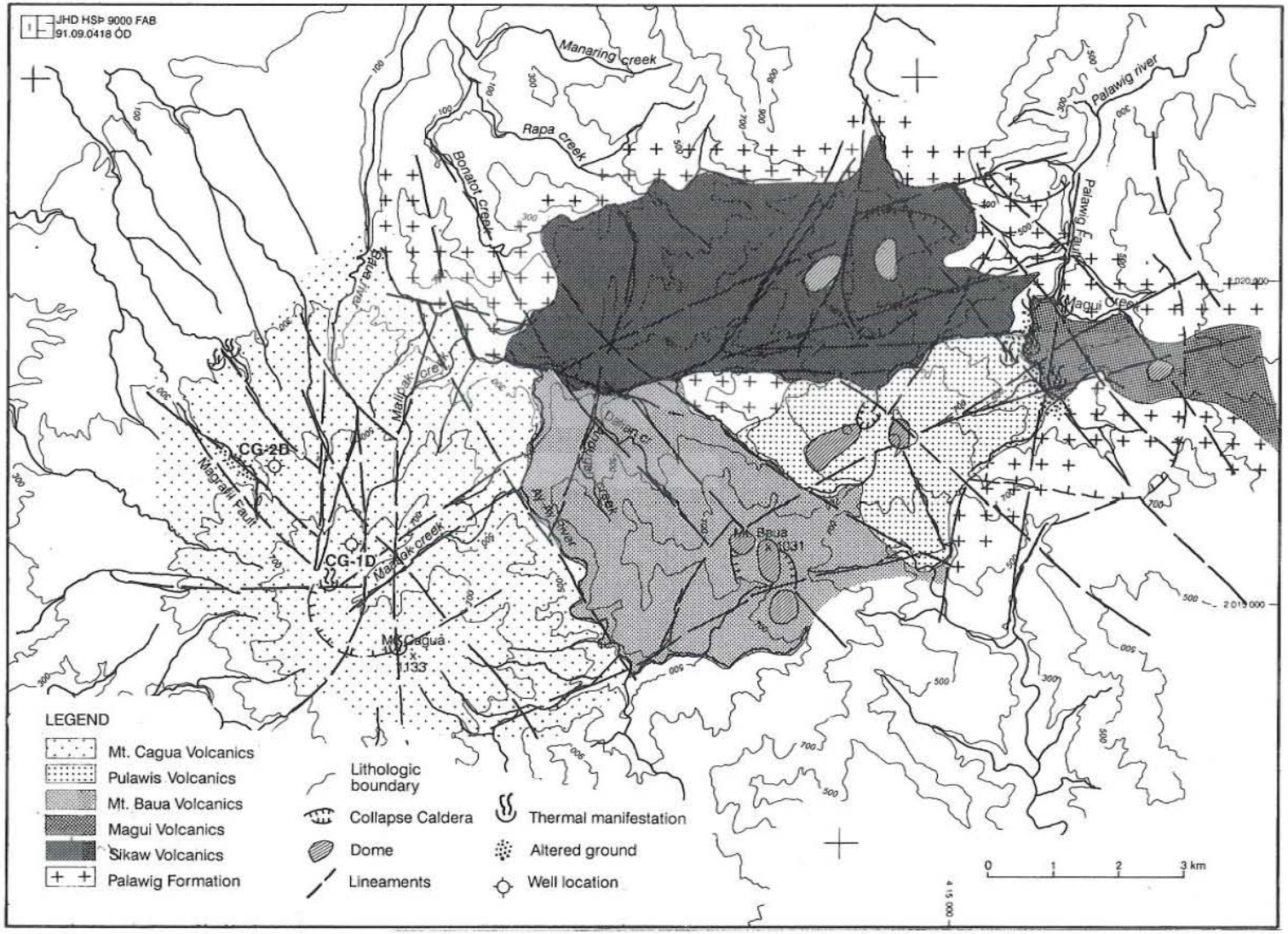

FIGURE 7: Simplified geologic map of Mt. Cagua geothermal prospect (modified from PNOC-EDC map)

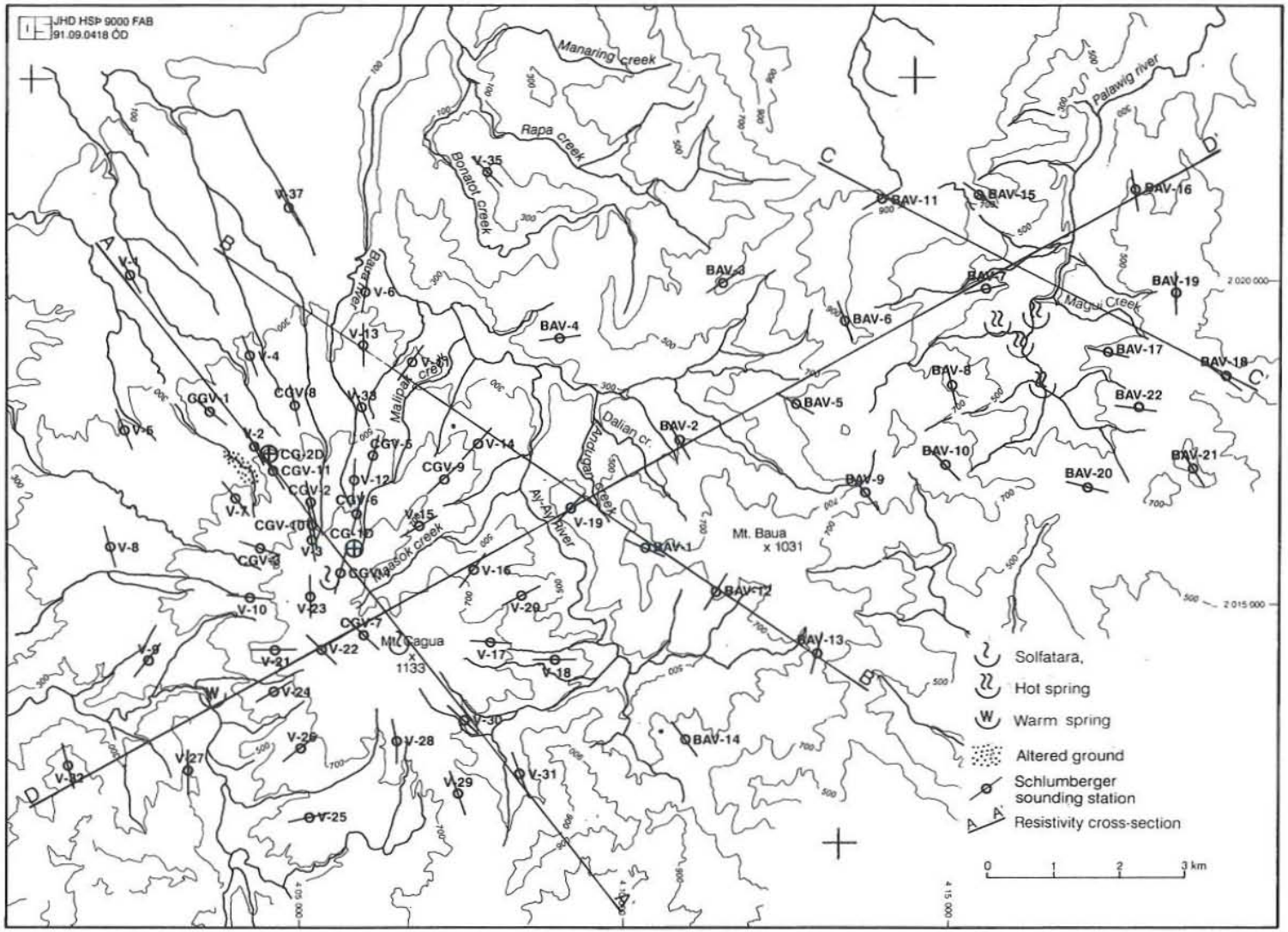

FIGURE 8: Mt. Cagua, location of resistivity soundings and cross-sections

thermal areas. Neutral-bicarbonate-sulfate springs like those at Paminta and Kabinlangan are found when the center of the resource is located at higher elevations where the topographic relief is high, and they are the result of the neutralization of acidic fluids by water-rock interaction.

3.3.3 Results of one-dimensional interpretation

Schlumberger sounding data from eighty-six stations were processed using the one-dimensional program ELLIPSE described in Section 3.2.3. The locations of the soundings and resistivity cross-sections are shown in Figure 8.

Resistivity cross-section A-A' (Figure 9): The section runs from northwest to southeast across the major thermal manifestations in the vicinity of Cagua Volcano. The same section was interpreted two-dimensionally (see Section 3.3.4). Twelve soundings are covered or projected into the profile and the two exploration wells, CG-1D and CG-2D. The last segment of the sounding curves is moderately increasing and appears to be levelling at both end stations of the cross-section (V-01 and V-31), while it is moderate-to-steeply descending in other stations except at CGV-07 where it is steeply ascending.

The surface layer is 20-60 m thick with varying resistivity of up to 6000 Ωm. It overlies a resistive layer of >500 Ωm of up to 200 m thickness. The model shows a low resistivity layer of less than 50 Ωm along the central part of the profile at depths of 50-250 m below the surface. The lowest resistivity values of 5-10 Ωm are recorded at V-23 and CGV-07 close to the rim of a collapse caldera and the solfataras. The conductive layer is apparently also detected at V-30, but the result

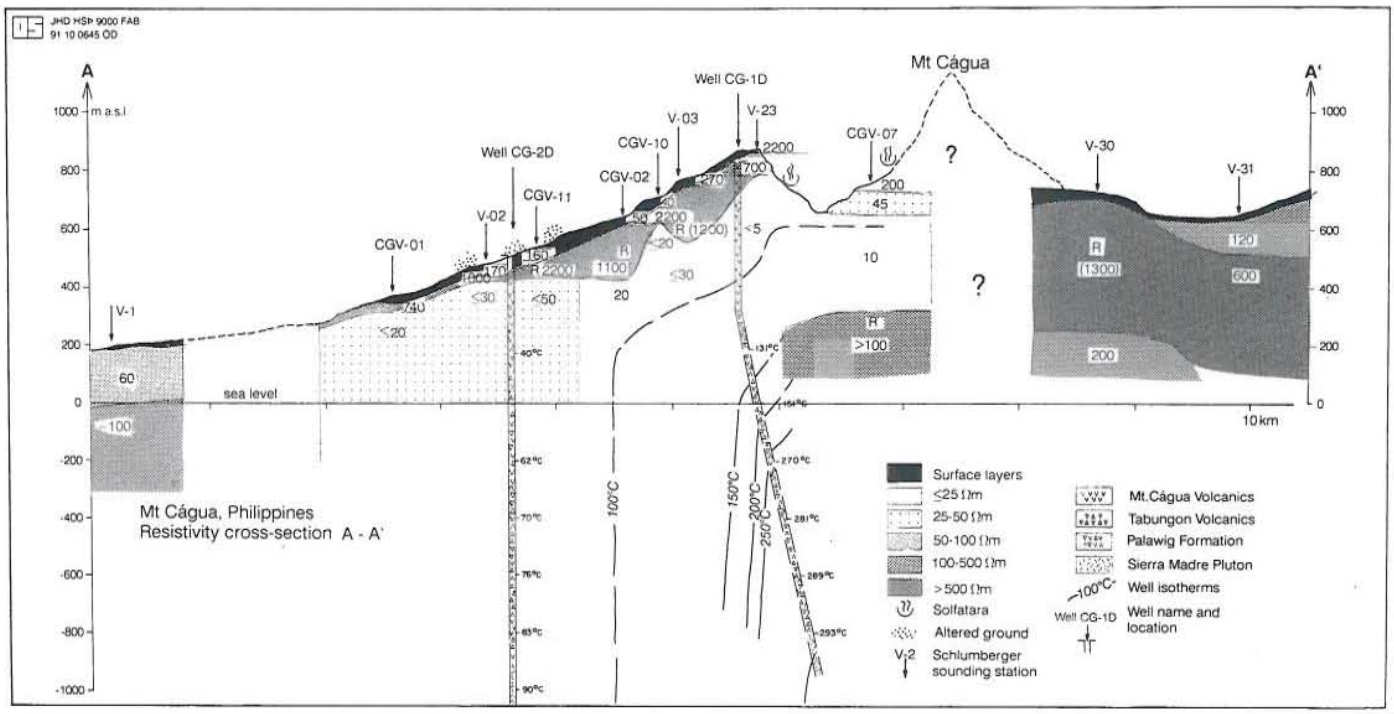

FIGURE 9: Resistivity cross-section A-A'

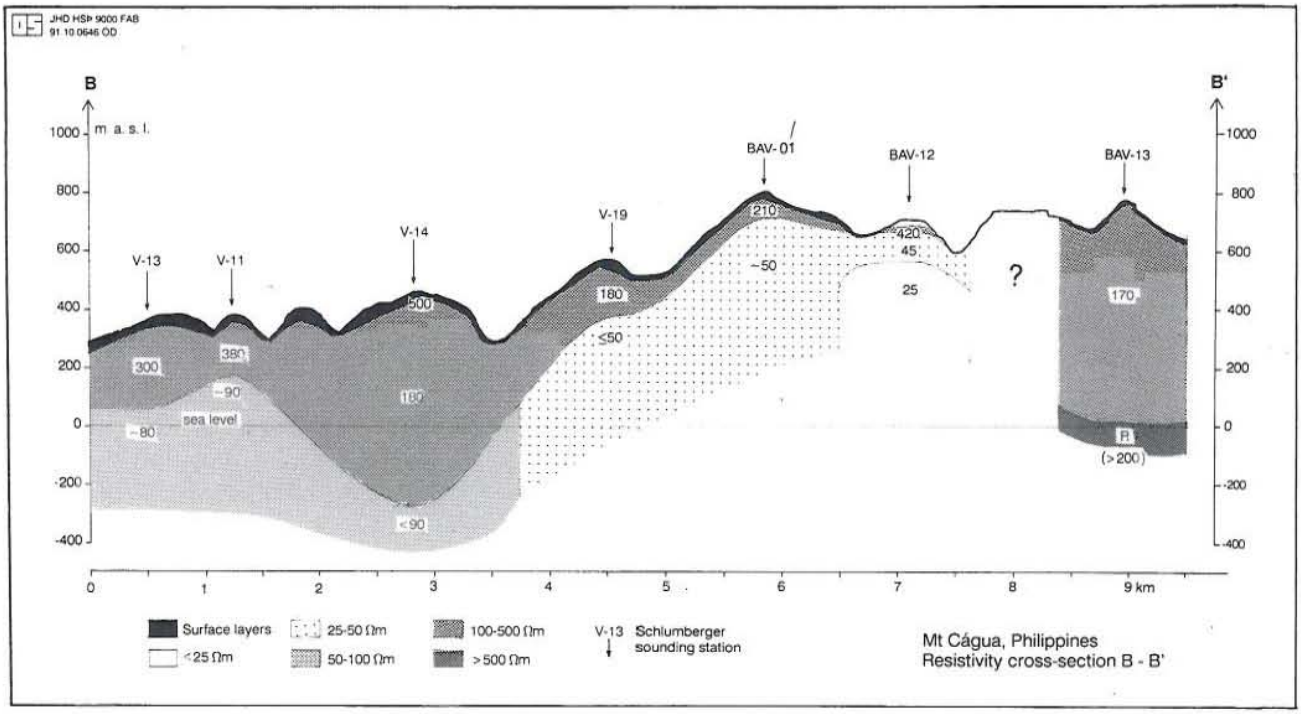

FIGURE 10: Resistivity cross-section B-B'

of the two-dimensional modelling indicates the decreasing resistivity at this station (≤200 Ωm) is caused by lateral resistivity changes. The low resistivity layer also appears to reach closer to the surface at CGV-10. The natural way to interpret this might be to assume a structure located close to this station. However, this can be attributed to topographic effect as can be seen later from the results of the two-dimensional interpretation. The bottom of the low resistivity layer was not detected in the soundings except at CGV-07 where it appears thinnest and the resistivity increases at depths (>100 Ωm). The resistivity contrast at stations V-30 and V-31 and below CGV-07 delineates the southern boundary of the conductive layer while it is bound to the northwest by station V-01.

From the stratigraphy of well CG-1D, the bottom of the low resistivity layer at CGV-07 coincides with the contact between Tabungon Volcanics and Palawig Formation, but more likely the resistivity values may reflect the high temperature alteration in this part of the well which is also reflected in the temperatures of more than 250°C. Relatively high resistivity values within the conductive layer (<50 Ωm) are observed close to well CG-2D at sounding station CGV-11. This correlates to the low temperature recorded in the well.

Resistivity cross-section B-B' (Figure 10): The section runs from northwest to southeast, a few kilometers northeast of Cagua Volcano. The surface layer is up to 50 m thick along this section with resistivity values of up to 3000 Ωm. A layer of medium resistivity values of 150-400 Ωm underlies the surface layer. A conductive layer of ≤50 Ωm was detected in three of the soundings, V-19, BAV-01 and BAV-12, while moderate values of 50-100 Ωm characterize the same layer in other stations to the northwest. The conductive body is centered at BAV-12 where the resistivity is lowest at 25 Ωm, however, there are no reported thermal manifestations in the vicinity of the station. As in cross-section A-A', the low resistivity layer is bound to the southwest by increasing resistivity at depths at BAV-13.

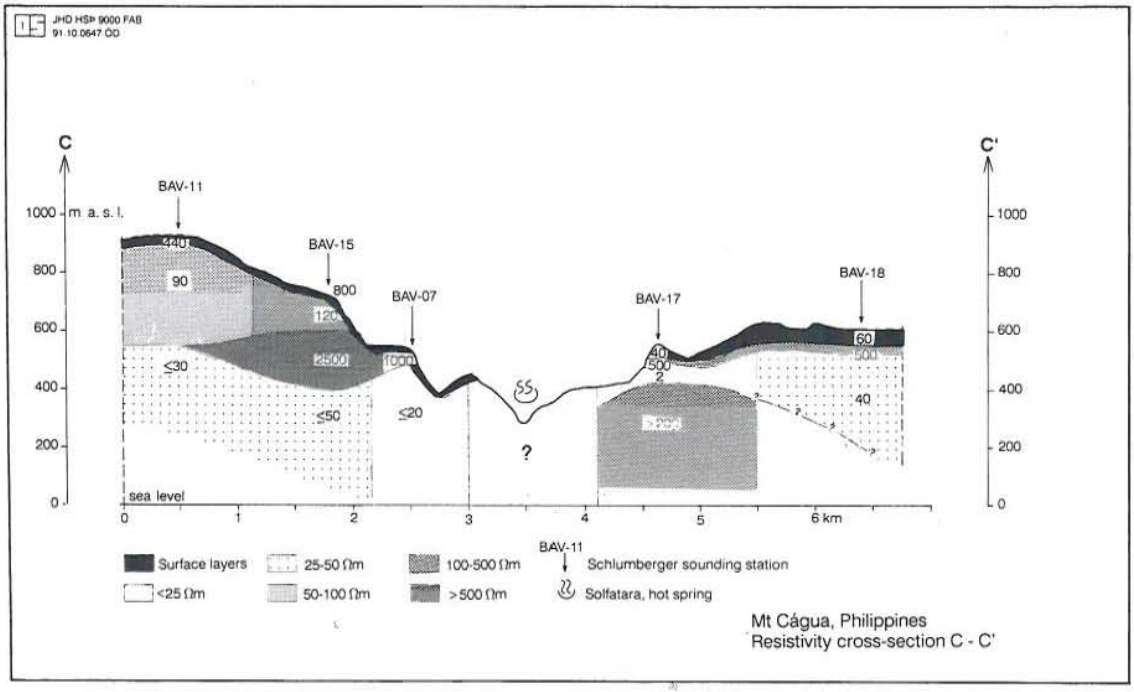

FIGURE 11: Resistivity cross-section C-C'

Resistivity cross-section C-C' (Figure 11): As with the first two, the section runs from northwest to southwest and is located at the northeastern edge of the survey area. The resistivity of the surface layer is only up to 800 Ωm and is lower compared to the other sections. This could reflect the alteration at the surface due to the thermal activity in the area. Medium resistivity values (>150 Ωm) underlie the surface layers at BAV-11 and BAV-15. A resistive layer (≥500 Ωm) underlies the surface at the other stations, BAV-07, BAV-17 and BAV-18 including the next layer at BAV-15. A conductive layer was detected at the bottom of all the soundings except at BAV-17 where it only appears as a thin layer above a resistive body. The conductive layer is centered at BAV-07 with the resistivity at ≤20 Ωm. At BAV-17 on the other hand, a very low resistivity of 2 Ωm was recorded for this layer at shallow levels, but underlying it is a resistive layer of >200 Ωm. The possible interconnection of this layer in BAV-07 and BAV-17 is uncertain. There is a possibility BAV-17 may be closest to the center of the heat source considering its location relative to the thermal manifestations at Magui Creek.

Resistivity cross-section D-D' (Figure 12): This 19-km section trending southwest-northeast cuts through the three other sections described above. It shows the extent of the conductive body northeast of Mt. Cagua and the possible interconnection of the geothermal system with Mt. Baua. Except for CGV-07 near Cagua Volcano, all the sounding curves have decreasing resistivity values at depths. The surface is underlain by a resistive layer of >200 Ωm to the southwest and northeast ends of the section and a moderate resistivity layer of <200 Ωm in the middle of the section. The conductive layer of ≤50 Ωm is detected beginning at station V-21 and it extends towards the northeast up to the hot springs near BAV-07. It is generally found at depths of 100-200 m below the surface. The resistivity of the layer in some of the soundings is not well defined and, in some cases, may be lower than the values shown in the figure. The conductive layer has the lowest resistivity values of 10-25 Ωm at CGV-07 and BAV-07 close to the postulated geothermal centers. There is no indication that the conductive layer extends to the location of Paminta hot springs in the southwest, and the hot water could be an outflow from the geothermal heat source at Cagua Volcano because of its proximity to the low resistivity boundary.

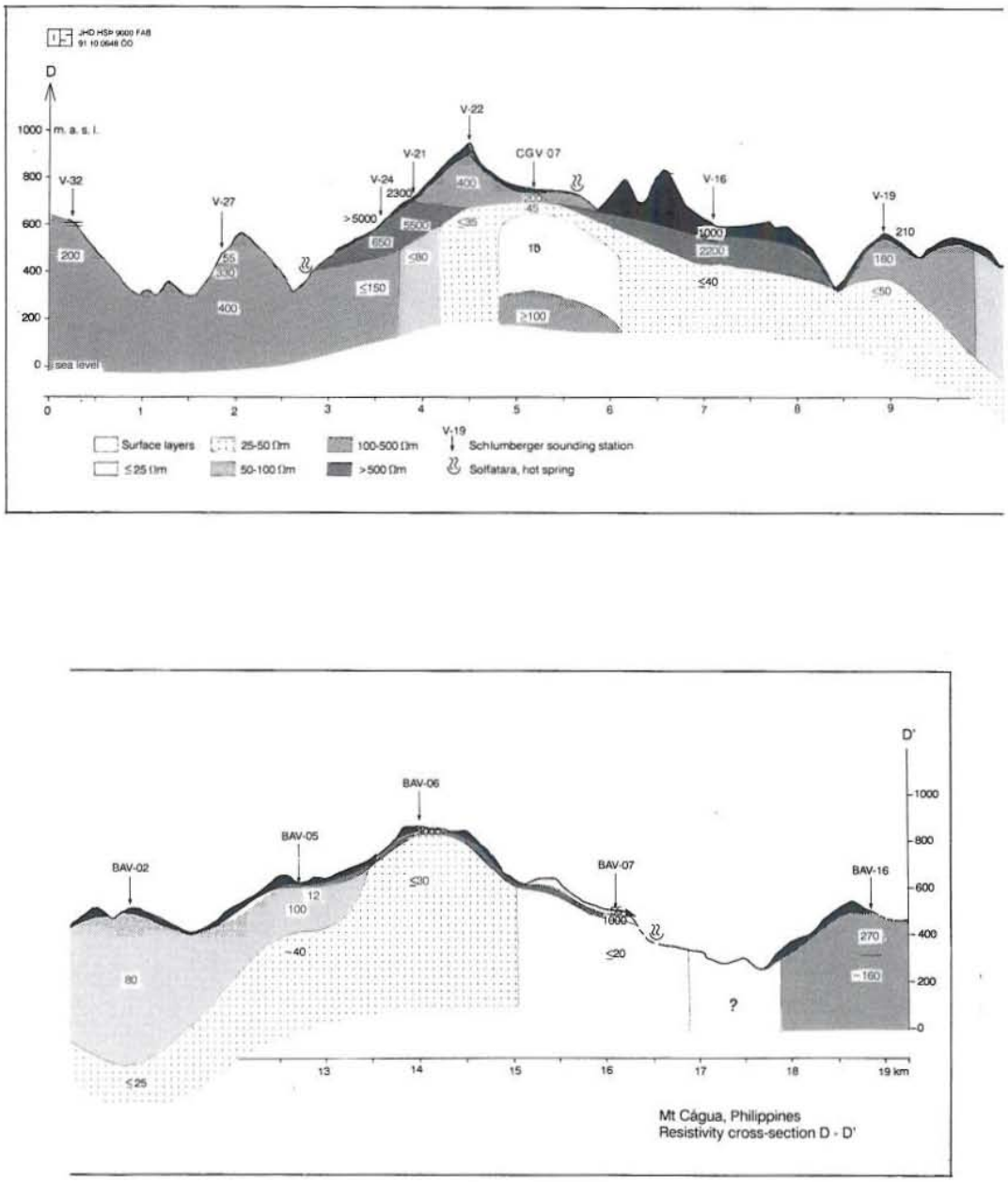

FIGURE 12: Resistivity cross-section D-D'

The isoresistivity maps: Figures 13, 14 and 15 show the isoresistivity maps contoured at elevations of 500, 300 and 100 m above sea level, respectively. The maps are based on the one-dimensional interpretation of the soundings. They are presented to delineate the boundary of the low resistivity anomaly at the given range of depths where the resistivity sounding data can be reliably interpreted. The geology of the prospect area was also taken into consideration in the drawing of the maps.

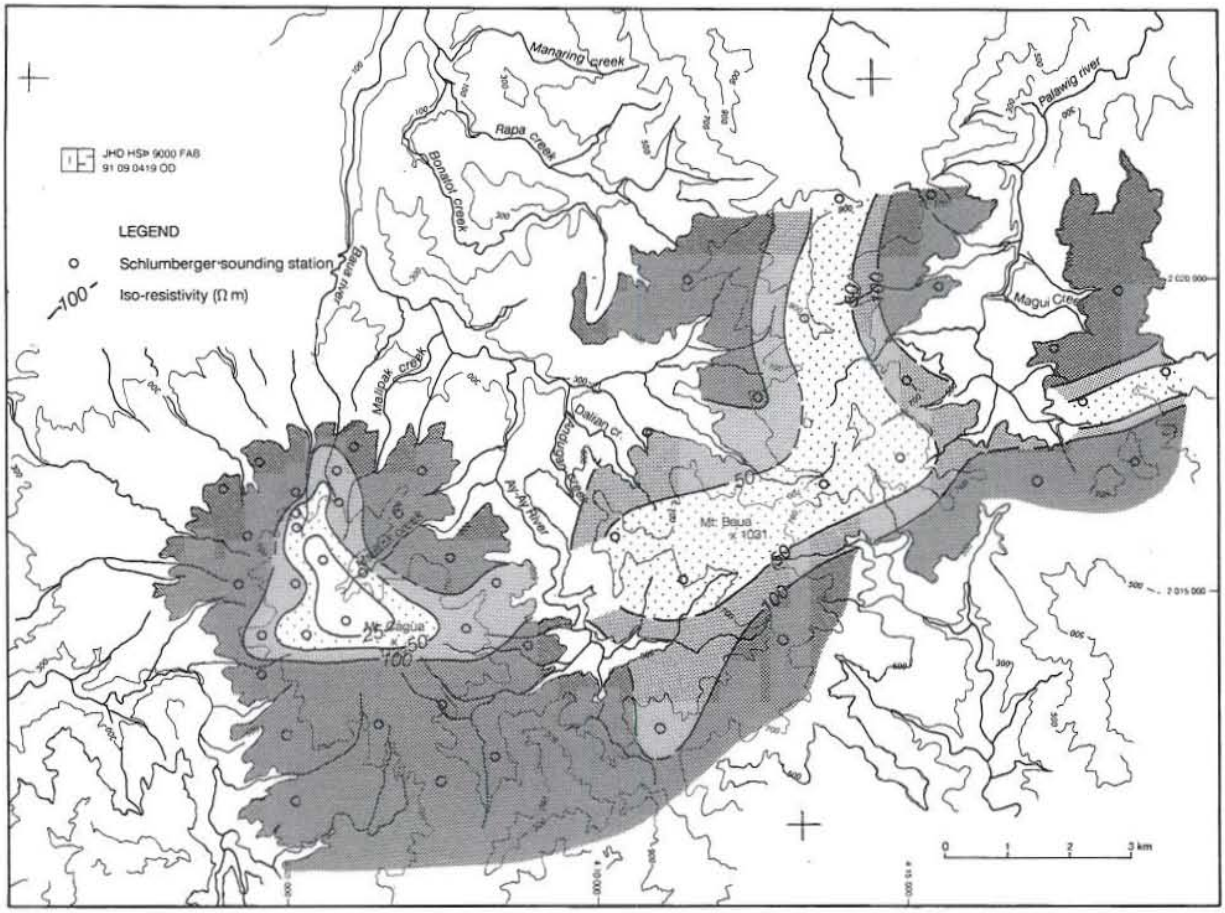

FIGURE 13: Isoresistivity map at 500 m a.s.l.

The maps depict the same trend of resisitivity values except at 500 m a.s.l. where the isolines are limited by the contour line of the topography. A southwest-east-northeast trending low resistivity anomaly defined by the 50-Ωm isoline covers the survey area. It is northeasterly dipping at depth in the west along cross-section A-A'. Two distinct centers defined by the 25-Ωm isoline are readily distinguished within the anomaly zone. The first center is located at the western part of the prospect area and is a confirmation of the low resistivity structure delineated by Bayrante et al. (1989). The resistivity anomaly trends in a NW direction parallel to cross-section A-A' and along the Magrafil Fault. It encloses the known thermal manifestations in the vicinity of Cagua volcano. The other center of the resistivity anomaly is situated northeast of Baua Volcano and encloses the thermal manifestations in the vicinity of Magui Creek.

Two other resistivity zones of ≤25 Ωm were delineated but are not depicted in the maps. One is located at BAV-02 but is detected below sea level (see Figure 12) and the other at BAV-12 (see Figure 10) where it is detected between 500 and 300 m a.s.l.. Considering the relative positions of these two stations, with regard to geology, another upflow zone might be suspected in the vicinity of Baua Volcano. The lateral boundaries of the low resistivity structure is well defined to the north and south but is open in the other two directions, towards the lowlands in the northwest and towards the Palawig Range in the east-northeast side of the anomaly.

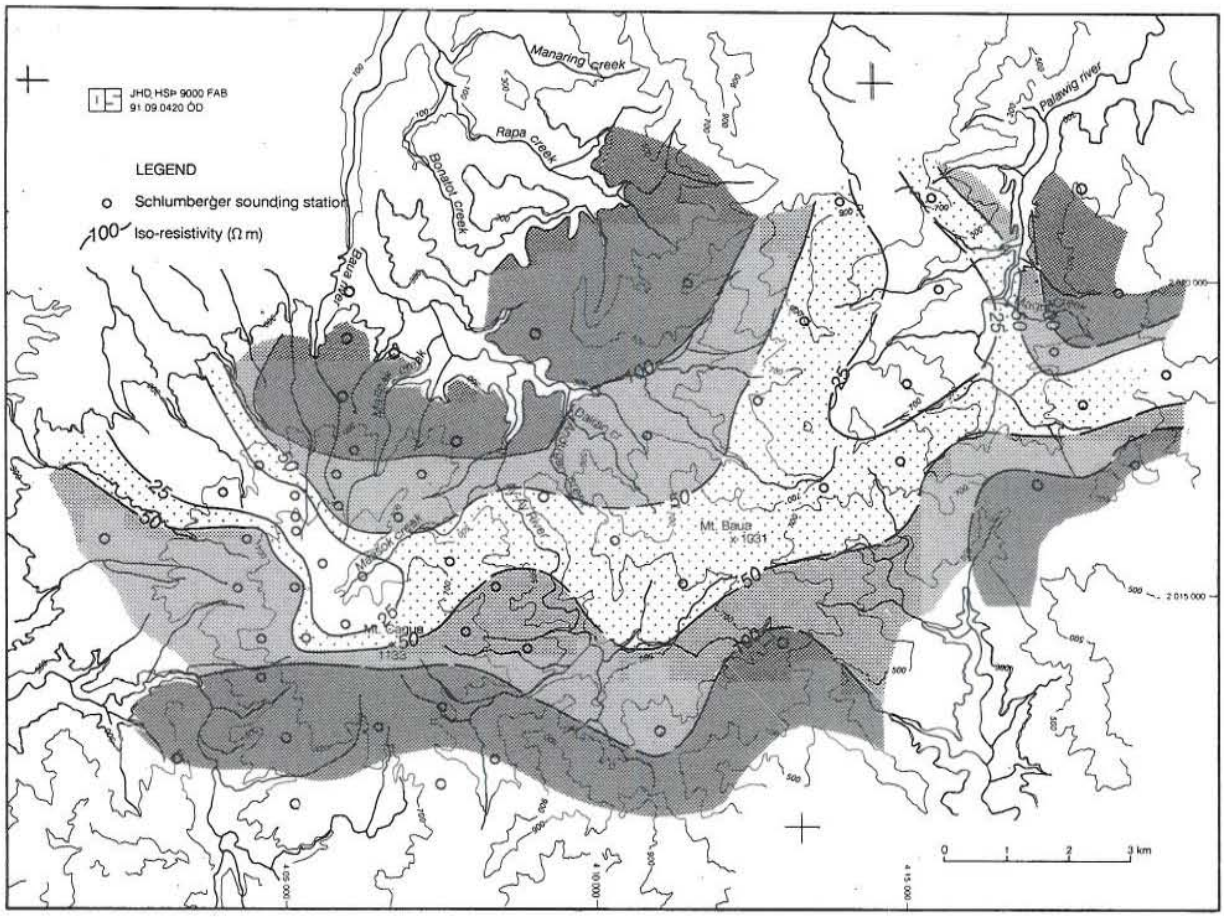

FIGURE 14: Isoresistivity map at 300 m a.s.l.

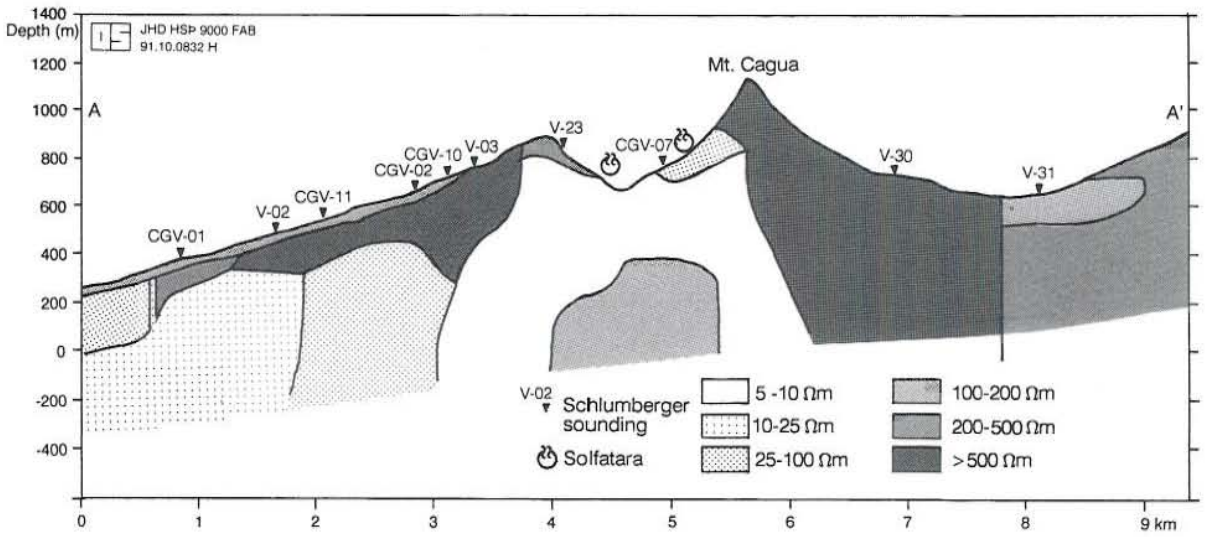

FIGURE 16: Two-dimensional resistivity cross-section A-A'

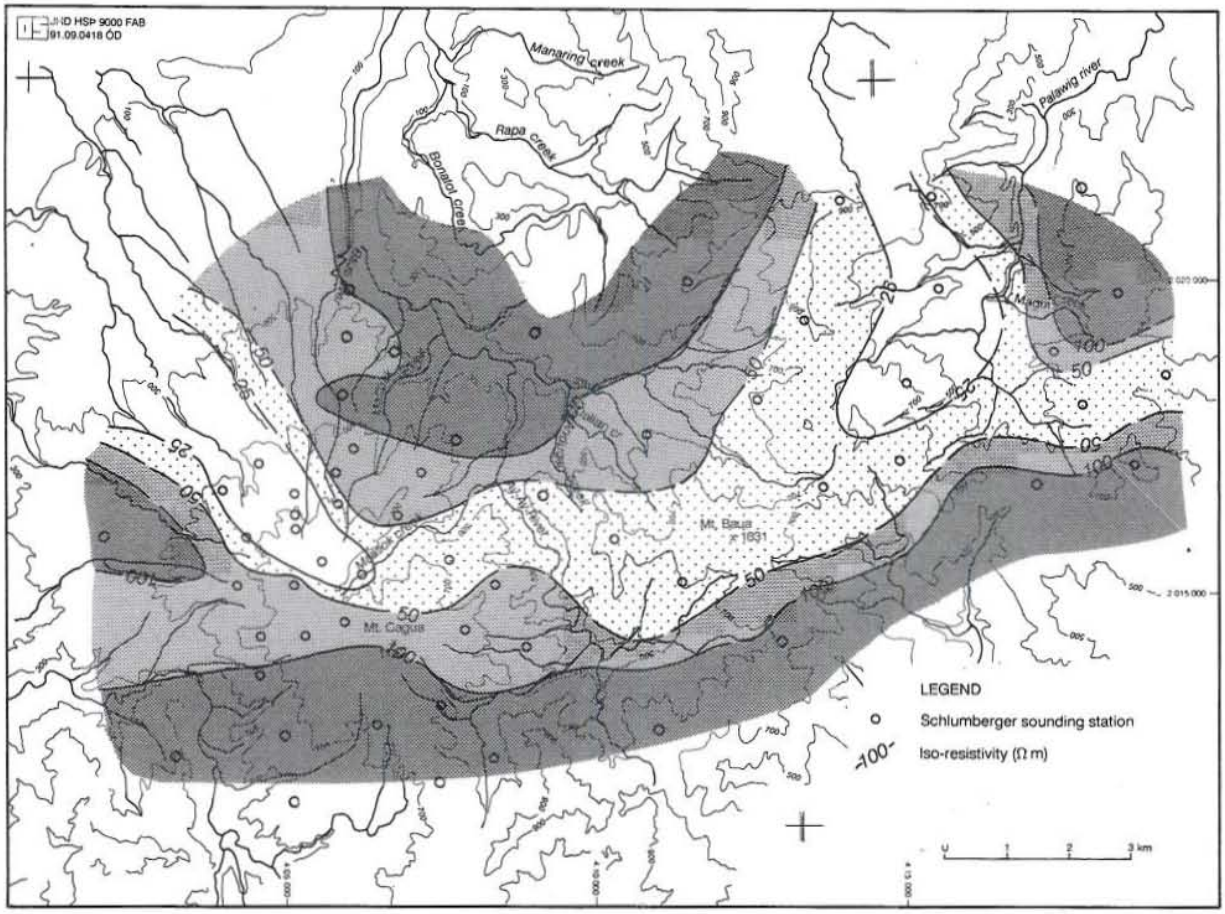

FIGURE 15: Isoresistivity map at 100 m a.s.l.

3.3.4 Two-dimensional modelling of cross-section A-A'

The two-dimensional interpretation of the Schlumberger soundings was done using the program FELIX described in Section 3.2.4. Results of the one-dimensional interpretation of ten Schlumberger sounding curves along cross-section A-A' were used as the basis for the starting model. The fitted curves are shown in Appendix B (Benito, 1991). The result of the 2-D modelling is shown in Figure 16.

It should be stated that the Schlumberger sounding survey conducted in Mt. Cagua was not designed for two-dimensional interpretation but cross-section A-A' was found the most logical and interesting choice for two-dimensional modelling due, primarily, to the orientation of the current arms of the sounding stations within it. However, the cross-section lies parallel to the inferred resistivity structure as can be seen from the isoresistivity maps and this is a weakness or a disadvantage in two-dimensional modelling. The soundings can be divided into three groups based on the orientations of the current arms as well as positions along the profile line. Soundings CGV-01, V-02 and CGV-11 go together as their current arms are oriented almost parallel and along the profile line. CGV-02, CGV-10, V-03 and V-23 have current arms oriented more than 10° from that of the profile line. CGV-07 on the other hand is dependent on V-23 while V-30 and V-31 are too far away from the probable heat source, according to the one-dimensional model, to have much influence on the interpretation of the low resistivity structure.

Surface layers were ignored and given the resistivity values measured beginning at 100 m depth. The interpretation started at V-23, one of the probable centers of the resistivity anomaly based on the one-dimensional model. This station was chosen instead of CGV-04 because the orientation of its current arm follows that of the other stations in the grouping. It is, however, located about 750 m away from the profile, so its location was critical and it had to be projected carefully into the cross-section. The last segment of the curve is steeply descending indicative of a sudden change from very high to very low resistivity value, reflecting its closeness to vertical boundaries in the northwest half of the collapse caldera. The sounding actually does not see much below 600 m as in the one-dimensional model, but the presence of the resistive body beneath the station was detected by its influence to sounding CGV-07.

The second layer at sounding V-03 (1100 Ωm) influenced the shape of the steeply descending segment of the sounding curve at V-23. The vertical boundary separating the high and low resistivity layers between the two stations was carefully located so as to get the best fit for the curves in both stations. The second layer is much thicker than the one-dimensional model. The conductive layer beneath this station has a resisitivity value of about 5 Ωm which is the same as that at V-23. The resistivity value shows that the geothermal activity extends to this station.

An example of the topographic effect is clearly demonstrated in stations CGV-10 and CGV-02. In the one-dimensional model, the conductive layer appears closest to the surface at CGV-10 and the resistive second layer is thicker at CGV-02. The two-dimensional interpretation showed just the opposite i.e., the second layer is thicker at CGV-10 and thinner at CGV-02.

The bottomlayer was not defined at CGV-10 and it is at the exact boundary of two contrasting resistivity bodies of 50 and 5 Ωm. The 50-Ωm block shown in the one-dimensional model at the bottom of CGV-11 extended beneath CGV-02 up to this boundary at CGV-10.

The resistivity curves of CGV-01 and V-02 are much influenced by the location of the second layers at these stations. A thin, vertical and conductive structure of 10 Ωm resistivity was detected southwest of CGV-01. The vertical structure caused the steeply descending portion of the curve at about 300 m depth.

A good correlation on the depth of the resistive bottom layer at CGV-07 was observed between the one- and two-dimensional models. The conductive layer was extended to the eastern half of the collapse caldera and beneath Mt. Cagua to get a better fit for this model.

A highly resistive body was interpreted from sounding V-30. The steeply descending last segment of the curve that gave a bottom resistivity value of ≤200 Ωm in the one-dimensional model at this station, is caused by lateral resistivity changes and reflects bodies of lower resistivity to the east.

The resistivity values at the uppermost layers at V-31 are different for both models but are in agreement on the bottomlayer.

3.3.5 Discussion of results

The results of one- and two-dimensional interpretation of the soundings reflect the permeability, hydrothermal alteration and the geological and structural features in the prospect area.

The 25 Ωm zone northwest of Cagua Volcano is in agreement with the results of the interpretations made by PNOC-EDC that the sharp decrease in resistivity with depth is attributed

to the presence of thermal springs and hydrothermal alterations associated with the geothermal system at Mt. Cagua. The shape of the anomaly is largely controlled by the northwest trending Magrafil Fault which provides a narrow conduit for fluid outflow from Mt. Cagua. Results of the one- and two-dimensional modelling show that in the center of this low resistivity area beneath the collapse caldera, there is a highly resistive body. Well CG-1D was drilled into this high resistivity structure and the presence of temperature in excess of 250°C shows that the high resistivity body is in the center of the geothermal system, and if experience in Iceland can be used as an example, then this could be an indication of intense high temperature mineralization of the epidote-chlorite type. On the other hand, this says little about the permeability which may be poor as shown by the result of well CG-1D. The conductive layer is confined to the upper levels and around the resistive body detected at CGV-07 and V-23. The temperature profile of CG-1D suggest that fluids flow at the contact of these low and high resistivity layers and possibly laterally and perpendicular to section A-A' and along the direction of section D-D'. As pointed out by Bayrante et al. (1989), the absence of magmatic gases rules out the possibility of a shallow magma body which could be attributed to this high resistivity body. Well CG-2D, on the other hand, was drilled into a medium resistivity layer according to the two-dimensional model. This correlates well with the recorded temperatures in the well.

The location of the other 25-Ωm zone and surface thermal manifestations at Magui Creek coincides with the contacts among the different rock formations along this creek (i.e. Palawis, Sikaw and Magui Volcanics and Palawig Formation) and is an indication of the high permeability of this location. The thermal manifestations are controlled mainly by the north-trending Palawig Fault (see Figure 7). Other noteworthy geological features are the series of domes and collapse calderas mapped in the vicinity of the thermal manifestations. These features follow the north-northeast trend of the major lineaments in the eastern part of the prospect area and could well provide increased permeability for the geothermal system. Therefore, the thermal manifestations at Magui Creek could be outflows from one of the domes or collapse structures mapped in the area.

The other possible heat source is Baua Volcano itself where low resistivity layers of ≤25 Ωm were detected at nearby BAV-12 and BAV-02. Although the two systems at Cagua and Baua areas are separate, they may be related as they are both inside the 50-Ωm isoline as in the case of Svartsengi and Eldvörp geothermal fields in Iceland (Georgsson, pers. comm.).

The anomaly is open to the east and follows the trend of the Magui Volcanics to this direction. It was necessary to leave the anomaly open-ended to the northeast as no resistivity data was available for use by the author to confirm the extent of the anomaly in this direction.

4. CENTRAL-LOOP TRANSIENT ELECTROMAGNETIC (TEM) METHOD

4.1 Introduction

As prevously mentioned, the Schlumberger sounding method of electrical surveying has been the most common method used in geothermal exploration. However, most of the high-temperature geothermal areas are located in volcanic zones where large parts of the surface can be covered with lava making current injection into the ground almost impossible, such that the use of direct current survey methods like the Schlumberger sounding is very difficult and time consuming (Arnason, 1989). In Iceland, the use of the central-loop transient electromagnetic method (TEM) is replacing the conventional Schlumberger sounding in geothermal exploration of areas of resistive surface conditions. Although the inversion of the sounding results, in terms of subsurface resistivity structure, is more complicated for the TEM-soundings than for Schlumberger soundings, experience in Iceland showed that the TEM method is, in many respects, superior to the conventional Schlumberger soundings (Arnason, 1990).

The TEM method is also best suited for locating conductive targets such as salt-water layers and has very good vertical resolution. It also provides a way of siting wells and monitoring salt-water interface migration in aquifers intruded by saltwater (Fitterman and Stewart, 1986).

The advantages of the TEM method over conventional sounding methods can be summarized as follows:

(a) The transmitter couples inductively to the earth and no current has to be injected to the ground, which is important in highly resistive surfaces.

(b) It is less dependent on local or surface inhomogeneities at the receiver site because the monitored signal at the surface is a decaying magnetic field rather than an electric field.

(c) It is less sensitive to lateral resistivity variations as the current induced in the ground diffuses downwards and outwards, resulting in increasing depth of penetration with time (Figure 17). The monitored signal at the surface is primarily dependent on the resistivity structure inside the diffuse current ring and thus, much more downward focused than the DC-soundings, where depth of penetration is obtained by increasing the distance between the current electrodes and the receiver dipole, making the monitored electric field dependent on a much larger volume of rocks.

(d) The monitored signal is stronger on lower subsurface resistivity, whereas in DC-soundings, the situation is the opposite and the monitored signal is drowned at a certain level by telluric noise.

The main disadvantages of TEM methods are relatively slow speed of operation mainly due to bulky equipment (but this can be overcome in the future with miniaturization of equipment) and the proneness of the receiving circuit to electrical noise since the circuit has to respond to a broad band of frequencies and cannot be tuned to a particular frequency in order to enhance the received signal, as can be done in continous-wave equipment (Parasnis, 1986).

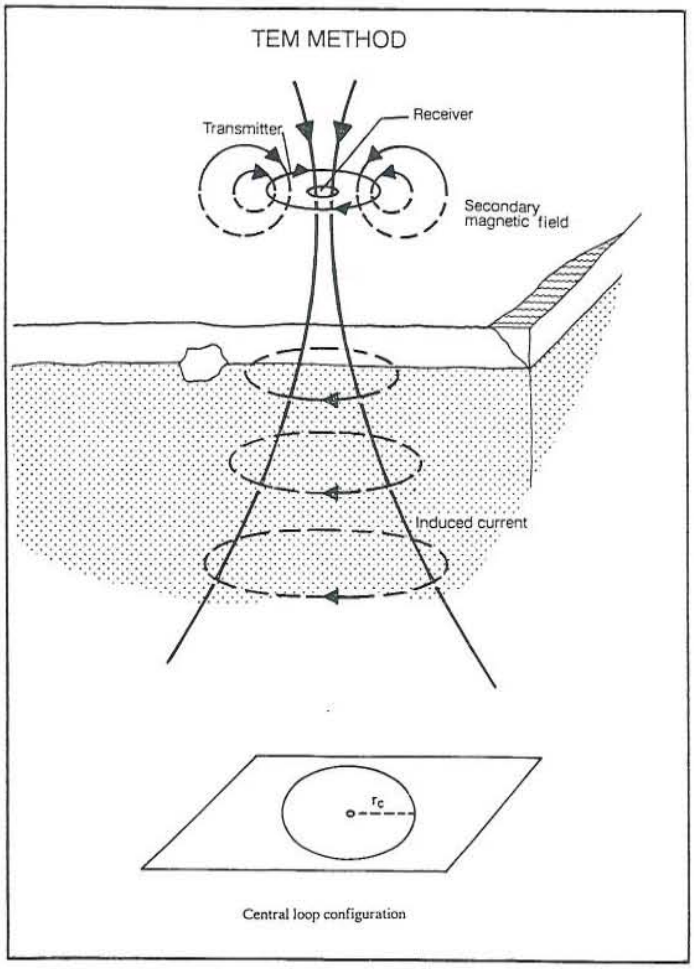

FIGURE 17: The central-loop transient electromagnetic (TEM) method

4.2 Basic principles

In the central-loop TEM sounding method the current in the ground is generated by a time varying magnetic field. It is different from the magnetotelluric method (MT) in that the magnetic field is not randomly varying but a field of a controlled magnitude generated by a source loop. A loop of wire is placed on the ground and a constant magnetic field of known strength is built up by transmitting a constant current into the loop. The current is then abruptly turned off. The decaying magnetic field induces electric current in the ground. The current distribution in the ground induces a secondary magnetic field decaying with time. The decay rate of the secondary magnetic field is monitored by measuring the voltage induced in a receiver coil (or a small loop) at the centre of the transmitter loop. The current distribution and the decay rate of the secondary magnetic field depend on the resisitivity structure of the earth. The decay rate, recorded as a function of time after the current in the transmitter loop is turned off, can, therefore, be interpreted in terms of the subsurface resisitivity structure. The depth of penetration in the central-loop TEM soundings is dependent on the geoelectrical section and how long the induction in the receiver can be traced in time before it is drowned in noise.

The physical basis of the TEM was discussed by Nabighian (1979), Fitterman and Stewart (1986) and Arnason (1989, 1990). The calculation of the sounding response for a known resistivity problem is more complicated for the TEM method than for DC methods. After the current I is turned off, the induced voltage in a receiver coil with an effective area A_r placed at the centre

of a circular transmitter loop of radius r is given, as a function of time t, by the cosine transform integral,

$$V(t,r) = \frac{2}{\pi}\int_0^\infty Re\left[\frac{V(\omega,r)}{-i\omega}\right]\cos(\omega,r)\ d\omega \tag{13}$$

In the case of a one-dimensional (1-D) resistivity structure of a horizontally layered earth, the frequency domain response $V(\omega,r)$ can be expressed by the Hankel transform integral,

$$V(\omega,r) = -IA_r i\omega\mu_0 r\int_0^\infty \frac{S_0}{S_0-T_0} J_1(\lambda r)\lambda\ d\lambda \tag{14}$$

The quantities S_0 and T_0 are determined recursively in terms of frequency and the resistivity and thickness of the successive layers. These integrals can be turned into convolution integrals and evaluated by the digital filter method by changing them to logarithmic variables (Arnason, 1989).

For a homogeneous half-space, the induced voltage in the receiver coil at the centre of the loop takes an asymptotic form,

$$V(r,t) = IA_r\frac{\mu_0 r^2}{20\pi^{1/2}}\frac{(\mu_0\sigma)^{3/2}}{t^{5/2}} \tag{15}$$

for large t. The sounding response is frequently expressed in terms of late time apparent resistivity which is defined by solving Equation 15 for the resistivity ($\rho = 1/\sigma$) of the half-space resulting in,

$$\rho_a(r,t) = \mu_0\left[\frac{IA_r\mu_0 r^2}{20\pi^{1/2}t^{5/2}V(r,t)}\right]^{2/3} \tag{16}$$

Expressed in this form, the response of a homogeneous half-space approaches the true resistivity for large t. For a layered half-space with thick layers, the late time apparent resistivity approximately displays the resistivity of successive layers as t increases. A numerical inversion of the data is needed to get any detailed information about the subsurface resistivity structure as it is difficult by visual inspection of the sounding curves.

4.3 Data acquisition and analysis

The central-loop TEM sounding field equipment used consists of a transmitter, receiver box, generator and receiver and transmitter loops. There are two receiver loops, a small coil with an effective area of 100 m^2 and a flexible loop with an effective area of 8112 m^2. Square transmitter loops of 200-300 m side length were used. The transmitter and receiver are synchronized through crystal clocks and the data are digitally recorded as voltage versus time in the receiver. The current turn-off time, which is the time it takes to turn the current off from its maximum value and to zero and is dependent on the size of the transmitter loop, was also recorded. The data was recorded over high and low frequency sweeps.

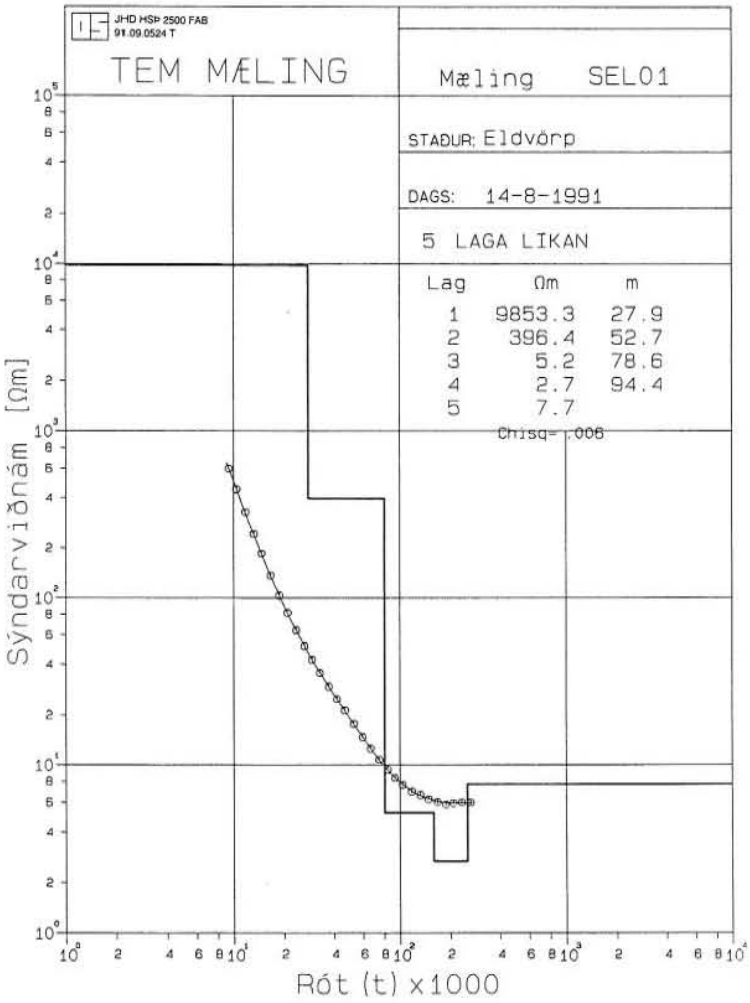

FIGURE 18: One-dimensional inversion of a TEM sounding using the program TINV

Preliminary data analysis includes stacking of the recorded voltages. The stacked data is then edited to remove any spurious measurements due to cultural noise and the result averaged to obtain induced voltage as a function of time. The induced voltage is then used to calculate apparent resistivity as a function of time by use of Equation 16.

4.4 The inversion program TINV

A non-linear least-squares inversion program TINV has been developed at the National Energy Authority of Iceland (Arnason, 1989) for the one-dimensional interpretation of TEM soundings. It uses a slightly modified Levenberg-Marquadt algorithm wherein the forward routine uses the digital filter method to evaluate the integrals in Equations 13 and 14. The aim is to determine the layered earth model whose response produces the measured value as closely as possible. TINV was developed on an IBM PC and written in standard FORTRAN 77 and can, in principle, be implemented on any machine supporting that language. Figure 18 shows an example of 1-D inversion of a TEM sounding using TINV. The data and the model curves are presented in Appendix C (Benito, 1991).

4.5 Central-loop TEM survey in Svartsengi-Eldvörp, SW-Iceland

4.5.1 Introduction

The Svartsengi and Eldvörp high-temperature geothermal fields are located on the outer part of of Reykjanes Peninsula, in southwest Iceland. The Reykjanes Peninsula is the landward extension of the Mid-Atlantic ridge and a part of the transition zone where the plate boundary is shifted toward the east. Hence, both rifting and transform faults are evident. The Peninsula is covered with postglacial basaltic lava flows with occasional hyaloclastite ridges, formed in subglacial eruptions (Georgsson, 1981 and 1984). The outer part of the Peninsula is saturated with seawater, and floating above the saline seawater is a lens of freshwater with an effective thickness of 40-60 m. The Svartsengi and Eldvörp, along with the Reykjanes, geothermal fields are within a continous low-resistivity zone and are associated with centers of recent magmatic activity and fracture zones in the Peninsula. The reservoir temperature of the fields is in the range of 240-290°C. The geothermal fluid is a brine approaching the salinity of seawater. The Svartsengi geothermal field has already been exploited for space heating and electrical generation for the past 15 years.

Monitoring of temperature and pressure in the Svartsengi geothermal reservoir have been systematically carried out since drilling started in 1971 and analysis of data collected are presented by Bjornsson and Steingrimsson (1991). The fluid production has caused more than 20 bars drawdown in the geothermal reservoir. It has also reduced pressure in the Eldvörp geothermal area by more than 10 bars. The pressure drawdown has also induced, among other things, an

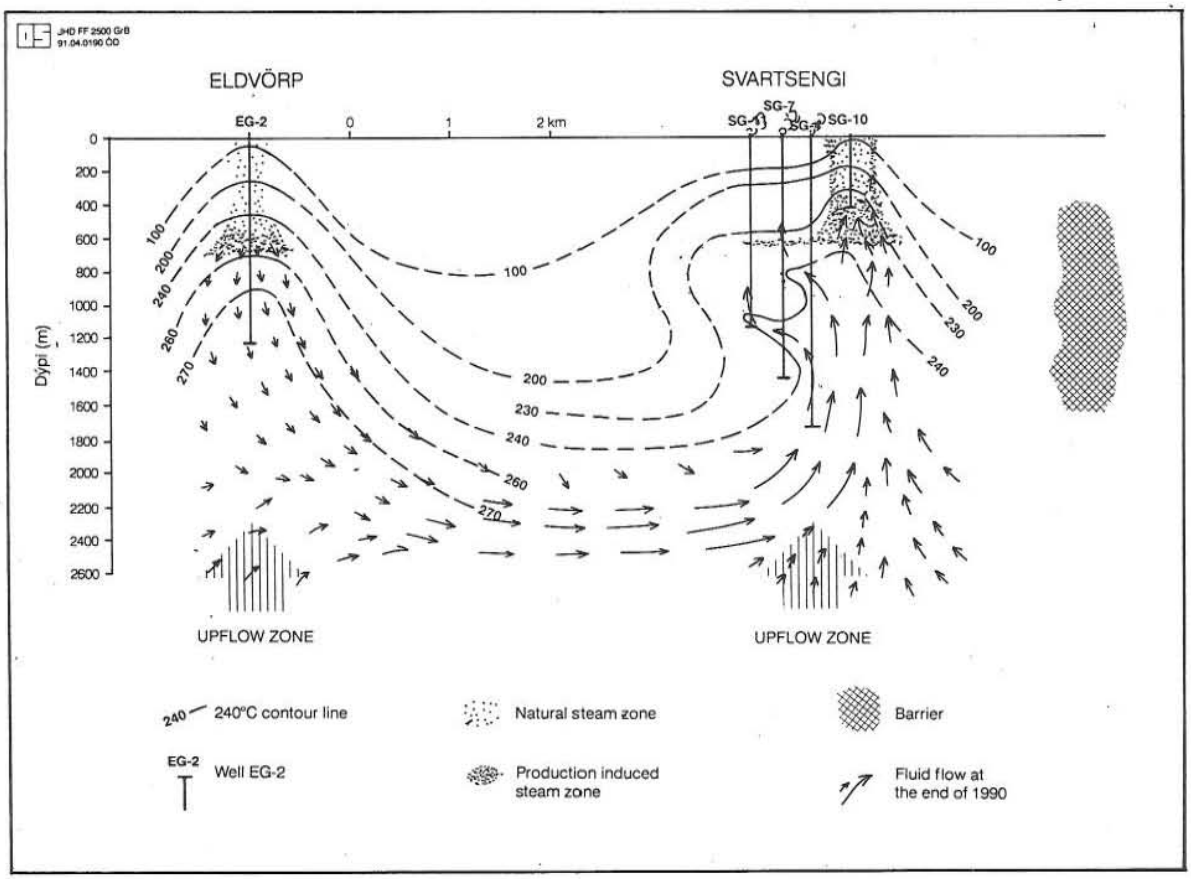

FIGURE 19: The conceptual model of the Svartsengi-Eldvörp geothermal area

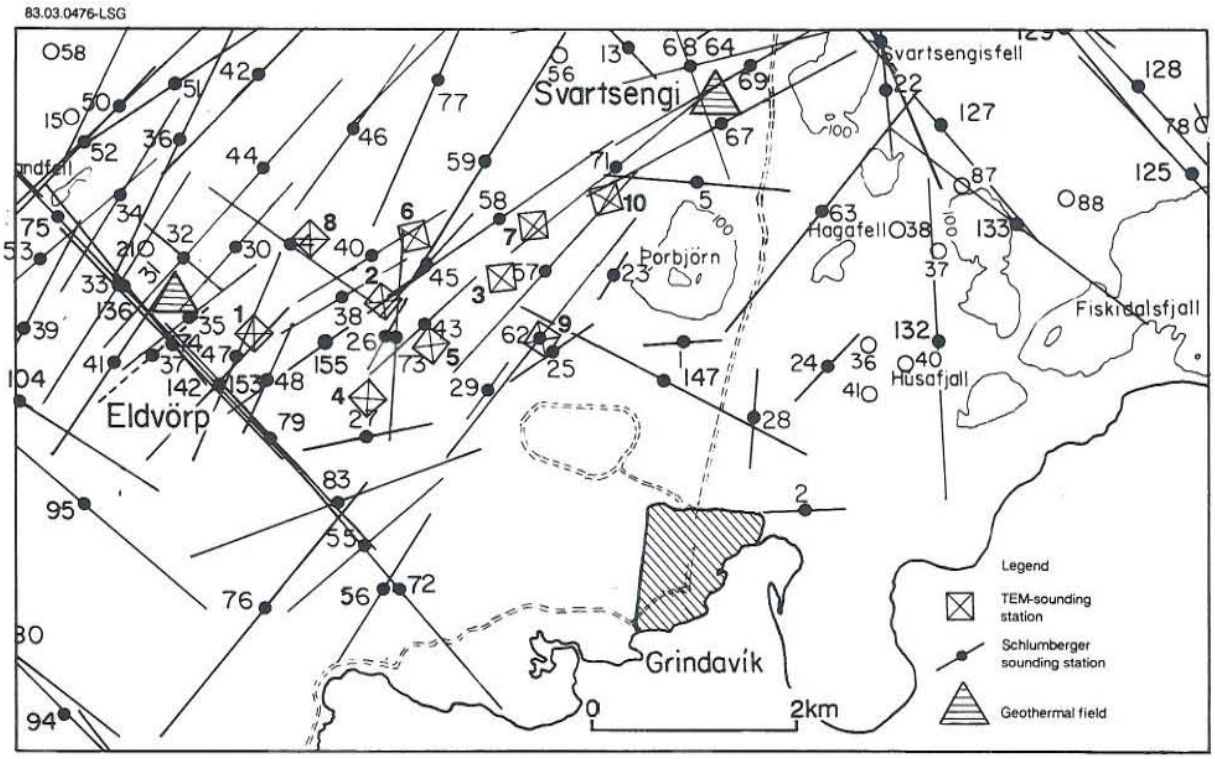

FIGURE 20: Location map of central-loop TEM soundings

inflow of colder geothermal fluids and calcite scaling in the wells. Based on the conceptual model of the Svartsengi-Eldvörp reservoir complex, geothermal fluids from Eldvörp are being drawn towards Svartsengi with the pressure connection of the two fields most likely along layers below 2000 m (Figure 19). Reservoir study showed that, to be able to offset excessive drawdown and maintain pressure in the Svartsengi reservoir, the reinjection of at least 50% of the produced fluids should be made. The reinjection well should be located between the two fields to prevent further cooling of the reservoir.

The central-loop TEM method is ideal for the purpose of locating the site for the reinjection well at Svartsengi because of the nature of the reservoir fluids i.e. brine approaching the salinity of sea water with a fresh water lens above it. Fitterman and Stewart (1986) and Arnason (1990) have shown applications of the TEM method in the detection of fresh water aquifers interfaced with salt or brackish water which are normally difficult to differentiate by DC methods. This is due to better vertical resolution of the TEM than DC methods.

Ten central-loop TEM soundings were measured between Svartsengi and Eldvörp for the purpose of locating the best site for the proposed reinjection well (Figure 20). The TEM stations are located inside the Schlumberger low-resistivity anomaly associated with the geothermal system in the Svartsengi-Eldvörp area.

4.5.2 Discussion of results

The TEM data was interpreted using the TINV program described in Section 4.4. Figure 21 shows a comparison of Schlumberger (station SE-62) and TEM (station SEL09) sounding data on the same location to test the vertical resolution of both methods. The resistive surface layer

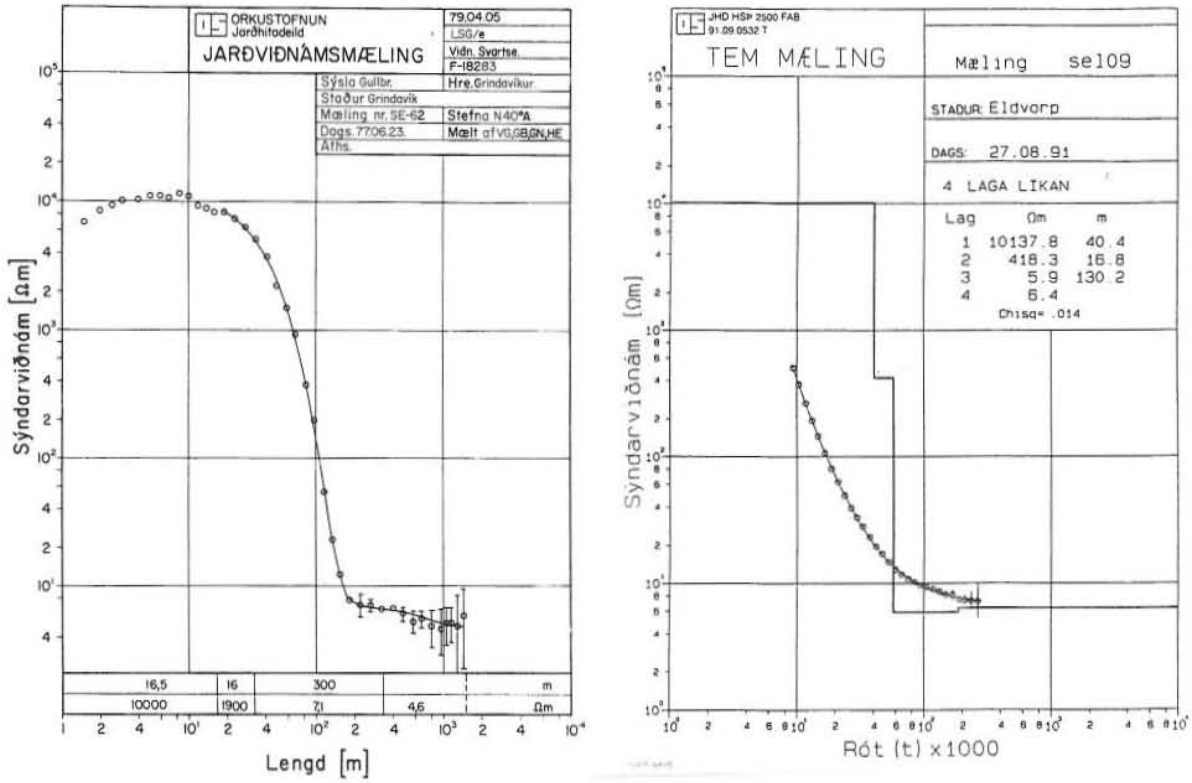

FIGURE 21: Comparison of TEM and Schlumberger sounding curves

was clearly defined by the Schlumberger method as it has measured the entire curve while the TEM has measured a limited portion of the curve. This is due to technical limitations of the TEM equipment; it cannot reliably sample transients in the early stage especially for a thick resistive first layer. Nevertheless, both methods gave similar resistivity values (≈10,000 Ωm) for the first layer, with the TEM value due more to the given starting model.

For the second layer, the resistivity values and thicknesses for both methods are far different, 1900 Ωm for SE-62 and 400 Ωm for SEL09. A similar trend is seen for all the stations within the anomaly towards Svartsengi: a drop in resistivity value for the second layer. A review of the resistivity values for the second layer in the Schlumberger soundings revealed that the TEM resistivity values are lower by about 80-90% than the Schlumberger values. A possible explanation for this may be the effects from the saline runoff water from Svartsengi. This layer corresponds to the fresh water lens, floating on the saline seawater. The flow direction of the runoff water from the Blue Lagoon, where the effluents are gathered, towards the sea is through the surveyed area. Since the Schlumberger data are more than ten years old, the effect of the runoff on the fresh water lens may now have been detected in the TEM soundings. However, it can also be stated that the resistivity values of this layer are poorly defined in the Schlumberger soundings due to equivalence. The thickness, on the other hand, is much better defined. For the succeeding layers, the data have relatively high uncertainty resulting in the ambiguity of interpretation, while in the TEM even the small change in the curve can be easily recognized even by visual inspection. This emphasizes the strength of the TEM method in conductive areas over the DC methods.

The result of the interpretation is shown in Figure 22 where the TEM data is superimposed on the Schlumberger resistivity map by Georgsson and Tulinius (1983) at depths of 200, 400 and 600 m b.s.l. The TEM data is presented in two ways: averaged resistivity values to reflect the contribution of each layer below the freshwater lens to the depth in question, and the actual resistivity values at that depth. The 6-Ωm isoline was selected for the TEM data as it represents best the resistivity trend when compared to the Schlumberger data. Except at 200 m depth b.s.l., the resistivity trend for both methods appear similar. However, reflected from the choice of the 6 Ωm line, resistivity values from TEM are slightly higher than from the Schlumberger.

The center of the TEM anomaly is located between stations SEL-02 and SEL-03 because they are both within the 6-Ωm anomaly zone in all the depths under consideration. It also appears that the anomaly is shifting from the southeast at deeper levels to the northwest at shallower levels (200 m b.s.l.). A narrow permeable zone trending in the northeast-southwest direction is inferred at the location of the shift, probably along the two mentioned TEM stations. This also correlates well with the Schlumberger data where the permeable zone can be inferred at the convergence of the 4-, 5- and 6-Ωm isoresistivity lines northeast of Eldvörp. The convergence of these isolines may also reflect the high permeability of this location which is ideal for the purpose of reinjection. The salinity of the reservoir fluids at Svartsengi approaches that of seawater and, in this case, ionic conduction dominates. Therefore, Archie's Law, which implies that there is an inverse correlation between resistivity and porosity and, consequently, the permeability of the rocks, holds true for the Svartsengi area. Thus, the low resistivity anomaly detected by TEM could be related to the high permeability of the area.

The recommended location for the reinjection well, therefore, is the area within the 6-Ωm isoline from the TEM anomaly near TEM station SEL03.

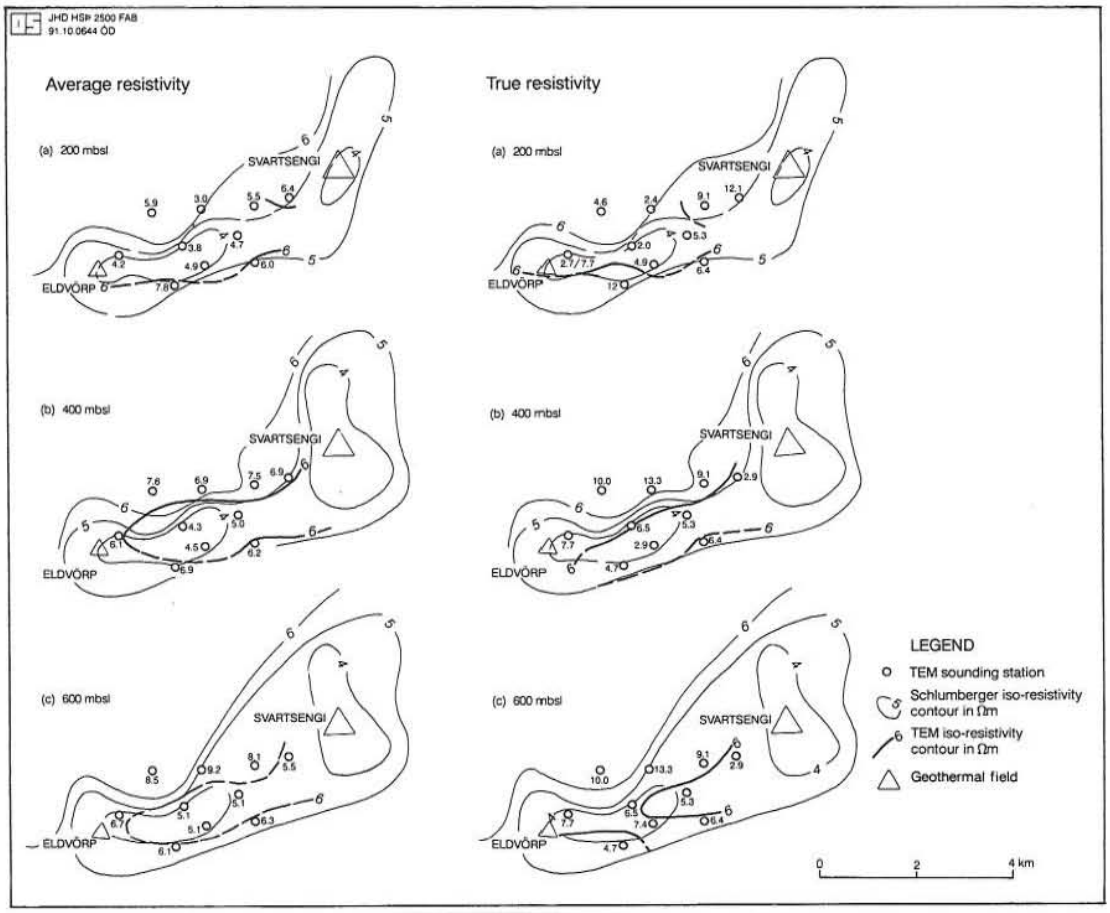

FIGURE 22: Combined TEM and Schlumberger isoresistivity maps at different depth levels

5. CONCLUSIONS AND RECOMMENDATIONS

5.1 Mt. Cagua geothermal prospect

As in any modelling process, equivalence is a common problem and one way of limiting it is the use of available geological or drillhole informations during the construction of the model. Since this information is lacking in the eastern part of the area, the problem of equivalence should not be overlooked.

The Schlumberger resistivity soundings were interpreted one- and two-dimensionally. It was shown how two-dimensional modelling provided more accurate and better interpretation and understanding of the resistivity structures in the prospect area. Parameters that can be related to the resistivity anomaly were discussed such as temperature, permeability, degree of hydrothermal alteration and structural as well as geological features in the area.

An elongated conductive structure has been delineated from the modelling and covers most parts of the prospect area. Two upflow zones are inferred, one is connected with the system at Cagua Volcano which has been identified in an earlier survey by PNOC-EDC and the other to the system at Baua Volcano.

One of the more significant findings in the present study is the good correlation of the resistivity structure from two-dimensional modelling with the result of the two wells drilled in the western part of the prospect. The geothermal system in this part of the area is confined to the western half of a collapse caldera. Conducting additional soundings in the vicinity of Baua Volcano (near BAV-12 and BAV-02) is recommended to test the extent of the conductive layers detected at these stations. Further detailed investigation of the eastern part seems justified.

5.2 Svartsengi-Eldvörp geothermal field

The TEM soundings in Svartsengi-Eldvörp area have shown the applicability of the central-loop TEM in resistive surfaces where current injection is almost impossible but low resistivity is found at depth. The soundings have confirmed the better vertical resolution of the TEM than the Schlumberger, especially in the more conductive part of the subsurface. Where the Schlumberger soundings detected uniform low resistivity layers at a station, the TEM has identified different layerings.

The site near station SEL03 is recommended for the planned reinjection well based on the result of the TEM sounding interpretation. Although the planned reinjection well could be sited anywhere within the resistivity anomaly delineated by the Schlumberger soundings with probable success, the results of the TEM soundings have clearly defined the area where the well could be best sited within the Schlumberger resistivity anomaly. Good permeability is also inferred in this area. Additional stations are also recommended around the surveyed area to delineate the lateral extent of the TEM anomaly.

5.3 Applicability of the methods in the Philippines

The importance of two-dimensional modelling was appreciated during the study, especially in the selection of drillsites. Comparison of results showed that the two-dimensional model approached that of the result from the drilled wells. The two-dimensional modelling process improved the

resolution of the results from the one-dimensional model. The high cost and low probability of success of drilling a well should encourage geothermal planners to use two-dimensional modelling as a standard exploration method. Future Schlumberger sounding surveys should, therefore, be designed to include two-dimensional modelling.

The TEM method, on the other hand, should also apply well in the Philippines where field conditions are similar with what the method is designed for i.e. resistive surfaces and mountainous terrains. The interpretation is much easier than the Schlumberger method presently used in the country.

ACKNOWLEDGEMENTS

I am grateful to the staff of UNU and Orkustofnun, most especially to Dr. Ingvar B. Fridleifsson, for the award of the Fellowship to the 1991 Geothermal Training Programme. I am also indebted to the following persons:

To my adviser, Mr. Ludvik Georgsson, for sharing his expertise and experience on the different geophysical methods as well as for supervising this work, for the fertile discussions during the writing of this report, and for his untiring support during our stay in Iceland.

To Dr. Knutur Arnason, who personally and patiently guided me through the geophysics lectures, and for his critical review of the manuscript. To Dr. Hjalmar Eysteinsson, for introducing me to the magnetotelluric method and his valuable time during the fieldworks.

To the Philippine National Oil Company-Energy Development Corporation (PNOC-EDC), through its Exploration Manager, Mr. Hermes P. Ferrer, for allowing me to use the geoscientific data from Mt. Cagua. To the staff of the Geothermal Division, Office of Energy Affairs, for their support.

To my wife and children who have to bear my long absence from home.

And most of all, I give back all the glory to God and to our Lord Jesus Christ, for He accomplished the work He has set for me to do.

REFERENCES

Arnason, K., 1984: The effect of finite electrode separation on Schlumberger soundings. 54th Annual International SEG Meeting, Society of Exploration Geophysicists, Atlanta, Ga. Extended Abstracts, 129-132.

Arnason, K., 1989: Central-loop transient electromagnetic soundings over a horizontally layered earth. Orkustofnun report OS-89032/JHD-06, Iceland, 128 pp.

Arnason, K. 1990: Central-loop transient electromagnetic soundings in geothermal and groundwater exploration, a step forward. Geothermal Resources Council Transactions, Vol. 14, Part II, 845-851.

Arnason, K., and Hersir, G.P., 1990: Surface geophysical exploration of the Nesjavellir geothermal field, SW Iceland. Orkustofnun draft report, Iceland, 23 pp.

Barnett, P.R., Española, O.S., and Ferrer, H.P., 1984: A review of Philippine geothermal exploration strategy. Proceedings of the 6th New Zealand Geothermal Workshop, University of Auckland Geothermal Institute, 55-59.

Bayrante, L.F., Ruiz, C.C., Layugan, D.B., Apuada, N.A., and Clemente, V.C., 1989: Geoscientific exploration and evaluation of Mt. Cagua geothermal prospect, northeastern Luzon. PNOC-Energy Development Corporation (unpublished internal report), Philippines, 107 pp.

Benito, F.A., 1991: Appendices to the report:Interpretation of Schlumberger soundings from Mt. Cagua, Philippines and TEM soundings from Svartsengi-Eldvorp, SW-Iceland. UNU G.T.P., Iceland, report 4 appendices, 30 pp.

Bjornsson, G., and Steingrimsson, B., 1991: Temperature and pressure in the Svartsengi geothermal reservoir, initial status and changes due to production. Orkustofnun, report OS-91016/JHD-04 (in Icelandic with English summary), Iceland, 56 pp.

Dahknov, V. N., 1962: Geophysical well logging. Quart. Colorado Sch. Mines, Vol. 57, No. 2, 445 pp.

Fitterman, D.V., and Stewart, M.T., 1986: Transient electromagnetic soundings for groundwater. Geophysics, Vol. 44, No. 10, 1700-1705.

Fox, R.C., Hohmann, G.W., and Rijo, L., 1978: Topographic effects in resistivity surveys. Earth Science Laboratory, Salt Lake City, Utah, 99 pp.

Georgsson, L.S., 1981: A resistivity survey on the plate boundaries in the western Reykjanes Peninsula, Iceland. Geothermal Resources Council Transactions, Vol. 5, 75-78.

Georgsson, L.S., 1984: Resistivity and temperature distribution of the outer Reykjanes Peninsula, Southwest Iceland. 54th Annual international SEG Meeting, Atlanta, Ga., Extended Abstracts, 81-84.

Georgsson, L.S., and Tulinius, H., 1983: Resistivity sounding of the outer Reykjanes Peninsula 1981 and 1982. Orkustofnun, report OS-83049/JHD-09 (in Icelandic), Iceland, 70 pp.

Hersir, G.P., and Bjornsson, A., 1991: Geophysical exploration for geothermal resources, principles and applications. UNU G.T.P., Iceland, report 15, 94 pp.

Hochstein, M.P., 1982: Introduction to Geothermal Prospecting. University of Auckland Geothermal Institute Lectures, 155 pp.

Johansen, H.K., 1977: A man/computer interpretation system for resistivity soundings over a horizontally stratified earth. Geophysical Prospecting, Vol. 25, 667-691.

Koefoed, O., 1979: Geosounding principles, 1: Resistivity sounding measurements. Elsevier Scientific Publishing Co., Amsterdam, 276 pp.

Nabighian, M.N., 1979: Quasi-static transient response of a conducting half-space - an approximate representation. Geophysics, Vol. 44, No. 10, 1700-1705.

Orellana, E., and Mooney, H.M., 1966: Master tables and curves for vertical electrical sounding over layered structures. Intersciencia, Madrid, 193 pp.

Parasnis, D.S., 1986: Principles of Applied Geophysics, Fourth Edition. Chapman and Hall, London, 402 pp.

Ward, S.H., and Sill, W.R., 1983: Resistivity, induced polarization and self-potential methods in geothermal exploration. UNU Geothermal Training Programme, Iceland, Report 6, 78 pp.

Report 4 appendices, 1991

APPENDICES TO THE REPORT: INTERPRETATION OF SCHLUMBERGER SOUNDINGS FROM MT. CAGUA, PHILIPPINES AND TEM SOUNDINGS FROM SVARTSENGI-ELDVORP, SW-ICELAND

Francisco A. Benito,
UNU Geothermal Training Programme,
Orkustofnun - National Energy Authority,
Grensásvegur 9,
108 Reykjavik,
ICELAND

Permanent Address:
Office of Energy Affairs,
Energy Development Services,
Geothermal Division,
Merritt Road, Fort Bonifacio,
Makati, Metro Manila 1201,
PHILIPPINES

The following are the appendices to the report entitled, **"Interpretation of Schlumberger Soundings from Mt. Cagua, Philippines and TEM soundings from Svartsengi-Eldvörp, SW-Iceland"**. It was written by Francisco A. Benito at the UNU Geothermal Training Programme in 1991. It is divided into three parts. The first part shows the result of one dimensional interpretation (models, mean deviations and fits between measured and modelled data) using the ELLIPSE program. The second part shows how well the calculated apparent resistivity curves from the two dimensional model of cross-section A-A' (see Figure 16 in the main report) fit with the measured curves using the FELIX program. The third part is the result of one dimensional interpretation of central-loop transient electromagnetic (TEM) soundings using the TINV program.

TABLE OF CONTENTS

APPENDIX A

One dimensional interpretation of Schlumberger soundings using the ELLIPSE program:

Models, corresponding calculated apparent resistivity curves (shown as continous curves) and measured apparent resistivity curves (shown as points).

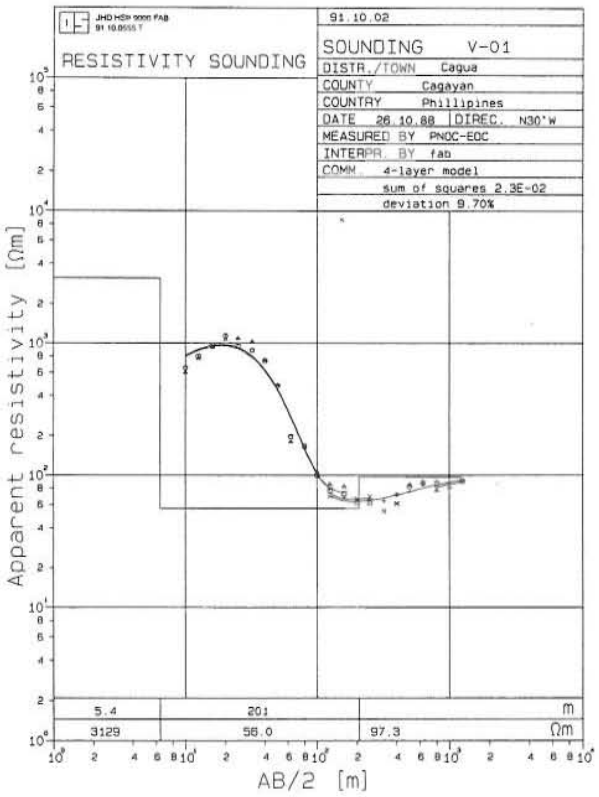
JHD HSP 9000 FAB
91.10.0555 T
91.10.02
RESISTIVITY SOUNDING
SOUNDING V-01
DISTR./TOWN Cagua
COUNTY Cagayan
COUNTRY Phillipines
DATE 26.10.88 | DIREC. N30°W
MEASURED BY PNOC-EDC
INTERPR. BY fab
COMM 4-layer model
sum of squares 2.3E-02
deviation 9.70%
Apparent resistivity [Ωm]
5.4 201 m
3129 56.0 97.3 Ωm
AB/2 [m]

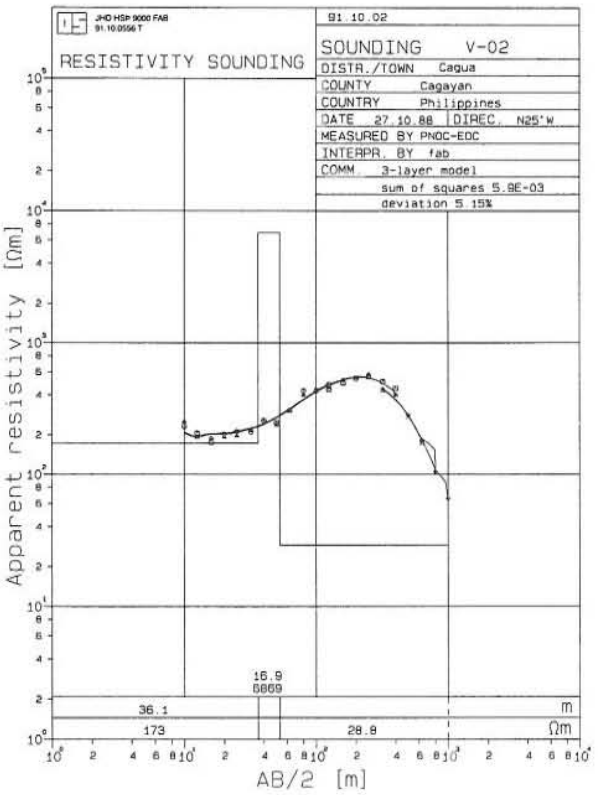
JHD HSP 9000 FAB
91.10.0556 T
91.10.02
RESISTIVITY SOUNDING
SOUNDING V-02
DISTR./TOWN Cagua
COUNTY Cagayan
COUNTRY Philippines
DATE 27.10.88 | DIREC. N25°W
MEASURED BY PNOC-EDC
INTERPR. BY fab
COMM 3-layer model
sum of squares 5.9E-03
deviation 5.15%
Apparent resistivity [Ωm]
16.9
6869
36.1 m
173 28.8 Ωm
AB/2 [m]

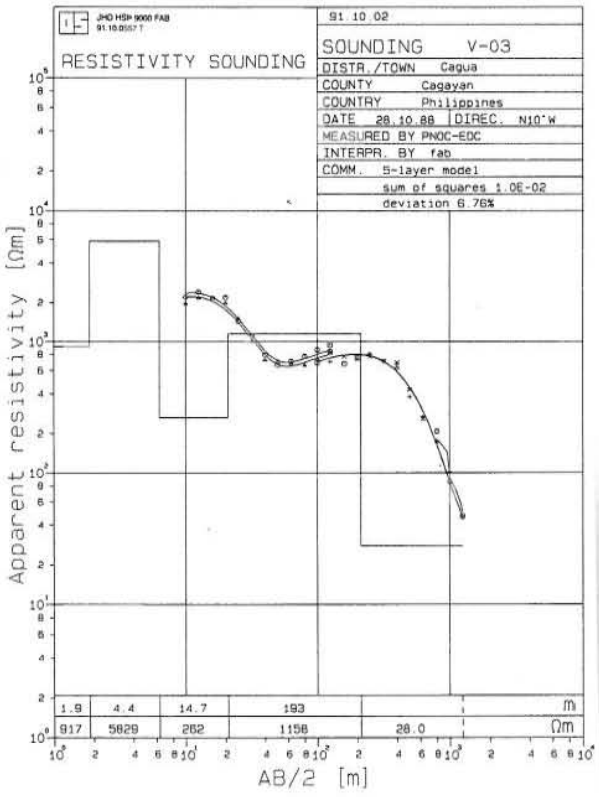
JHD HSP 9000 FAB
91.10.0557 T
91.10.02
RESISTIVITY SOUNDING
SOUNDING V-03
DISTR./TOWN Cagua
COUNTY Cagayan
COUNTRY Philippines
DATE 28.10.88 | DIREC. N10°W
MEASURED BY PNOC-EDC
INTERPR. BY fab
COMM. 5-layer model
sum of squares 1.0E-02
deviation 6.76%
Apparent resistivity [Ωm]
1.9 4.4 14.7 193 m
917 5829 262 1158 28.0 Ωm
AB/2 [m]

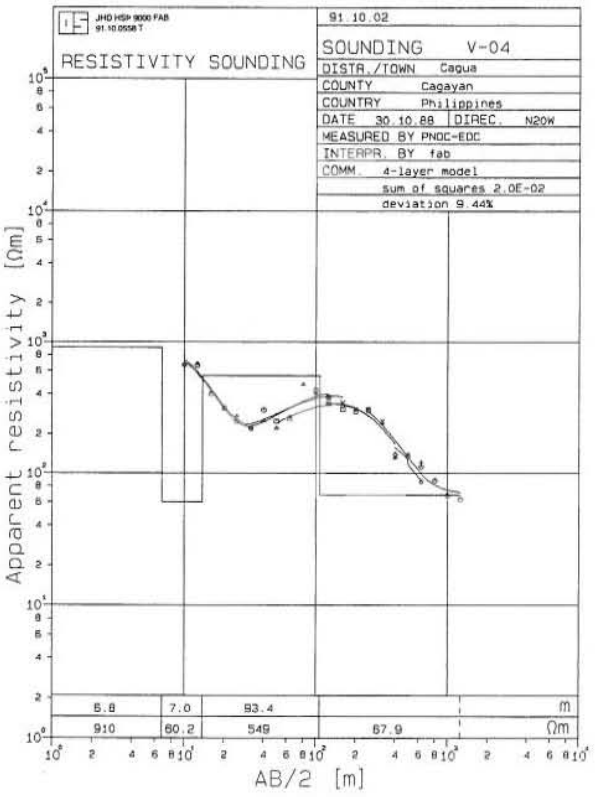
JHD HSP 9000 FAB
91.10.0558 T
91.10.02
RESISTIVITY SOUNDING
SOUNDING V-04
DISTR./TOWN Cagua
COUNTY Cagayan
COUNTRY Philippines
DATE 30.10.88 | DIREC. N20W
MEASURED BY PNOC-EDC
INTERPR. BY fab
COMM. 4-layer model
sum of squares 2.0E-02
deviation 9.44%
Apparent resistivity [Ωm]
5.8 7.0 93.4 m
910 80.2 549 67.9 Ωm
AB/2 [m]

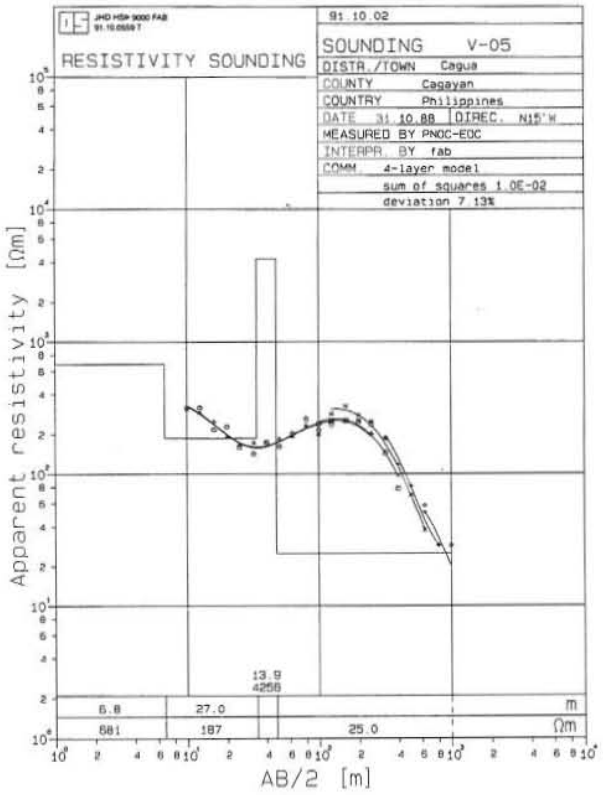
91.10.02
RESISTIVITY SOUNDING
SOUNDING V-05
DISTR./TOWN Cagua
COUNTY Cagayan
COUNTRY Philippines
DATE 31.10.88 DIREC. N15°W
MEASURED BY PNOC-EDC
INTERPR. BY fab
COMM. 4-layer model
sum of squares 1.0E-02
deviation 7.13%
Apparent resistivity [Ωm]
AB/2 [m]
m
Ωm
6.8
27.0
13.9
4256
25.0
681
187

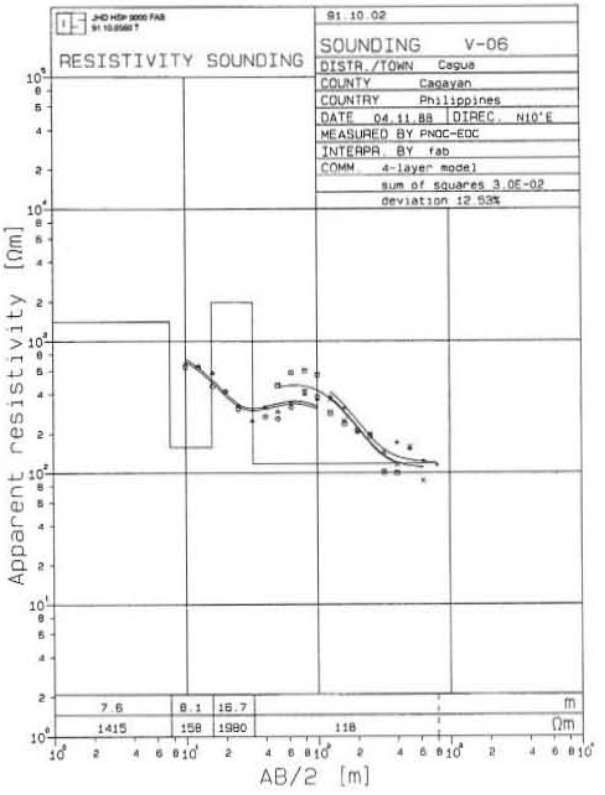
91.10.02
RESISTIVITY SOUNDING
SOUNDING V-06
DISTR./TOWN Cagua
COUNTY Cagayan
COUNTRY Philippines
DATE 04.11.88 DIREC. N10°E
MEASURED BY PNOC-EDC
INTERPR. BY fab
COMM. 4-layer model
sum of squares 3.0E-02
deviation 12.53%
Apparent resistivity [Ωm]
AB/2 [m]
m
Ωm
7.6
8.1
16.7
1415
158
1980
118

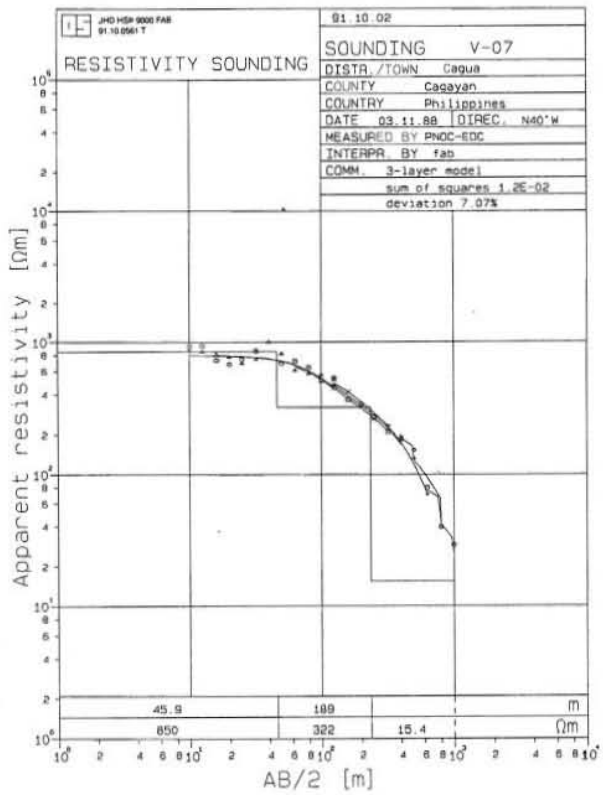
91.10.02
RESISTIVITY SOUNDING
SOUNDING V-07
DISTR./TOWN Cagua
COUNTY Cagayan
COUNTRY Philippines
DATE 03.11.88 DIREC. N40°W
MEASURED BY PNOC-EDC
INTERPR. BY fab
COMM. 3-layer model
sum of squares 1.2E-02
deviation 7.07%
Apparent resistivity [Ωm]
AB/2 [m]
m
Ωm
45.9
189
850
322
15.4

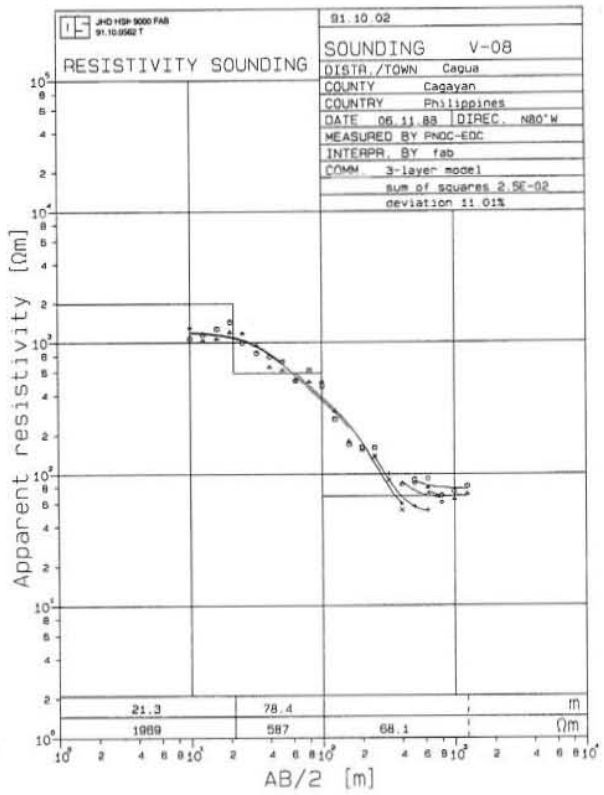
91.10.02
RESISTIVITY SOUNDING
SOUNDING V-08
DISTR./TOWN Cagua
COUNTY Cagayan
COUNTRY Philippines
DATE 06.11.88 DIREC. N80°W
MEASURED BY PNOC-EDC
INTERPR. BY fab
COMM. 3-layer model
sum of squares 2.5E-02
deviation 11.01%
Apparent resistivity [Ωm]
AB/2 [m]
m
Ωm
21.3
78.4
1989
587
68.1

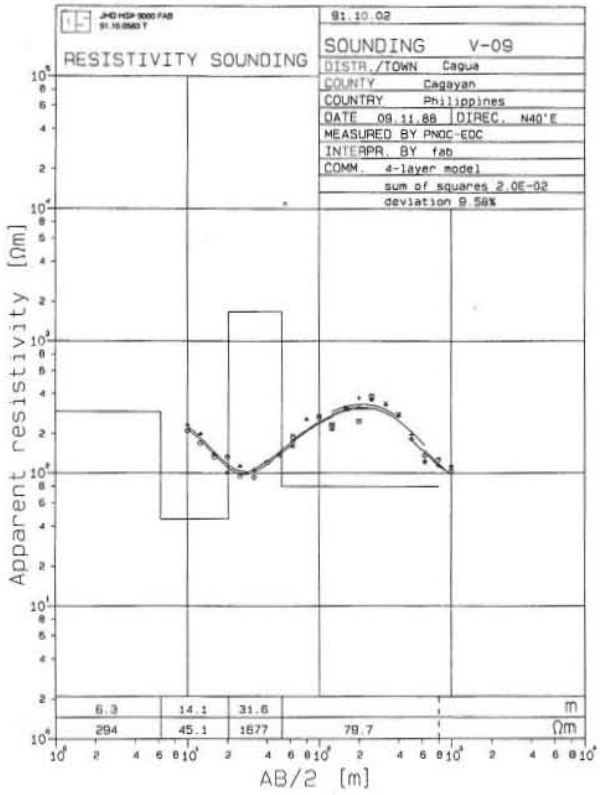
91.10.02
RESISTIVITY SOUNDING
SOUNDING V-09
DISTR./TOWN Cagua
COUNTY Cagayan
COUNTRY Philippines
DATE 09.11.88 | DIREC. N40°E
MEASURED BY PNOC-EDC
INTERPR. BY fab
COMM. 4-layer model
sum of squares 2.0E-02
deviation 9.58%
Apparent resistivity [Ωm]
AB/2 [m]
6.3 14.1 31.6 m
294 45.1 1677 79.7 Ωm

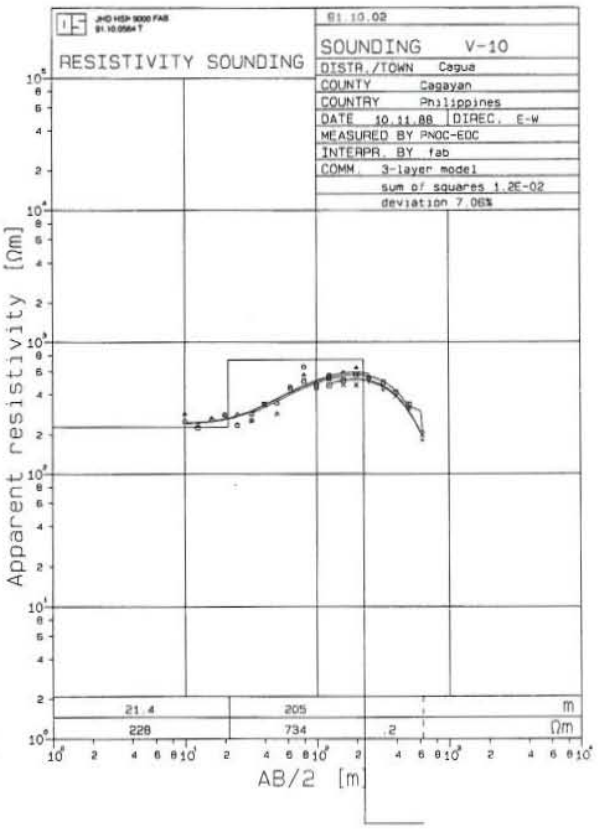
91.10.02
RESISTIVITY SOUNDING
SOUNDING V-10
DISTR./TOWN Cagua
COUNTY Cagayan
COUNTRY Philippines
DATE 10.11.88 | DIREC. E-W
MEASURED BY PNOC-EDC
INTERPR. BY fab
COMM. 3-layer model
sum of squares 1.2E-02
deviation 7.06%
Apparent resistivity [Ωm]
AB/2 [m]
21.4 205 m
228 734 .2 Ωm

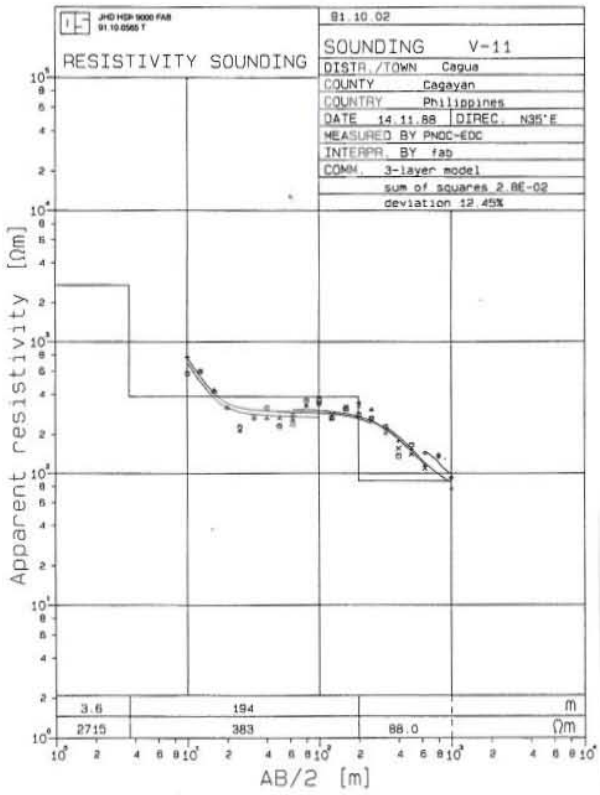
91.10.02
RESISTIVITY SOUNDING
SOUNDING V-11
DISTR./TOWN Cagua
COUNTY Cagayan
COUNTRY Philippines
DATE 14.11.88 | DIREC. N35°E
MEASURED BY PNOC-EDC
INTERPR. BY fab
COMM. 3-layer model
sum of squares 2.8E-02
deviation 12.45%
Apparent resistivity [Ωm]
AB/2 [m]
3.6 194 m
2715 383 88.0 Ωm

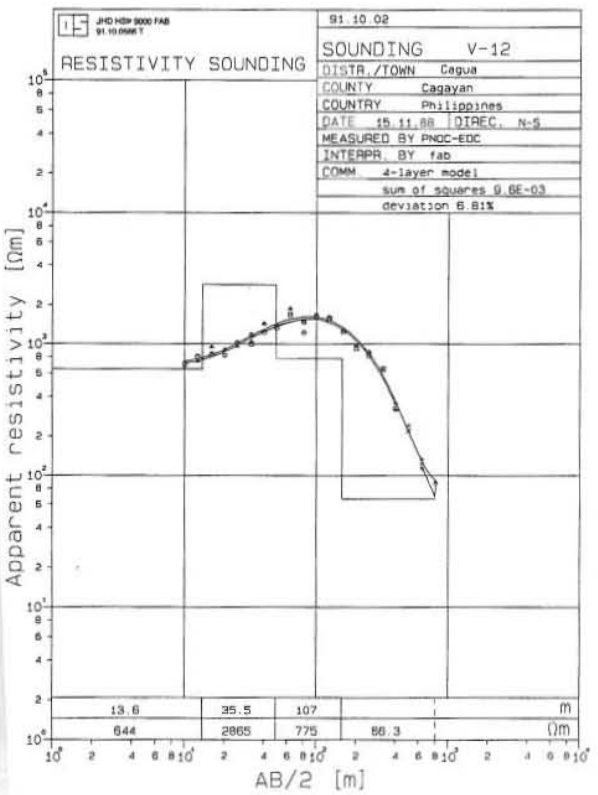
91.10.02
RESISTIVITY SOUNDING
SOUNDING V-12
DISTR./TOWN Cagua
COUNTY Cagayan
COUNTRY Philippines
DATE 15.11.88 | DIREC. N-S
MEASURED BY PNOC-EDC
INTERPR. BY fab
COMM. 4-layer model
sum of squares 9.6E-03
deviation 6.81%
Apparent resistivity [Ωm]
AB/2 [m]
13.6 35.5 107 m
644 2865 775 86.3 Ωm

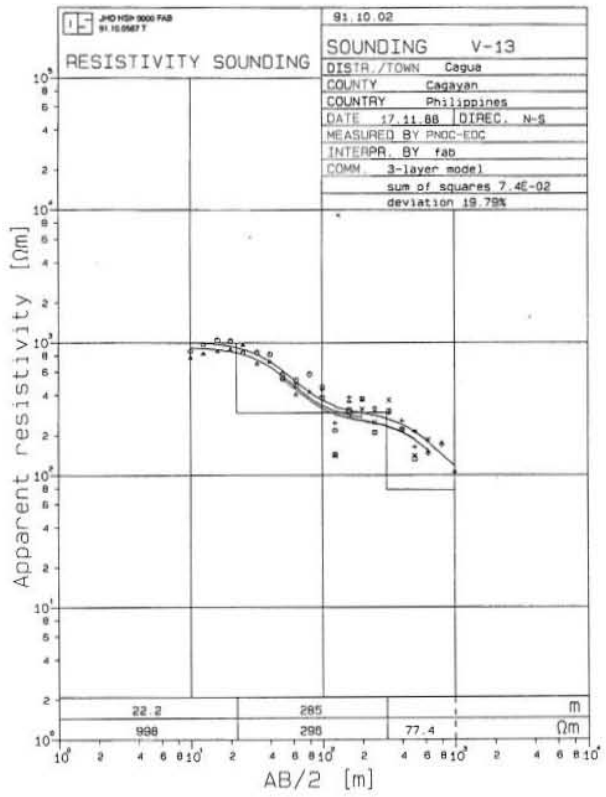
91.10.02
RESISTIVITY SOUNDING
SOUNDING V-13
DISTR./TOWN Cagua
COUNTY Cagayan
COUNTRY Philippines
DATE 17.11.88 DIREC. N-S
MEASURED BY PNOC-EDC
INTERPR. BY fab
COMM. 3-layer model
sum of squares 7.4E-02
deviation 19.79%
Apparent resistivity [Ωm]
AB/2 [m]
22.2
285
m
998
298
77.4
Ωm

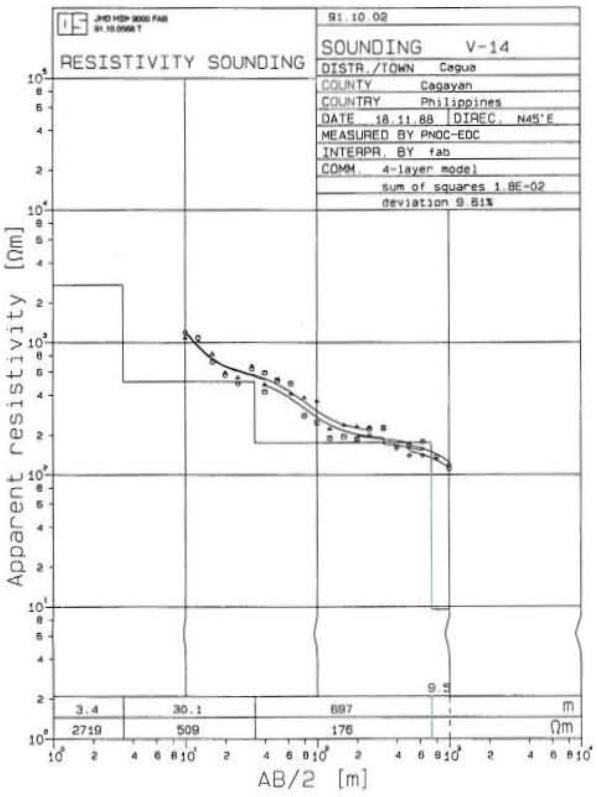
91.10.02
RESISTIVITY SOUNDING
SOUNDING V-14
DISTR./TOWN Cagua
COUNTY Cagayan
COUNTRY Philippines
DATE 18.11.88 DIREC. N45°E
MEASURED BY PNOC-EDC
INTERPR. BY fab
COMM. 4-layer model
sum of squares 1.8E-02
deviation 9.81%
Apparent resistivity [Ωm]
AB/2 [m]
3.4
30.1
697
m
2719
509
176
Ωm

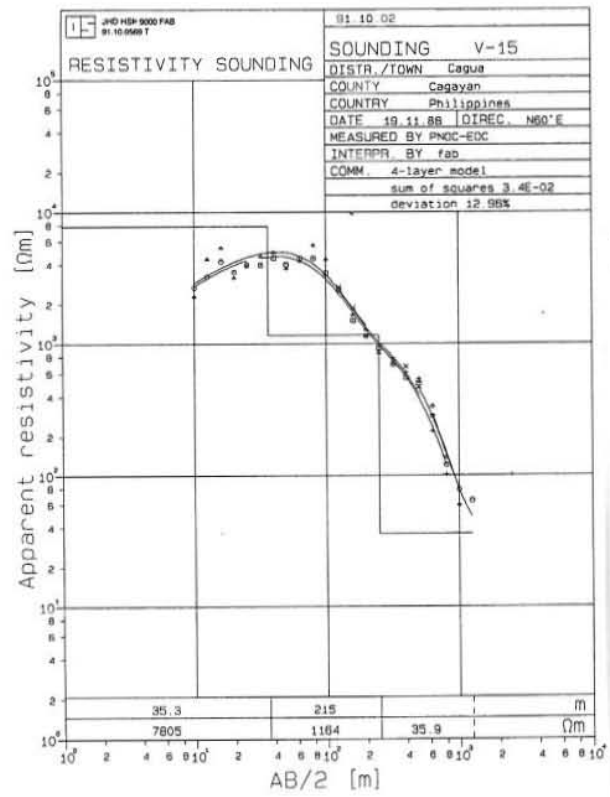
91.10.02
RESISTIVITY SOUNDING
SOUNDING V-15
DISTR./TOWN Cagua
COUNTY Cagayan
COUNTRY Philippines
DATE 19.11.88 DIREC. N60°E
MEASURED BY PNOC-EDC
INTERPR. BY fab
COMM. 4-layer model
sum of squares 3.4E-02
deviation 12.96%
Apparent resistivity [Ωm]
AB/2 [m]
35.3
215
m
7805
1164
35.9
Ωm

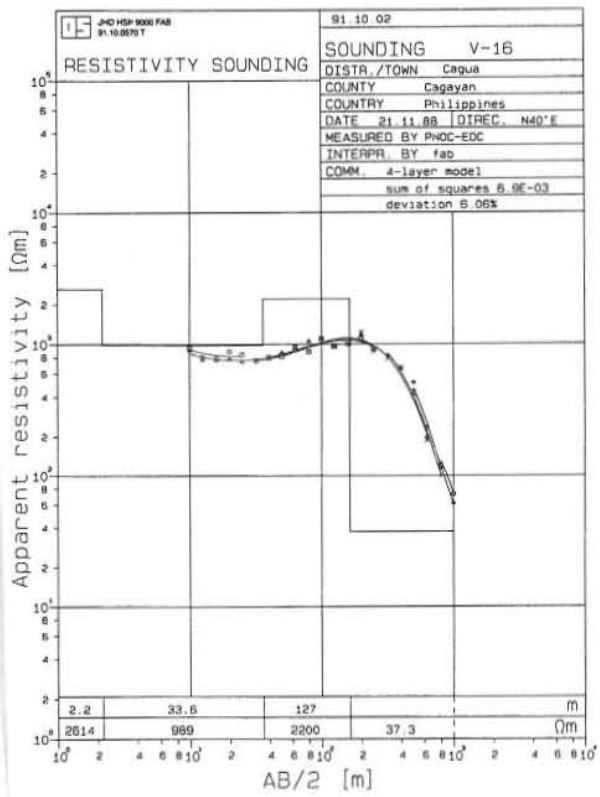
91.10.02
RESISTIVITY SOUNDING
SOUNDING V-16
DISTR./TOWN Cagua
COUNTY Cagayan
COUNTRY Philippines
DATE 21.11.88 DIREC. N40°E
MEASURED BY PNOC-EDC
INTERPR. BY fab
COMM. 4-layer model
sum of squares 6.9E-03
deviation 6.06%
Apparent resistivity [Ωm]
AB/2 [m]
2.2
33.6
127
m
2614
989
2200
37.3
Ωm

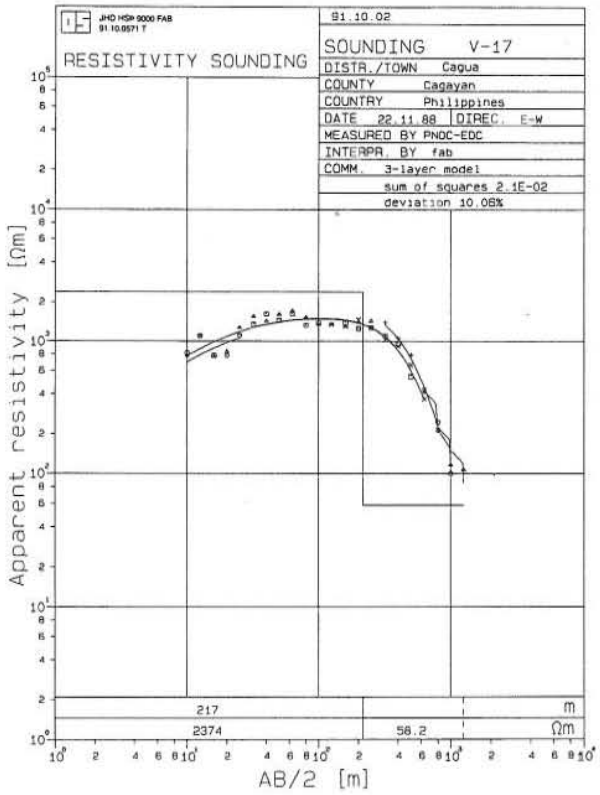
JHD HSP 9000 FAB
91.10.0571 T
91.10.02
RESISTIVITY SOUNDING
SOUNDING V-17
DISTR./TOWN Cagua
COUNTY Cagayan
COUNTRY Philippines
DATE 22.11.88 DIREC. E-W
MEASURED BY PNOC-EDC
INTERPR. BY fab
COMM. 3-layer model
sum of squares 2.1E-02
deviation 10.06%
Apparent resistivity [Ωm]
217
2374
56.2
m
Ωm
AB/2 [m]

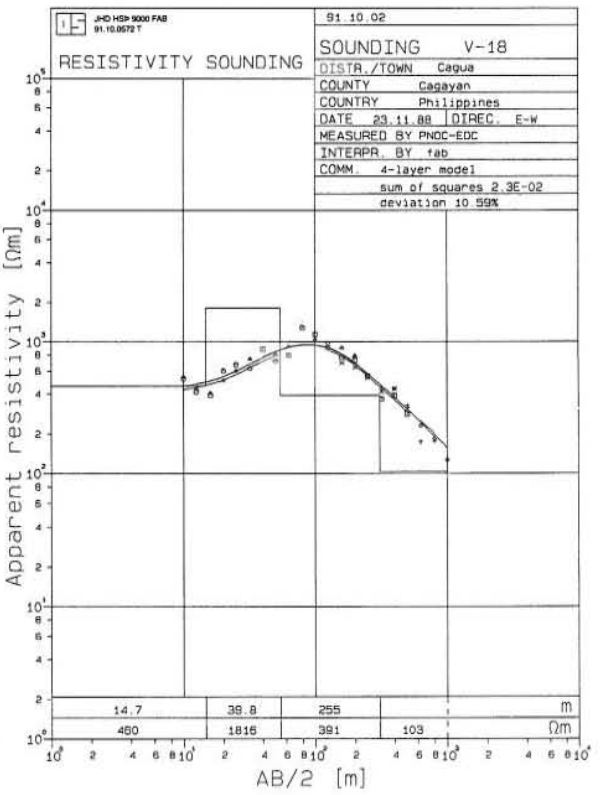
JHD HSP 9000 FAB
91.10.0572 T
91.10.02
RESISTIVITY SOUNDING
SOUNDING V-18
DISTR./TOWN Cagua
COUNTY Cagayan
COUNTRY Philippines
DATE 23.11.88 DIREC. E-W
MEASURED BY PNOC-EDC
INTERPR. BY fab
COMM. 4-layer model
sum of squares 2.3E-02
deviation 10.59%
Apparent resistivity [Ωm]
14.7
39.8
255
480
1816
391
103
m
Ωm
AB/2 [m]

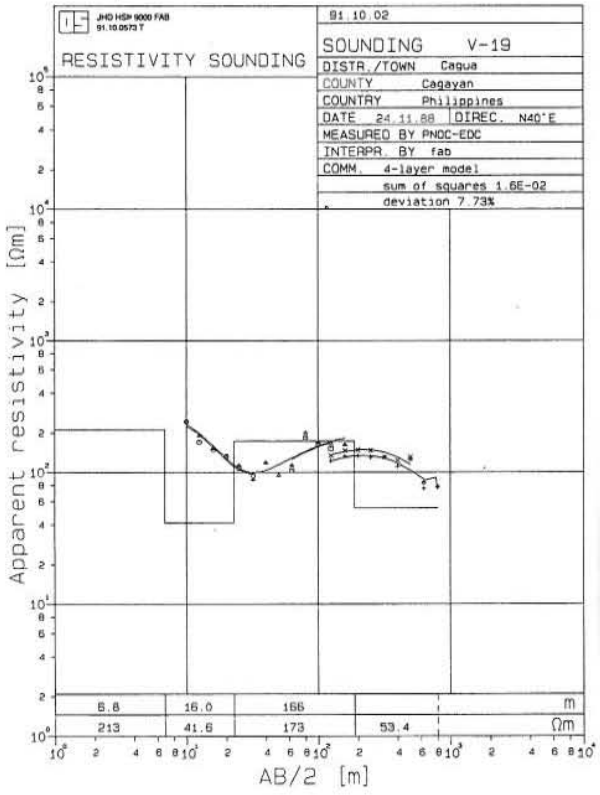
JHD HSP 9000 FAB
91.10.0573 T
91.10.02
RESISTIVITY SOUNDING
SOUNDING V-19
DISTR./TOWN Cagua
COUNTY Cagayan
COUNTRY Philippines
DATE 24.11.88 DIREC. N40°E
MEASURED BY PNOC-EDC
INTERPR. BY fab
COMM. 4-layer model
sum of squares 1.6E-02
deviation 7.73%
Apparent resistivity [Ωm]
6.8
16.0
166
213
41.6
173
53.4
m
Ωm
AB/2 [m]

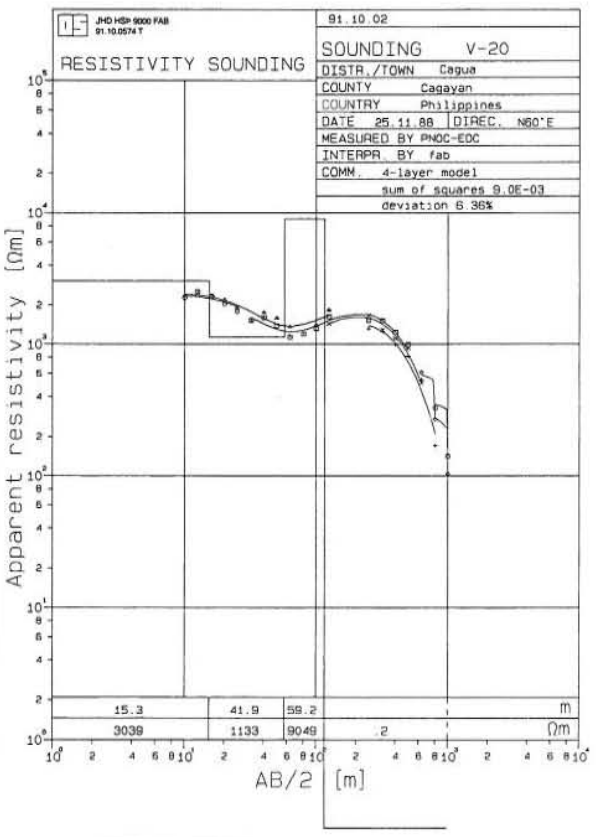
JHD HSP 9000 FAB
91.10.0574 T
91.10.02
RESISTIVITY SOUNDING
SOUNDING V-20
DISTR./TOWN Cagua
COUNTY Cagayan
COUNTRY Philippines
DATE 25.11.88 DIREC. N60°E
MEASURED BY PNOC-EDC
INTERPR. BY fab
COMM. 4-layer model
sum of squares 9.0E-03
deviation 6.36%
Apparent resistivity [Ωm]
15.3
41.9
58.2
3039
1133
9049
m
Ωm
AB/2 [m]

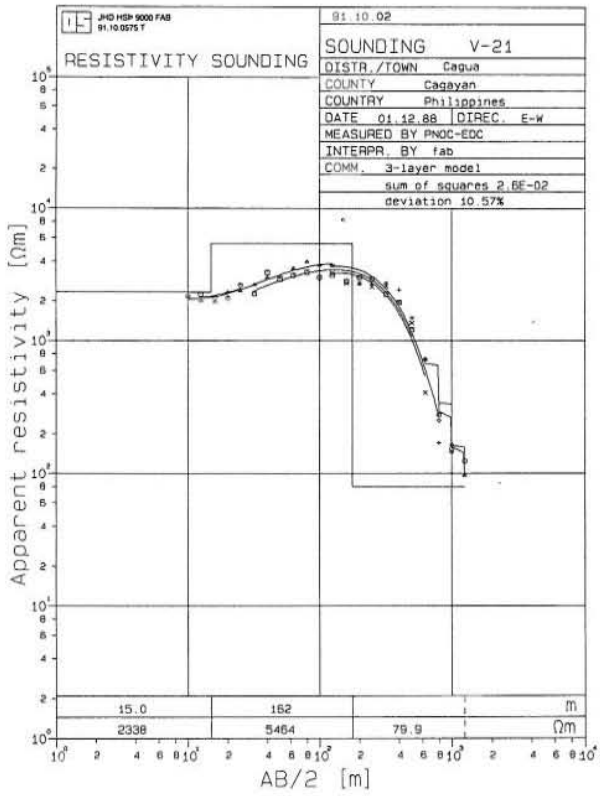
JHD HSP 9000 FAB
91.10.0575 T
RESISTIVITY SOUNDING
91.10.02
SOUNDING V-21
DISTR./TOWN Cagua
COUNTY Cagayan
COUNTRY Philippines
DATE 01.12.88 DIREC. E-W
MEASURED BY PNOC-EDC
INTERPR. BY fab
COMM. 3-layer model
sum of squares 2.6E-02
deviation 10.57%
15.0 162 m
2338 5464 79.9 Ωm
Apparent resistivity [Ωm]
AB/2 [m]

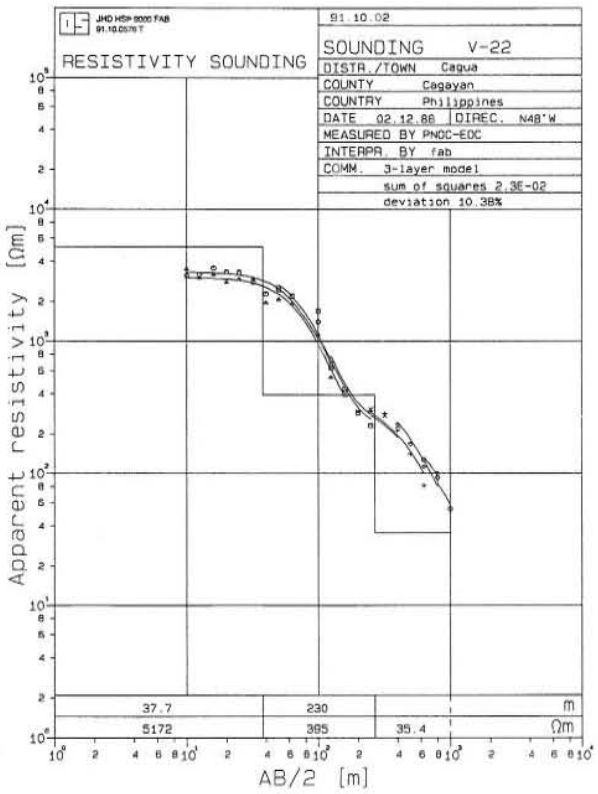
JHD HSP 9000 FAB
RESISTIVITY SOUNDING
91.10.02
SOUNDING V-22
DISTR./TOWN Cagua
COUNTY Cagayan
COUNTRY Philippines
DATE 02.12.88 DIREC. N48°W
MEASURED BY PNOC-EDC
INTERPR. BY fab
COMM. 3-layer model
sum of squares 2.3E-02
deviation 10.38%
37.7 230 m
5172 385 35.4 Ωm
Apparent resistivity [Ωm]
AB/2 [m]

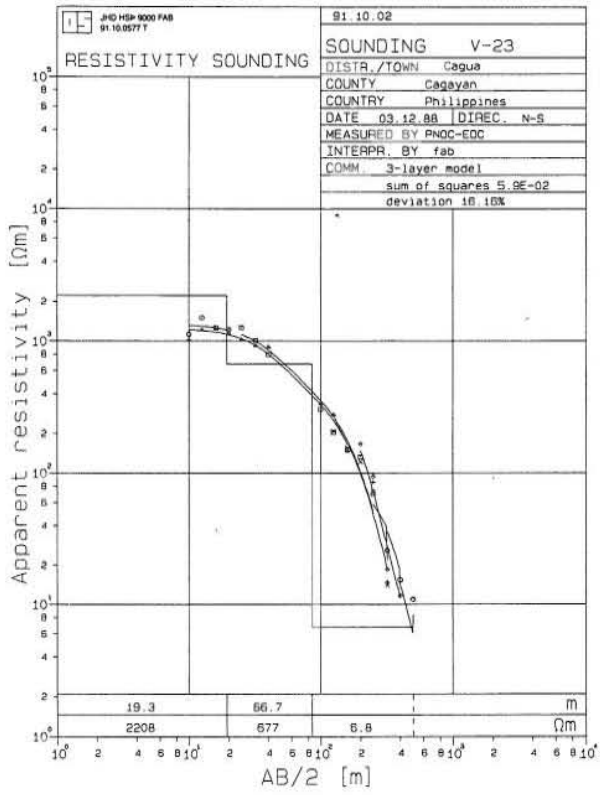
JHD HSP 9000 FAB
91.10.0577 T
RESISTIVITY SOUNDING
91.10.02
SOUNDING V-23
DISTR./TOWN Cagua
COUNTY Cagayan
COUNTRY Philippines
DATE 03.12.88 DIREC. N-S
MEASURED BY PNOC-EDC
INTERPR. BY fab
COMM. 3-layer model
sum of squares 5.9E-02
deviation 16.16%
19.3 66.7 m
2208 677 6.8 Ωm
Apparent resistivity [Ωm]
AB/2 [m]

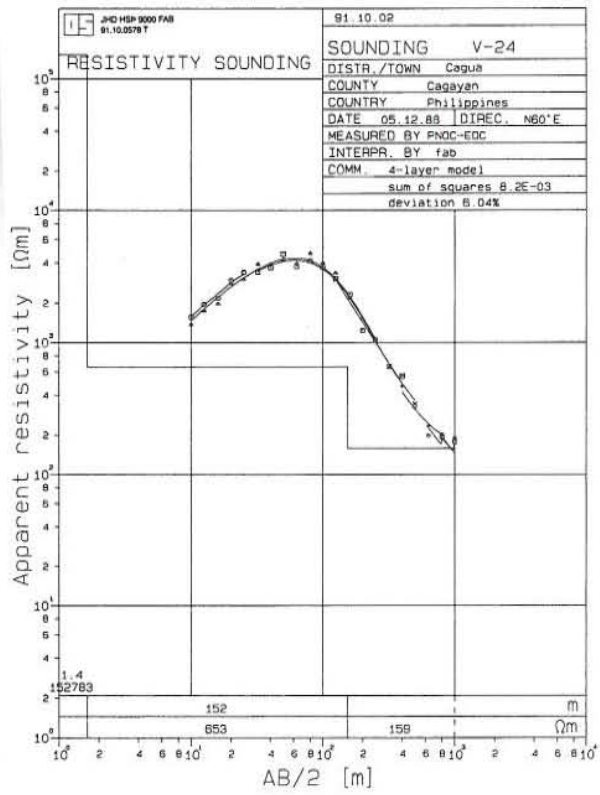
JHD HSP 9000 FAB
91.10.0578 T
RESISTIVITY SOUNDING
91.10.02
SOUNDING V-24
DISTR./TOWN Cagua
COUNTY Cagayan
COUNTRY Philippines
DATE 05.12.88 DIREC. N60°E
MEASURED BY PNOC-EDC
INTERPR. BY fab
COMM. 4-layer model
sum of squares 8.2E-03
deviation 6.04%
1.4
152783
152 m
653 159 Ωm
Apparent resistivity [Ωm]
AB/2 [m]

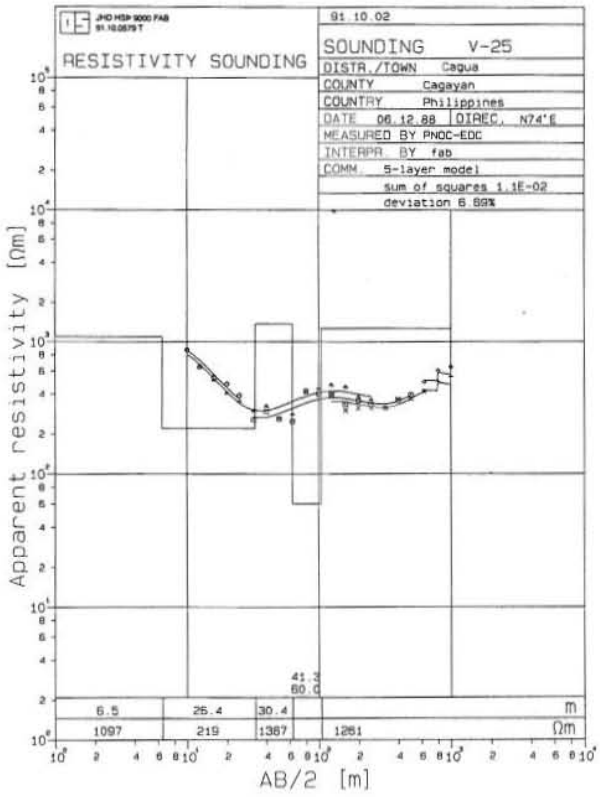
91.10.02
RESISTIVITY SOUNDING
SOUNDING V-25
DISTR./TOWN Cagua
COUNTY Cagayan
COUNTRY Philippines
DATE 06.12.88 DIREC. N74°E
MEASURED BY PNOC-EDC
INTERPR. BY fab
COMM. 5-layer model
sum of squares 1.1E-02
deviation 6.89%
Apparent resistivity [Ωm]
AB/2 [m]
6.5 25.4 30.4 41.3 60.0 m
1097 219 1367 1261 Ωm

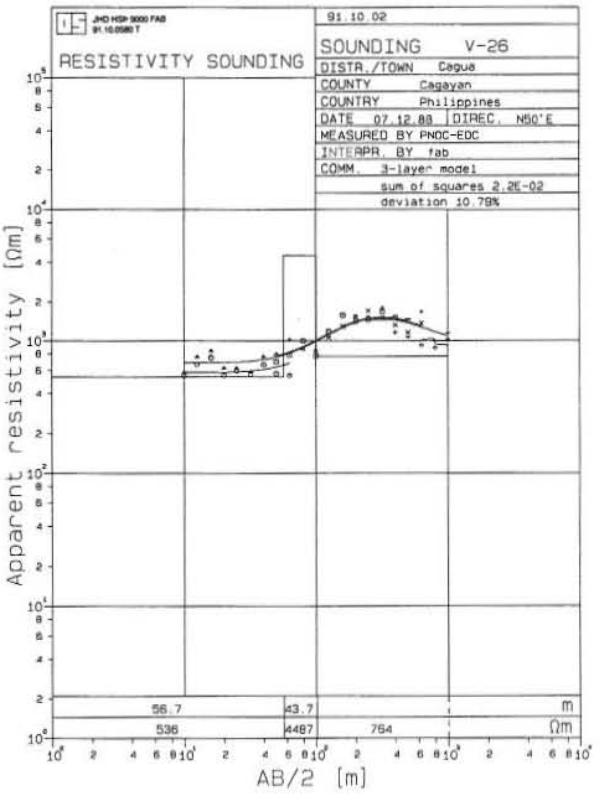
91.10.02
RESISTIVITY SOUNDING
SOUNDING V-26
DISTR./TOWN Cagua
COUNTY Cagayan
COUNTRY Philippines
DATE 07.12.88 DIREC. N50°E
MEASURED BY PNOC-EDC
INTERPR. BY fab
COMM. 3-layer model
sum of squares 2.2E-02
deviation 10.79%
Apparent resistivity [Ωm]
AB/2 [m]
56.7 43.7 m
536 4487 764 Ωm

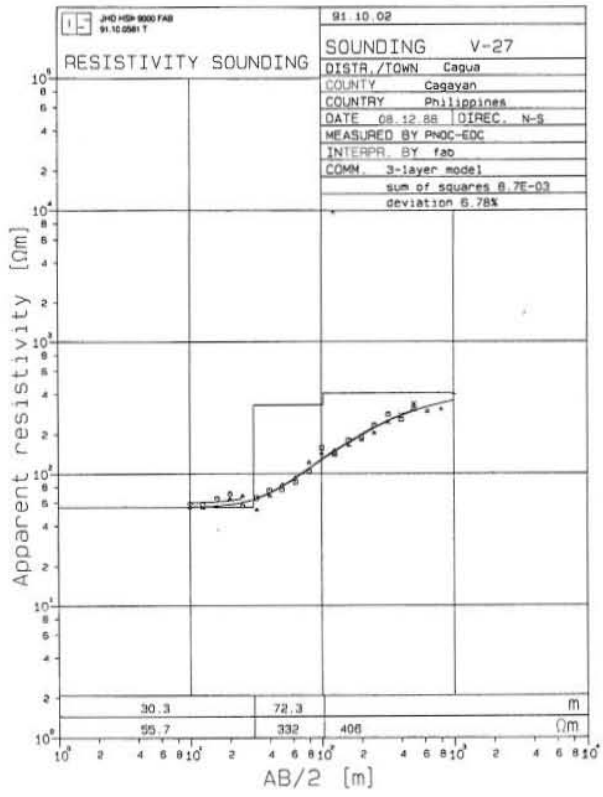
91.10.02
RESISTIVITY SOUNDING
SOUNDING V-27
DISTR./TOWN Cagua
COUNTY Cagayan
COUNTRY Philippines
DATE 08.12.88 DIREC. N-S
MEASURED BY PNOC-EDC
INTERPR. BY fab
COMM. 3-layer model
sum of squares 8.7E-03
deviation 6.78%
Apparent resistivity [Ωm]
AB/2 [m]
30.3 72.3 m
55.7 332 406 Ωm

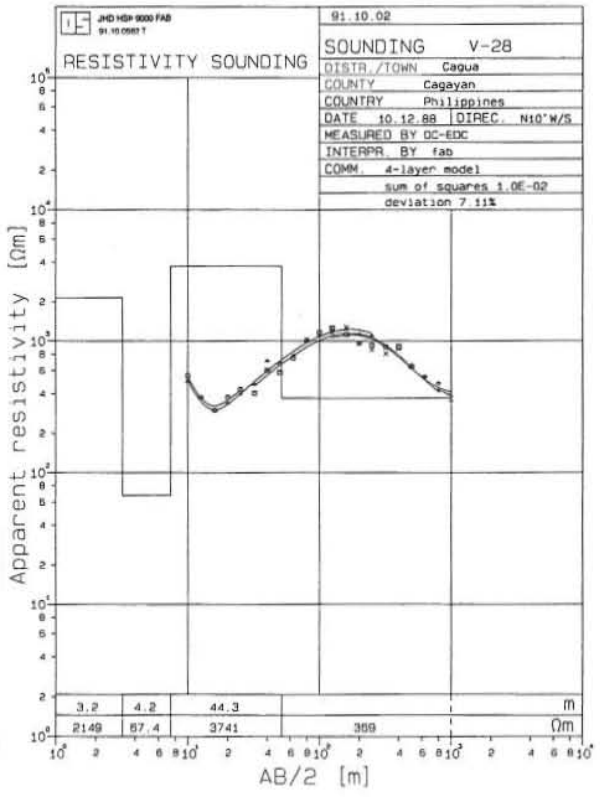
91.10.02
RESISTIVITY SOUNDING
SOUNDING V-28
DISTR./TOWN Cagua
COUNTY Cagayan
COUNTRY Philippines
DATE 10.12.88 DIREC. N10°W/S
MEASURED BY OC-EDC
INTERPR. BY fab
COMM. 4-layer model
sum of squares 1.0E-02
deviation 7.11%
Apparent resistivity [Ωm]
AB/2 [m]
3.2 4.2 44.3 m
2149 67.4 3741 369 Ωm

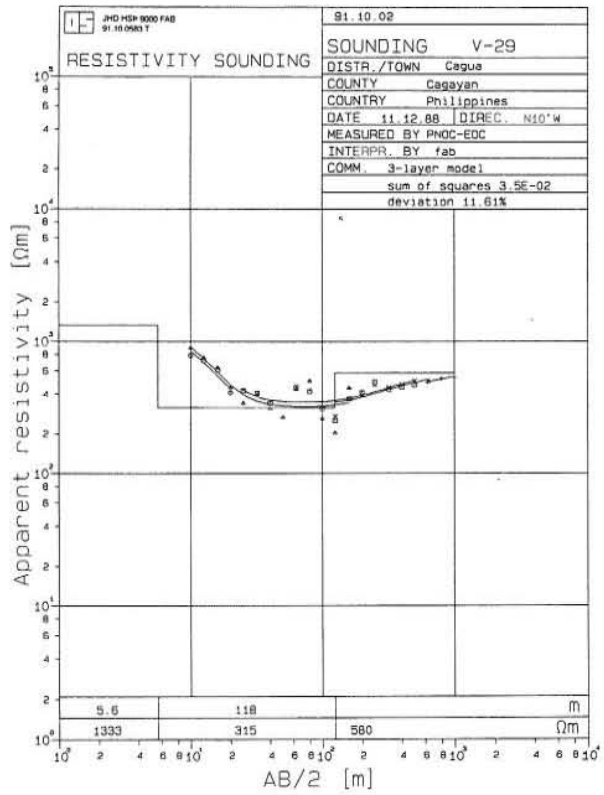
RESISTIVITY SOUNDING
91.10.02
SOUNDING V-29
DISTR./TOWN Cagua
COUNTY Cagayan
COUNTRY Philippines
DATE 11.12.88 DIREC. N10°W
MEASURED BY PNOC-EDC
INTERPR. BY fab
COMM. 3-layer model
sum of squares 3.5E-02
deviation 11.61%
Apparent resistivity [Ωm]
AB/2 [m]
5.6 118 m
1333 315 580 Ωm

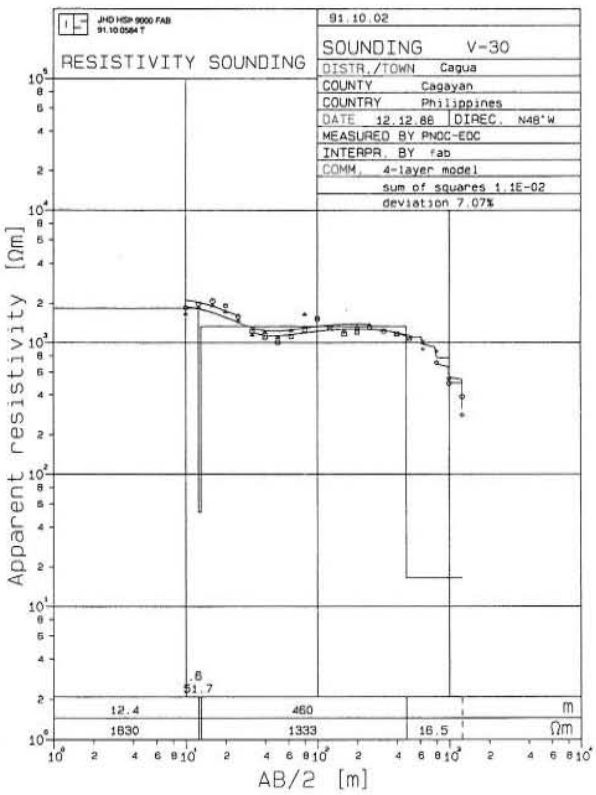
RESISTIVITY SOUNDING
91.10.02
SOUNDING V-30
DISTR./TOWN Cagua
COUNTY Cagayan
COUNTRY Philippines
DATE 12.12.88 DIREC. N48°W
MEASURED BY PNOC-EDC
INTERPR. BY fab
COMM. 4-layer model
sum of squares 1.1E-02
deviation 7.07%
Apparent resistivity [Ωm]
AB/2 [m]
.8 .7
12.4 460 m
1830 1333 16.5 Ωm

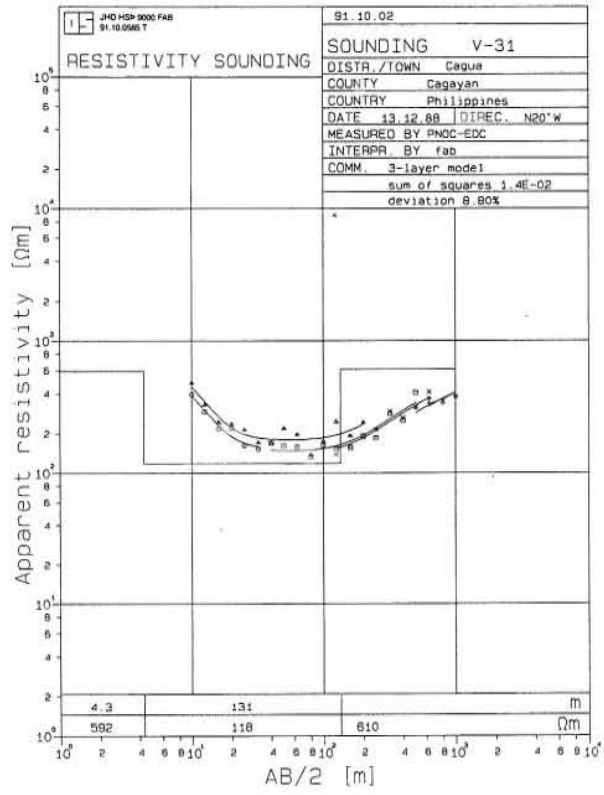
RESISTIVITY SOUNDING
91.10.02
SOUNDING V-31
DISTR./TOWN Cagua
COUNTY Cagayan
COUNTRY Philippines
DATE 13.12.88 DIREC. N20°W
MEASURED BY PNOC-EDC
INTERPR. BY fab
COMM. 3-layer model
sum of squares 1.4E-02
deviation 8.80%
Apparent resistivity [Ωm]
AB/2 [m]
4.3 131 m
592 118 610 Ωm

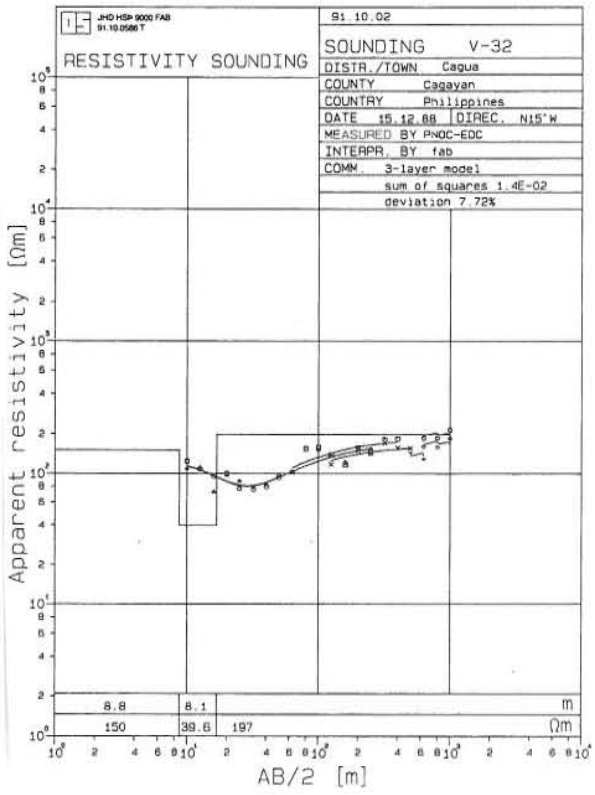
RESISTIVITY SOUNDING
91.10.02
SOUNDING V-32
DISTR./TOWN Cagua
COUNTY Cagayan
COUNTRY Philippines
DATE 15.12.88 DIREC. N15°W
MEASURED BY PNOC-EDC
INTERPR. BY fab
COMM. 3-layer model
sum of squares 1.4E-02
deviation 7.72%
Apparent resistivity [Ωm]
AB/2 [m]
8.8 8.1 m
150 39.6 197 Ωm

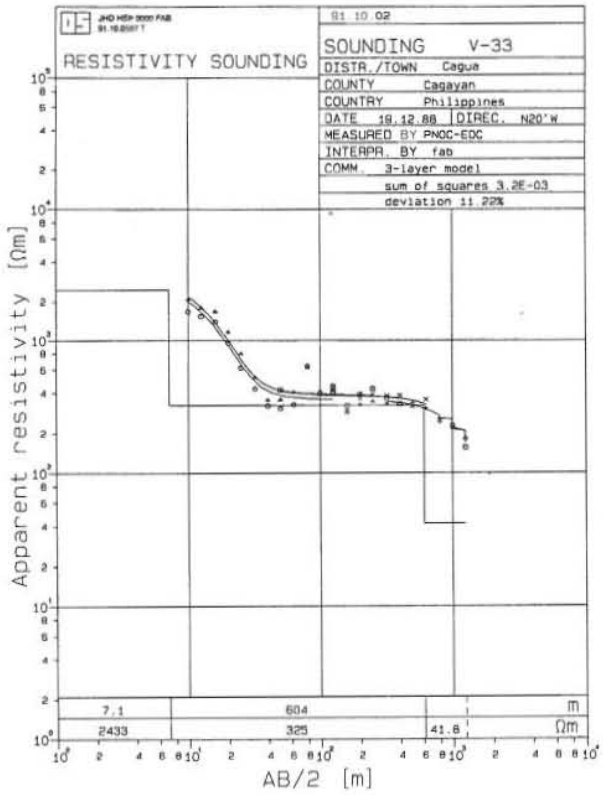
91.10.02
RESISTIVITY SOUNDING
SOUNDING V-33
DISTR./TOWN Cagua
COUNTY Cagayan
COUNTRY Philippines
DATE 19.12.88 | DIREC. N20°W
MEASURED BY PNOC-EDC
INTERPR. BY fab
COMM. 3-layer model
sum of squares 3.2E-03
deviation 11.22%
Apparent resistivity [Ωm]
AB/2 [m]
7.1 | 604 | m
2433 | 325 | 41.8 | Ωm

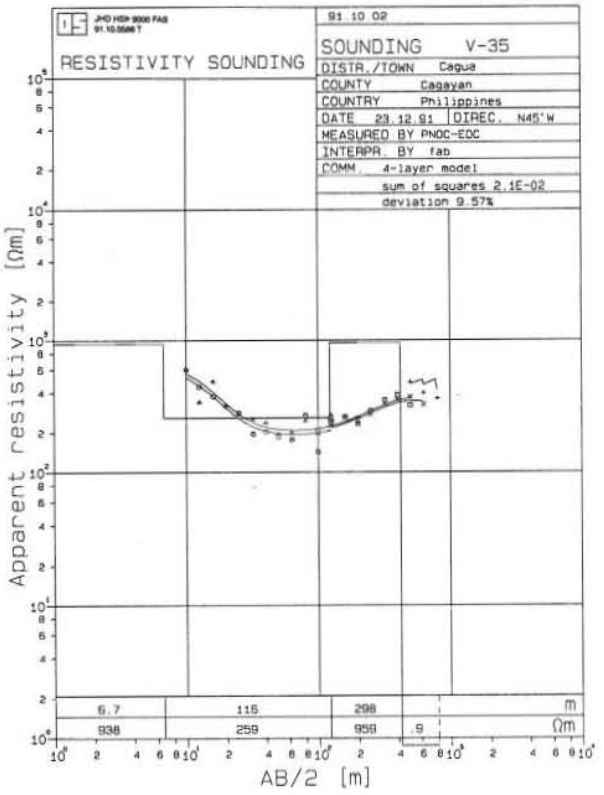
91.10.02
RESISTIVITY SOUNDING
SOUNDING V-35
DISTR./TOWN Cagua
COUNTY Cagayan
COUNTRY Philippines
DATE 23.12.91 | DIREC. N45°W
MEASURED BY PNOC-EDC
INTERPR. BY fab
COMM. 4-layer model
sum of squares 2.1E-02
deviation 9.57%
Apparent resistivity [Ωm]
AB/2 [m]
6.7 | 116 | 298 | m
938 | 259 | 959 | .9 | Ωm

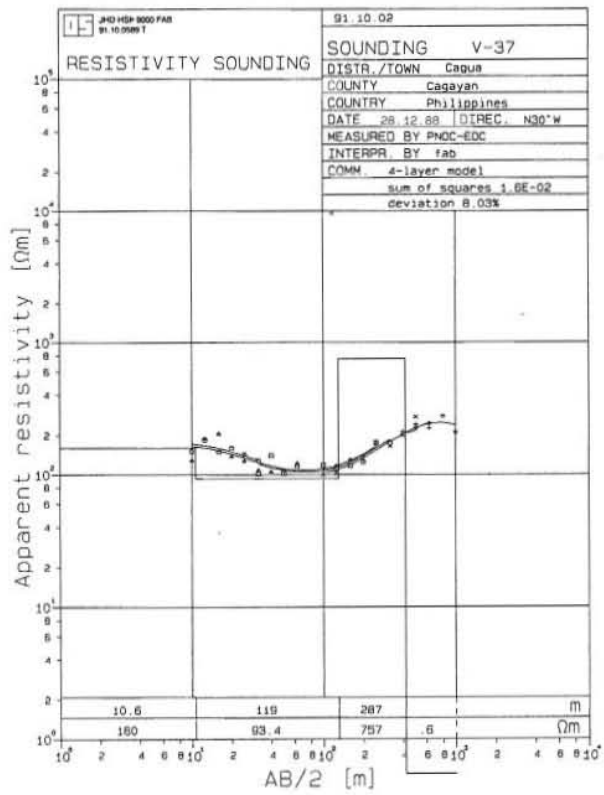
91.10.02
RESISTIVITY SOUNDING
SOUNDING V-37
DISTR./TOWN Cagua
COUNTY Cagayan
COUNTRY Philippines
DATE 28.12.88 | DIREC. N30°W
MEASURED BY PNOC-EDC
INTERPR. BY fab
COMM. 4-layer model
sum of squares 1.6E-02
deviation 8.03%
Apparent resistivity [Ωm]
AB/2 [m]
10.6 | 119 | 287 | m
160 | 93.4 | 757 | .6 | Ωm

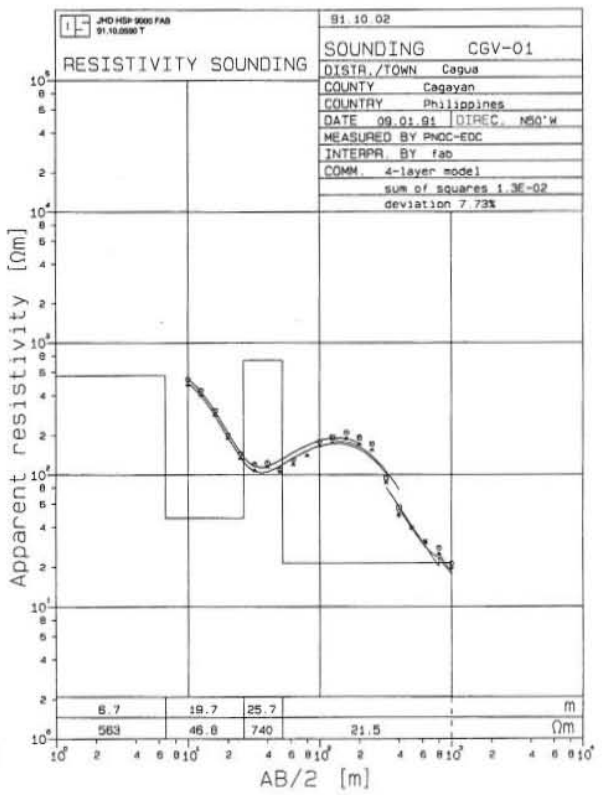
91.10.02
RESISTIVITY SOUNDING
SOUNDING CGV-01
DISTR./TOWN Cagua
COUNTY Cagayan
COUNTRY Philippines
DATE 09.01.91 | DIREC. N50°W
MEASURED BY PNOC-EDC
INTERPR. BY fab
COMM. 4-layer model
sum of squares 1.3E-02
deviation 7.73%
Apparent resistivity [Ωm]
AB/2 [m]
6.7 | 19.7 | 25.7 | m
563 | 46.8 | 740 | 21.5 | Ωm

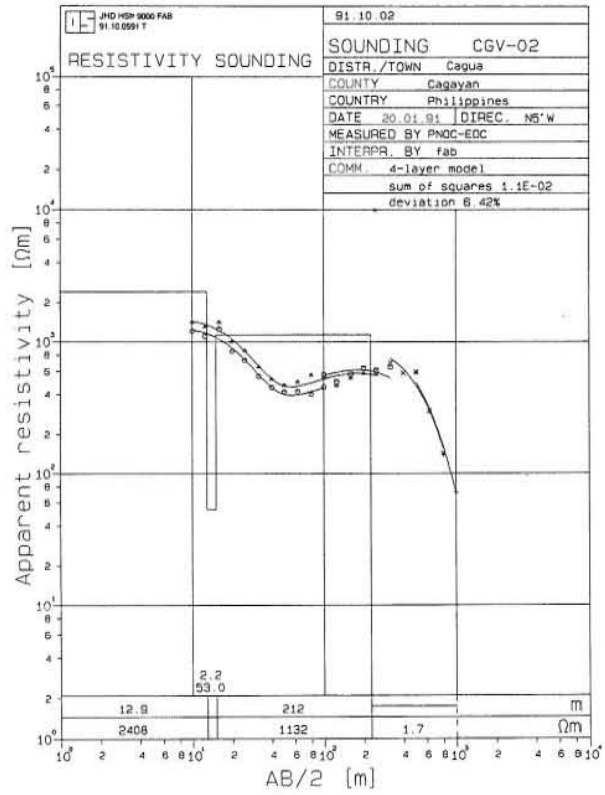
JHD HSP 9000 FAB
91.10.0591 T
91.10.02
RESISTIVITY SOUNDING
SOUNDING CGV-02
DISTR./TOWN Cagua
COUNTY Cagayan
COUNTRY Philippines
DATE 20.01.91 DIREC. N5°W
MEASURED BY PNOC-EDC
INTERPR. BY fab
COMM. 4-layer model
sum of squares 1.1E-02
deviation 6.42%
Apparent resistivity [Ωm]
2.2
53.0
12.9 212 m
2408 1132 1.7 Ωm
AB/2 [m]

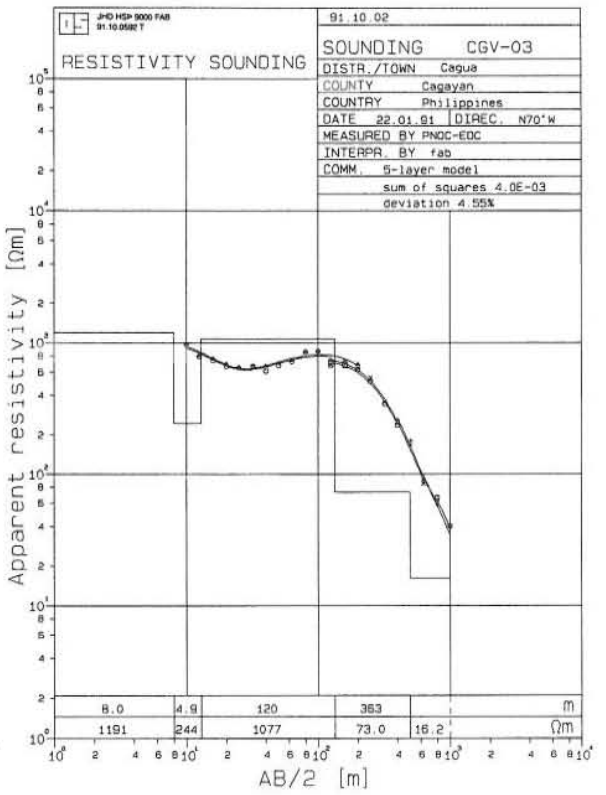
JHD HSP 9000 FAB
91.10.0592 T
91.10.02
RESISTIVITY SOUNDING
SOUNDING CGV-03
DISTR./TOWN Cagua
COUNTY Cagayan
COUNTRY Philippines
DATE 22.01.91 DIREC. N70°W
MEASURED BY PNOC-EDC
INTERPR. BY fab
COMM. 5-layer model
sum of squares 4.0E-03
deviation 4.55%
Apparent resistivity [Ωm]
8.0 4.9 120 363 m
1191 244 1077 73.0 16.2 Ωm
AB/2 [m]

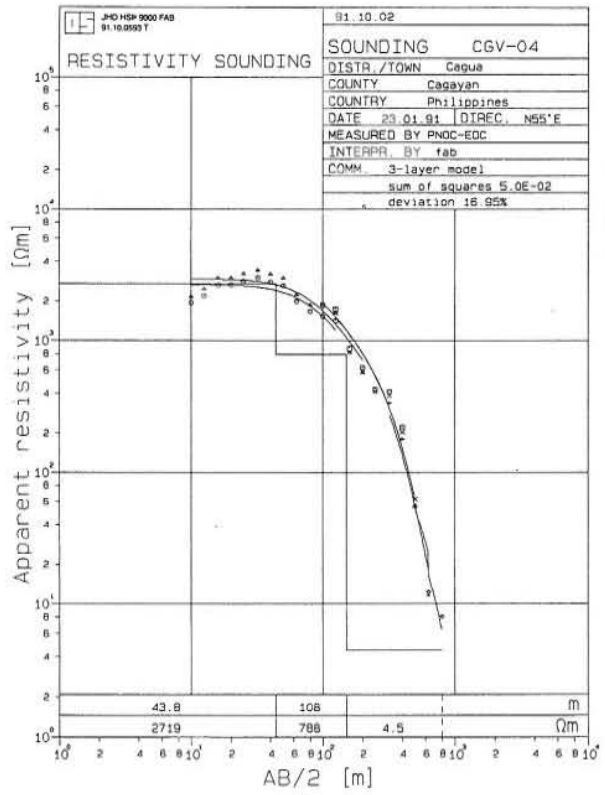
JHD HSP 9000 FAB
91.10.0593 T
91.10.02
RESISTIVITY SOUNDING
SOUNDING CGV-04
DISTR./TOWN Cagua
COUNTY Cagayan
COUNTRY Philippines
DATE 23.01.91 DIREC. N55°E
MEASURED BY PNOC-EDC
INTERPR. BY fab
COMM. 3-layer model
sum of squares 5.0E-02
deviation 16.95%
Apparent resistivity [Ωm]
43.8 108 m
2719 788 4.5 Ωm
AB/2 [m]

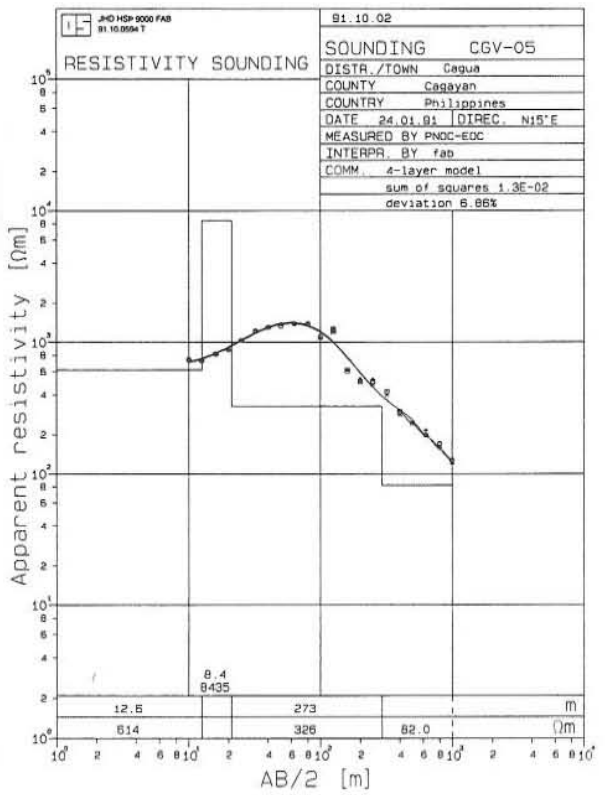
JHD HSP 9000 FAB
91.10.0594 T
91.10.02
RESISTIVITY SOUNDING
SOUNDING CGV-05
DISTR./TOWN Cagua
COUNTY Cagayan
COUNTRY Philippines
DATE 24.01.91 DIREC. N15°E
MEASURED BY PNOC-EDC
INTERPR. BY fab
COMM. 4-layer model
sum of squares 1.3E-02
deviation 6.86%
Apparent resistivity [Ωm]
8.4
8435
12.6 273 m
614 326 82.0 Ωm
AB/2 [m]

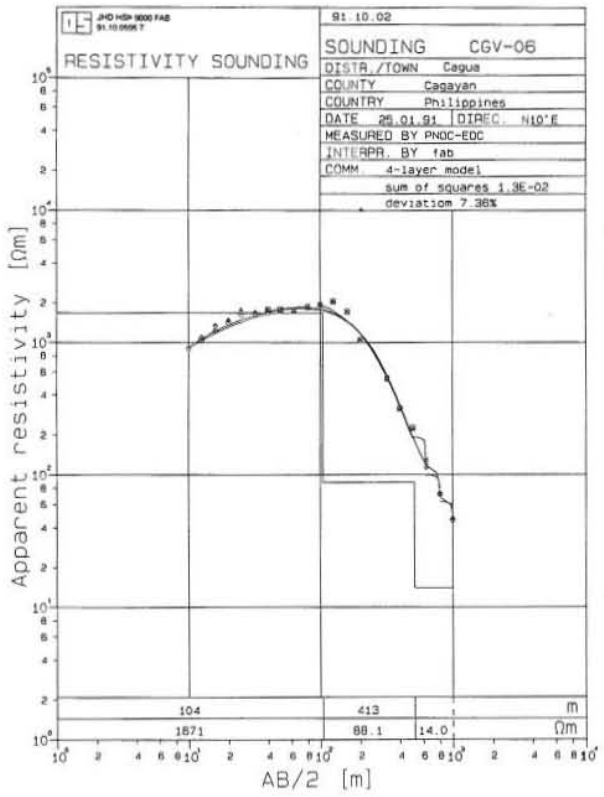
91.10.02
RESISTIVITY SOUNDING
SOUNDING CGV-06
DISTR./TOWN Cagua
COUNTY Cagayan
COUNTRY Philippines
DATE 26.01.91 | DIREC. N10°E
MEASURED BY PNOC-EDC
INTERPR. BY fab
COMM. 4-layer model
sum of squares 1.3E-02
deviation 7.38%
104 413 m
1871 88.1 14.0 Ωm
Apparent resistivity [Ωm]
AB/2 [m]

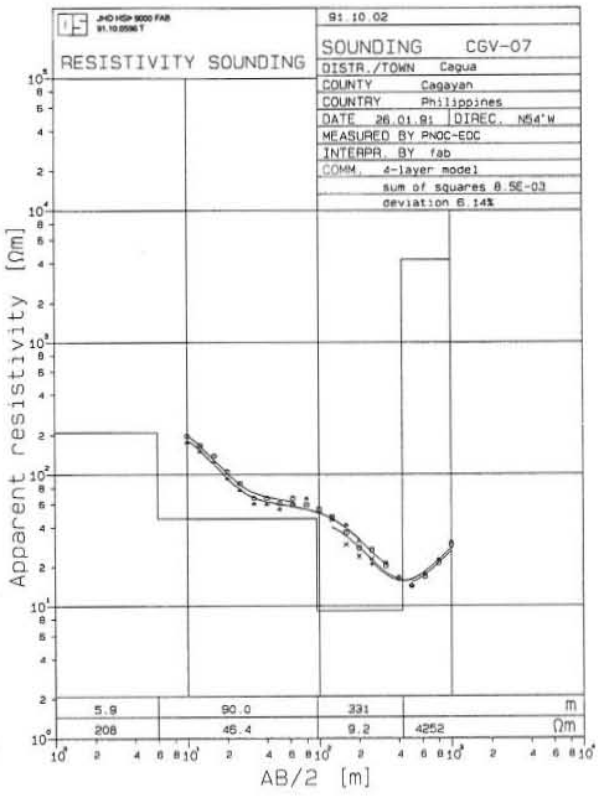
91.10.02
RESISTIVITY SOUNDING
SOUNDING CGV-07
DISTR./TOWN Cagua
COUNTY Cagayan
COUNTRY Philippines
DATE 26.01.91 | DIREC. N54°W
MEASURED BY PNOC-EDC
INTERPR. BY fab
COMM. 4-layer model
sum of squares 8.5E-03
deviation 6.14%
5.9 90.0 331 m
208 46.4 9.2 4252 Ωm
Apparent resistivity [Ωm]
AB/2 [m]

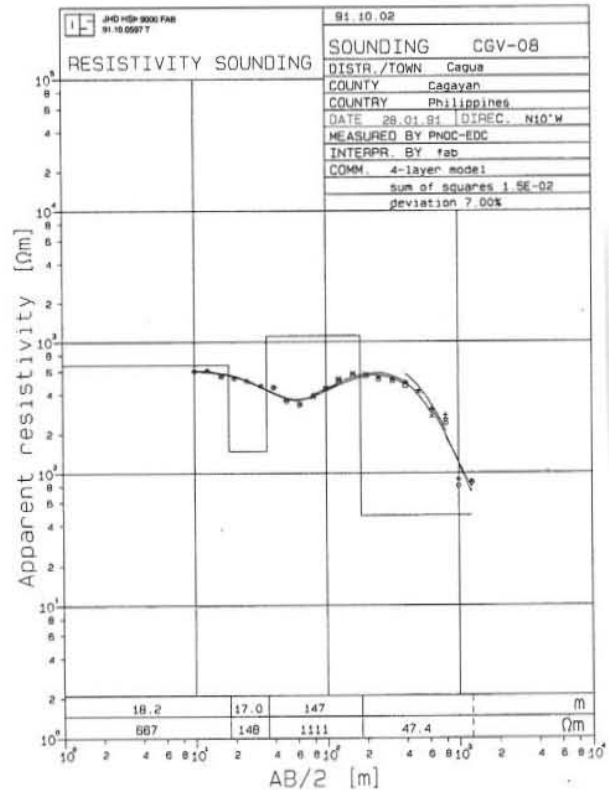
91.10.02
RESISTIVITY SOUNDING
SOUNDING CGV-08
DISTR./TOWN Cagua
COUNTY Cagayan
COUNTRY Philippines
DATE 28.01.91 | DIREC. N10°W
MEASURED BY PNOC-EDC
INTERPR. BY fab
COMM. 4-layer model
sum of squares 1.5E-02
deviation 7.00%
18.2 17.0 147 m
667 148 1111 47.4 Ωm
Apparent resistivity [Ωm]
AB/2 [m]

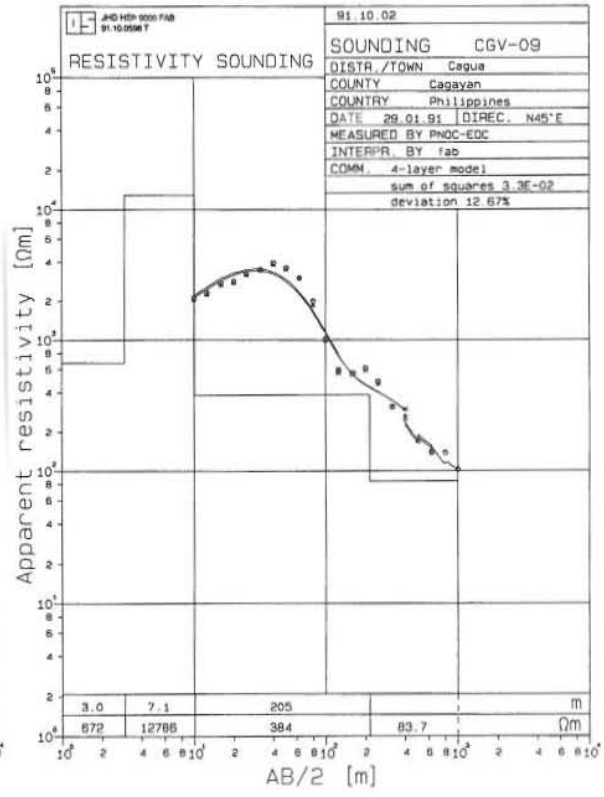
91.10.02
RESISTIVITY SOUNDING
SOUNDING CGV-09
DISTR./TOWN Cagua
COUNTY Cagayan
COUNTRY Philippines
DATE 29.01.91 | DIREC. N45°E
MEASURED BY PNOC-EDC
INTERPR. BY fab
COMM. 4-layer model
sum of squares 3.3E-02
deviation 12.67%
3.0 7.1 205 m
672 12786 384 83.7 Ωm
Apparent resistivity [Ωm]
AB/2 [m]

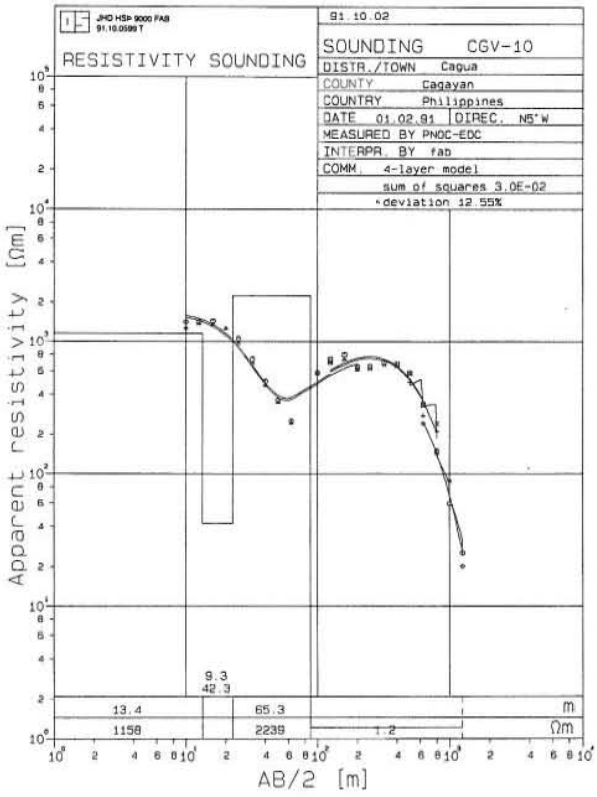
JHD HSP 9000 FAB
91.10.0599 T
91.10.02
RESISTIVITY SOUNDING
SOUNDING CGV-10
DISTR./TOWN Cagua
COUNTY Cagayan
COUNTRY Philippines
DATE 01.02.91 DIREC. N5°W
MEASURED BY PNOC-EDC
INTERPR. BY fab
COMM. 4-layer model
sum of squares 3.0E-02
deviation 12.55%
Apparent resistivity [Ωm]
AB/2 [m]
9.3
42.3
13.4
65.3
m
1158
2239
Ωm

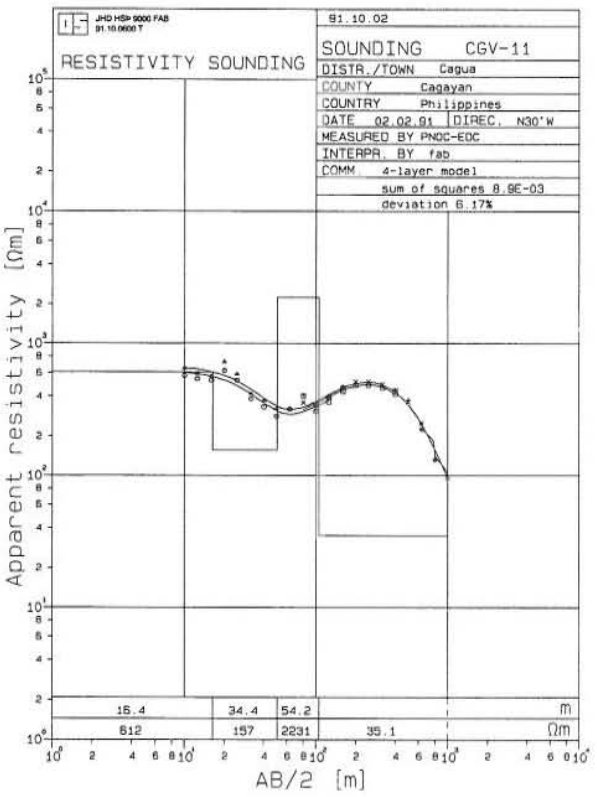
JHD HSP 9000 FAB
91.10.0600 T
91.10.02
RESISTIVITY SOUNDING
SOUNDING CGV-11
DISTR./TOWN Cagua
COUNTY Cagayan
COUNTRY Philippines
DATE 02.02.91 DIREC. N30°W
MEASURED BY PNOC-EDC
INTERPR. BY fab
COMM. 4-layer model
sum of squares 8.9E-03
deviation 6.17%
Apparent resistivity [Ωm]
AB/2 [m]
15.4
34.4
54.2
m
612
157
2231
35.1
Ωm

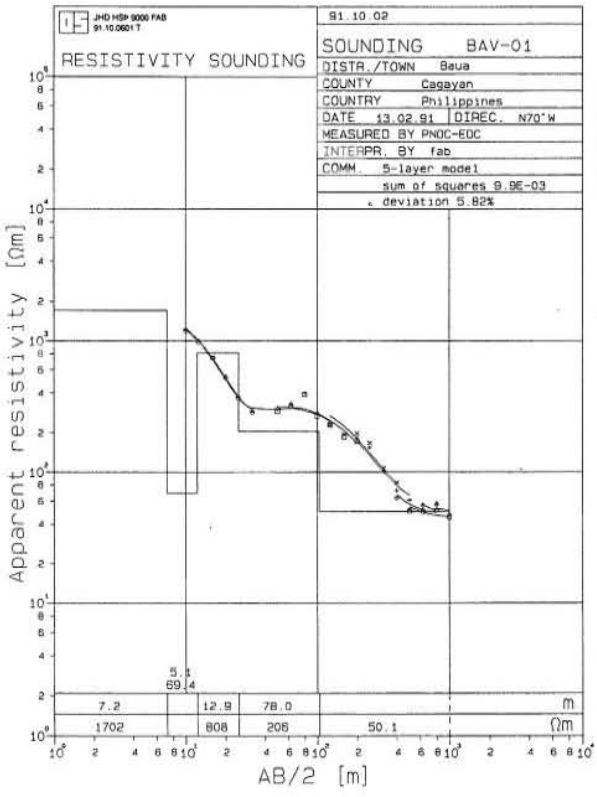
JHD HSP 9000 FAB
91.10.0601 T
91.10.02
RESISTIVITY SOUNDING
SOUNDING BAV-01
DISTR./TOWN Baua
COUNTY Cagayan
COUNTRY Philippines
DATE 13.02.91 DIREC. N70°W
MEASURED BY PNOC-EDC
INTERPR. BY fab
COMM. 5-layer model
sum of squares 9.9E-03
deviation 5.82%
Apparent resistivity [Ωm]
AB/2 [m]
5.1
69.4
7.2
12.9
78.0
m
1702
808
206
50.1
Ωm

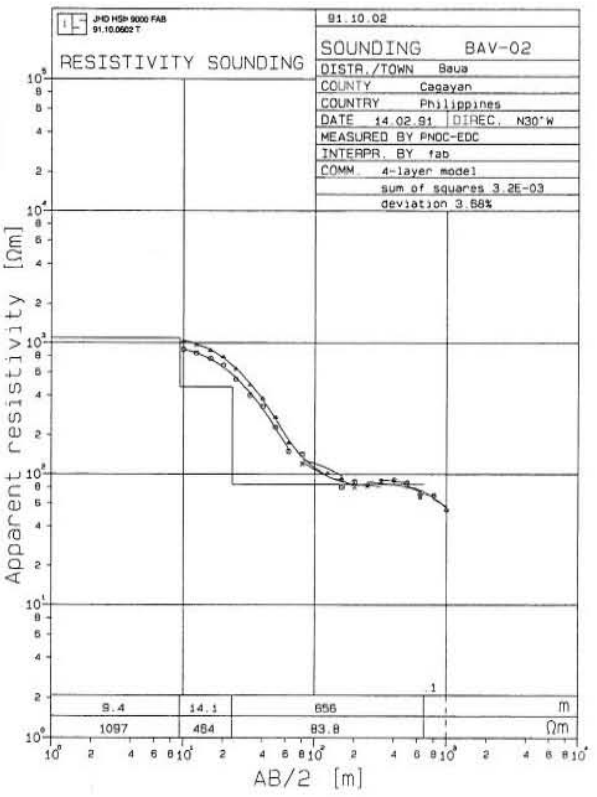
JHD HSP 9000 FAB
91.10.0602 T
91.10.02
RESISTIVITY SOUNDING
SOUNDING BAV-02
DISTR./TOWN Baua
COUNTY Cagayan
COUNTRY Philippines
DATE 14.02.91 DIREC. N30°W
MEASURED BY PNOC-EDC
INTERPR. BY fab
COMM. 4-layer model
sum of squares 3.2E-03
deviation 3.68%
Apparent resistivity [Ωm]
AB/2 [m]
9.4
14.1
656
m
1097
464
83.8
Ωm

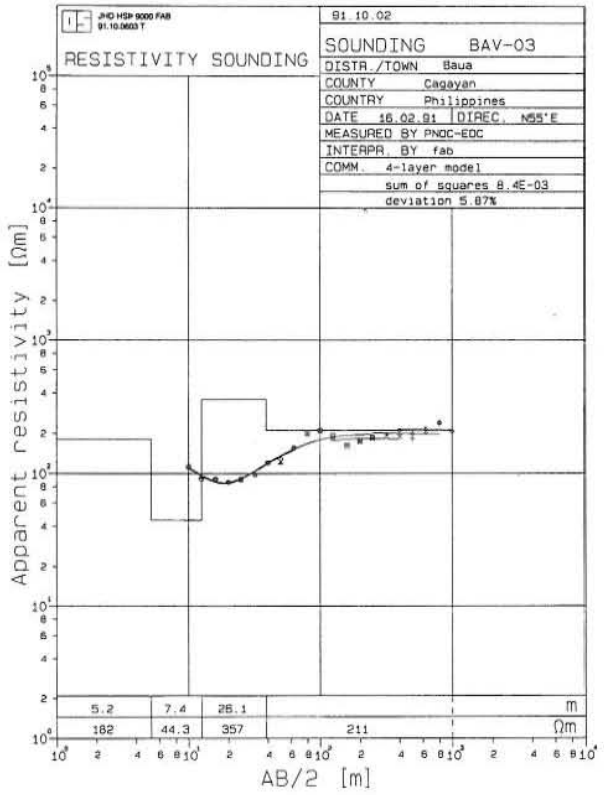
91.10.02
RESISTIVITY SOUNDING
SOUNDING BAV-03
DISTR./TOWN Baua
COUNTY Cagayan
COUNTRY Philippines
DATE 16.02.91 DIREC. N55°E
MEASURED BY PNOC-EDC
INTERPR. BY fab
COMM. 4-layer model
sum of squares 8.4E-03
deviation 5.87%
Apparent resistivity [Ωm]
AB/2 [m]
5.2 7.4 26.1 m
182 44.3 357 211 Ωm

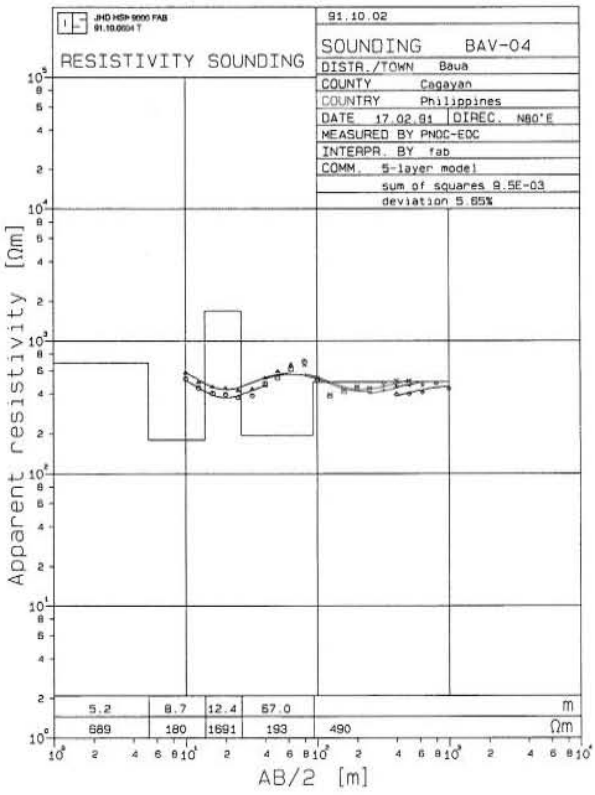
91.10.02
RESISTIVITY SOUNDING
SOUNDING BAV-04
DISTR./TOWN Baua
COUNTY Cagayan
COUNTRY Philippines
DATE 17.02.91 DIREC. N80°E
MEASURED BY PNOC-EDC
INTERPR. BY fab
COMM. 5-layer model
sum of squares 9.5E-03
deviation 5.65%
Apparent resistivity [Ωm]
AB/2 [m]
5.2 8.7 12.4 67.0 m
689 180 1691 193 490 Ωm

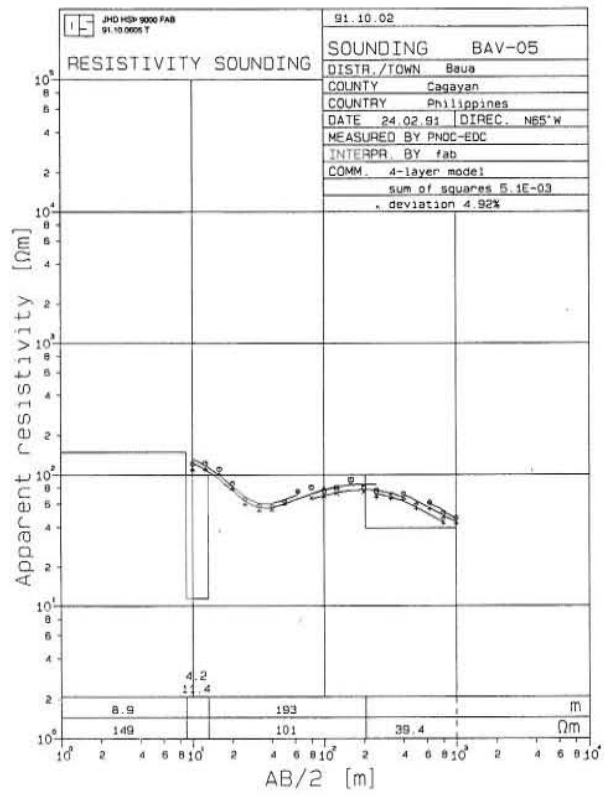
91.10.02
RESISTIVITY SOUNDING
SOUNDING BAV-05
DISTR./TOWN Baua
COUNTY Cagayan
COUNTRY Philippines
DATE 24.02.91 DIREC. N65°W
MEASURED BY PNOC-EDC
INTERPR. BY fab
COMM. 4-layer model
sum of squares 5.1E-03
deviation 4.92%
Apparent resistivity [Ωm]
AB/2 [m]
4.2
11.4
8.9 193 m
149 101 39.4 Ωm

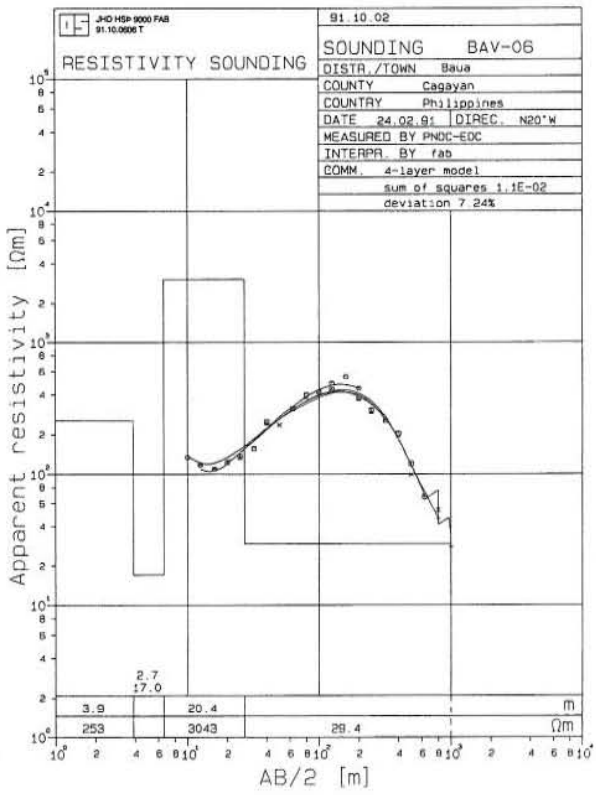
91.10.02
RESISTIVITY SOUNDING
SOUNDING BAV-06
DISTR./TOWN Baua
COUNTY Cagayan
COUNTRY Philippines
DATE 24.02.91 DIREC. N20°W
MEASURED BY PNOC-EDC
INTERPR. BY fab
COMM. 4-layer model
sum of squares 1.1E-02
deviation 7.24%
Apparent resistivity [Ωm]
AB/2 [m]
2.7
17.0
3.9 20.4 m
253 3043 29.4 Ωm

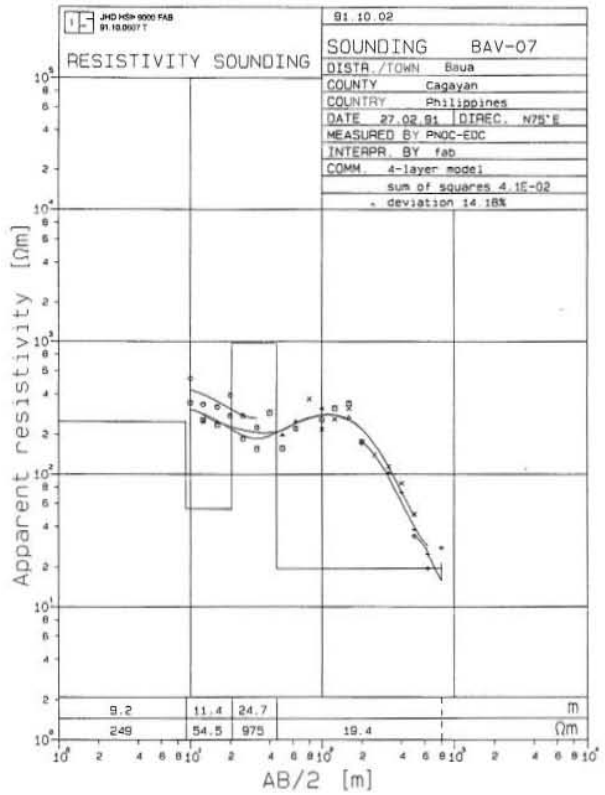
JHD HSP 9000 FAB
91.10.0607 T
91.10.02
RESISTIVITY SOUNDING
SOUNDING BAV-07
DISTR./TOWN Baua
COUNTY Cagayan
COUNTRY Philippines
DATE 27.02.91 | DIREC. N75°E
MEASURED BY PNOC-EDC
INTERPR. BY fab
COMM. 4-layer model
sum of squares 4.1E-02
deviation 14.18%
Apparent resistivity [Ωm]
9.2 11.4 24.7 m
249 54.5 975 19.4 Ωm
AB/2 [m]

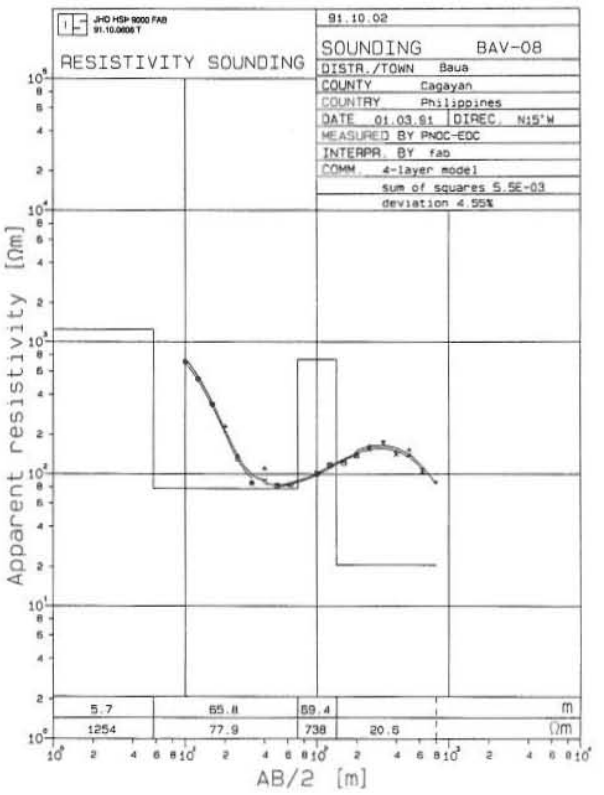
JHD HSP 9000 FAB
91.10.0606 T
91.10.02
RESISTIVITY SOUNDING
SOUNDING BAV-08
DISTR./TOWN Baua
COUNTY Cagayan
COUNTRY Philippines
DATE 01.03.91 | DIREC. N15°W
MEASURED BY PNOC-EDC
INTERPR. BY fab
COMM. 4-layer model
sum of squares 5.5E-03
deviation 4.55%
Apparent resistivity [Ωm]
5.7 65.8 89.4 m
1254 77.9 738 20.6 Ωm
AB/2 [m]

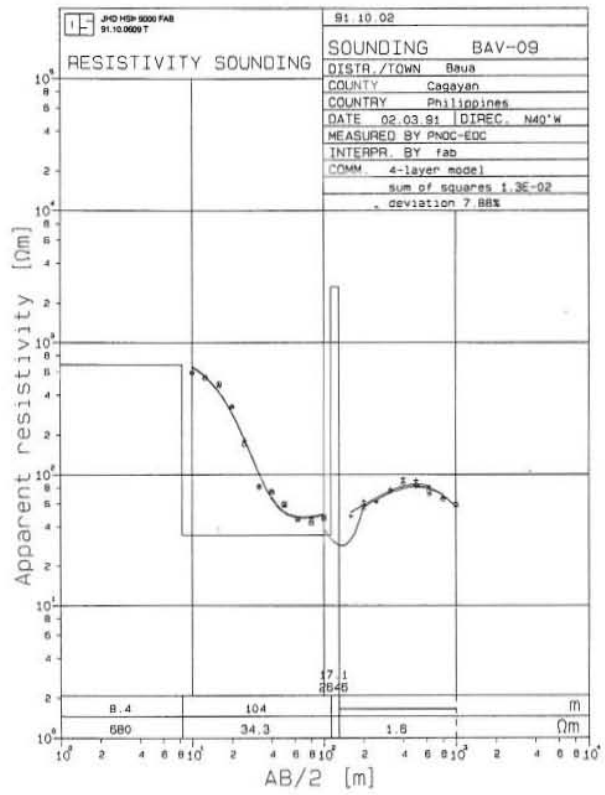
JHD HSP 9000 FAB
91.10.0609 T
91.10.02
RESISTIVITY SOUNDING
SOUNDING BAV-09
DISTR./TOWN Baua
COUNTY Cagayan
COUNTRY Philippines
DATE 02.03.91 | DIREC. N40°W
MEASURED BY PNOC-EDC
INTERPR. BY fab
COMM. 4-layer model
sum of squares 1.3E-02
deviation 7.88%
Apparent resistivity [Ωm]
17.1
2646
8.4 104 m
680 34.3 1.6 Ωm
AB/2 [m]

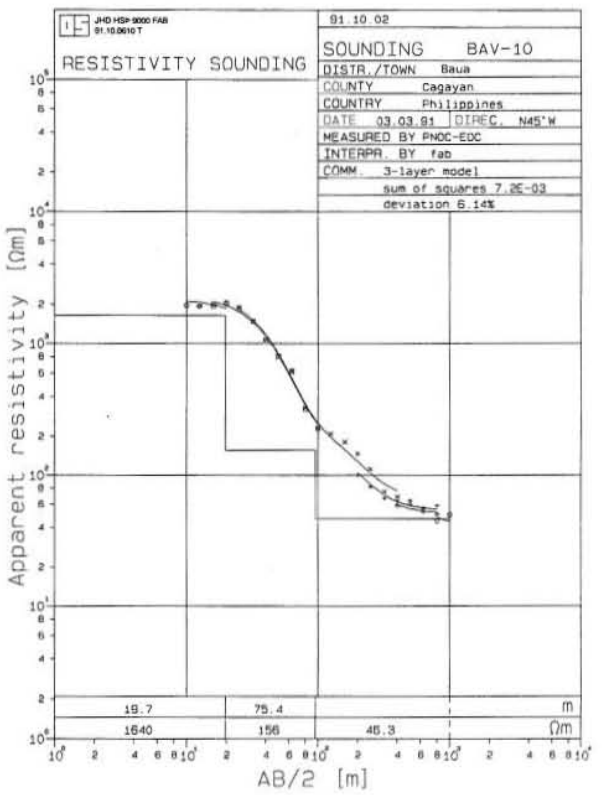
JHD HSP 9000 FAB
91.10.0610 T
91.10.02
RESISTIVITY SOUNDING
SOUNDING BAV-10
DISTR./TOWN Baua
COUNTY Cagayan
COUNTRY Philippines
DATE 03.03.91 | DIREC. N45°W
MEASURED BY PNOC-EDC
INTERPR. BY fab
COMM. 3-layer model
sum of squares 7.2E-03
deviation 6.14%
Apparent resistivity [Ωm]
19.7 75.4 m
1640 156 46.3 Ωm
AB/2 [m]

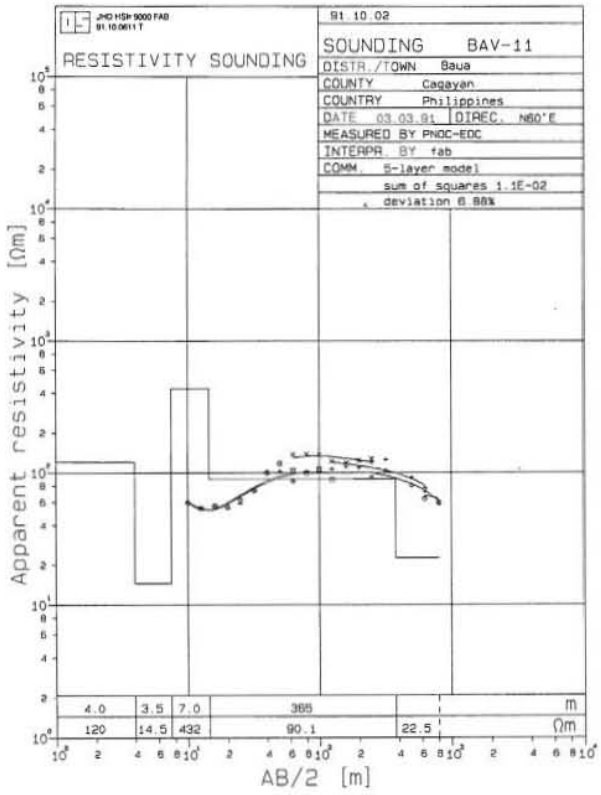
JHD HSP 9000 FAB
91.10.0611 T
91.10.02
RESISTIVITY SOUNDING
SOUNDING BAV-11
DISTR./TOWN Baua
COUNTY Cagayan
COUNTRY Philippines
DATE 03.03.91 DIREC. N60°E
MEASURED BY PNOC-EDC
INTERPR. BY fab
COMM. 5-layer model
sum of squares 1.1E-02
deviation 6.88%
Apparent resistivity [Ωm]
4.0 3.5 7.0 365 m
120 14.5 432 90.1 22.5 Ωm
AB/2 [m]

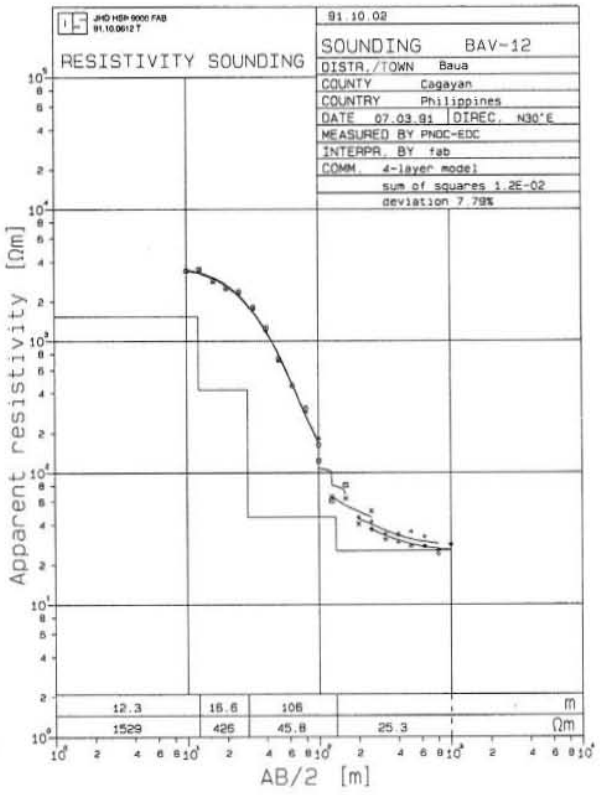
JHD HSP 9000 FAB
91.10.0612 T
91.10.02
RESISTIVITY SOUNDING
SOUNDING BAV-12
DISTR./TOWN Baua
COUNTY Cagayan
COUNTRY Philippines
DATE 07.03.91 DIREC. N30°E
MEASURED BY PNOC-EDC
INTERPR. BY fab
COMM. 4-layer model
sum of squares 1.2E-02
deviation 7.79%
Apparent resistivity [Ωm]
12.3 16.6 106 m
1529 426 45.8 25.3 Ωm
AB/2 [m]

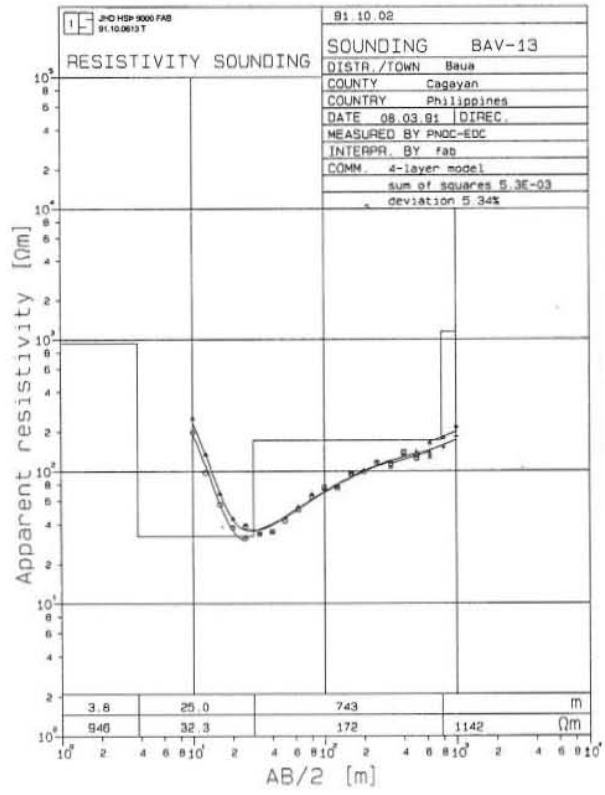
JHD HSP 9000 FAB
91.10.0613 T
91.10.02
RESISTIVITY SOUNDING
SOUNDING BAV-13
DISTR./TOWN Baua
COUNTY Cagayan
COUNTRY Philippines
DATE 08.03.91 DIREC.
MEASURED BY PNOC-EDC
INTERPR. BY fab
COMM. 4-layer model
sum of squares 5.3E-03
deviation 5.34%
Apparent resistivity [Ωm]
3.8 25.0 743 m
946 32.3 172 1142 Ωm
AB/2 [m]

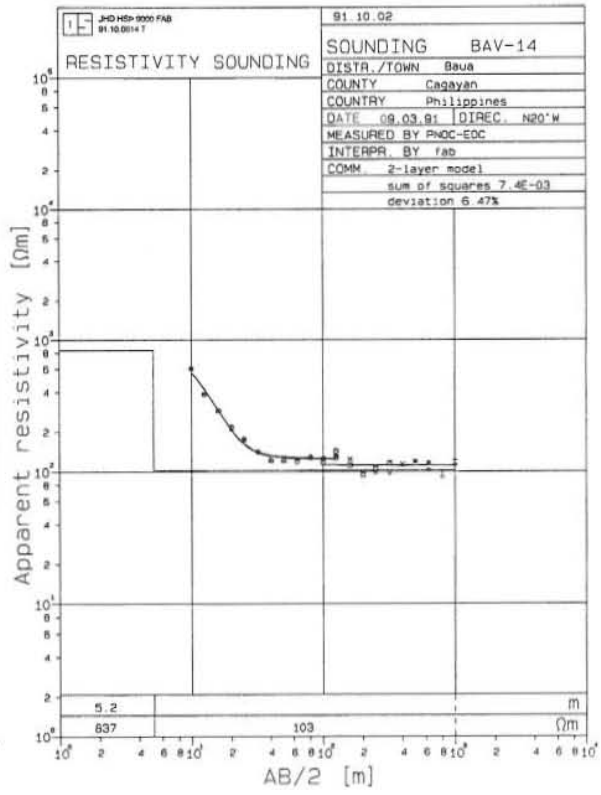
JHD HSP 9000 FAB
91.10.0614 T
91.10.02
RESISTIVITY SOUNDING
SOUNDING BAV-14
DISTR./TOWN Baua
COUNTY Cagayan
COUNTRY Philippines
DATE 09.03.91 DIREC. N20°W
MEASURED BY PNOC-EDC
INTERPR. BY fab
COMM. 2-layer model
sum of squares 7.4E-03
deviation 6.47%
Apparent resistivity [Ωm]
5.2 m
637 103 Ωm
AB/2 [m]

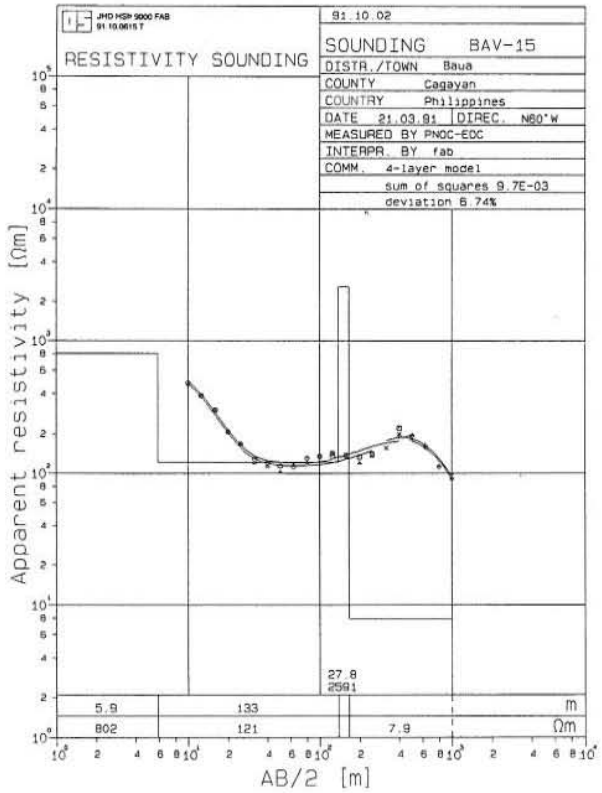
JHD HSP 9000 FAB
91.10.0615 T
91.10.02
RESISTIVITY SOUNDING
SOUNDING BAV-15
DISTR./TOWN Baua
COUNTY Cagayan
COUNTRY Philippines
DATE 21.03.91 | DIREC. N80°W
MEASURED BY PNOC-EDC
INTERPR. BY fab
COMM. 4-layer model
sum of squares 9.7E-03
deviation 6.74%
Apparent resistivity [Ωm]
27.8
2591
5.9 133 m
802 121 7.9 Ωm
AB/2 [m]

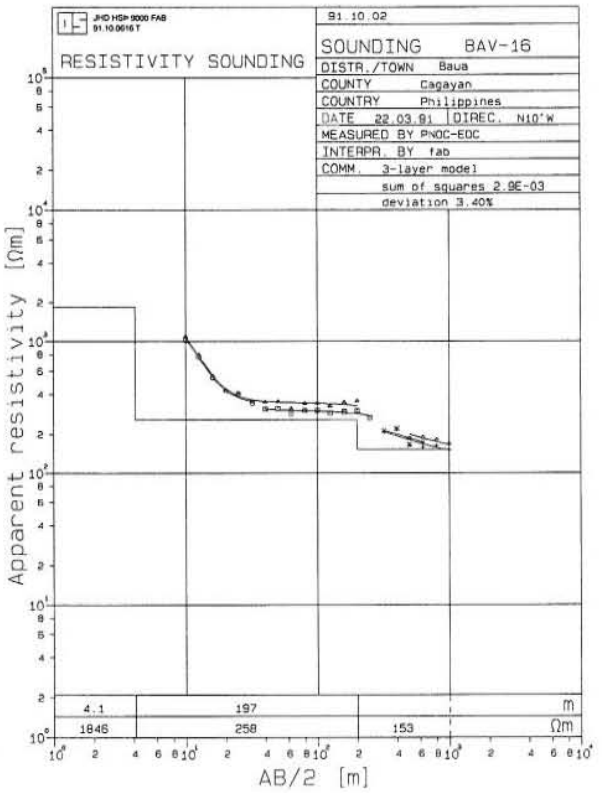
JHD HSP 9000 FAB
91.10.0616 T
91.10.02
RESISTIVITY SOUNDING
SOUNDING BAV-16
DISTR./TOWN Baua
COUNTY Cagayan
COUNTRY Philippines
DATE 22.03.91 | DIREC. N10°W
MEASURED BY PNOC-EDC
INTERPR. BY fab
COMM. 3-layer model
sum of squares 2.9E-03
deviation 3.40%
Apparent resistivity [Ωm]
4.1 197 m
1846 258 153 Ωm
AB/2 [m]

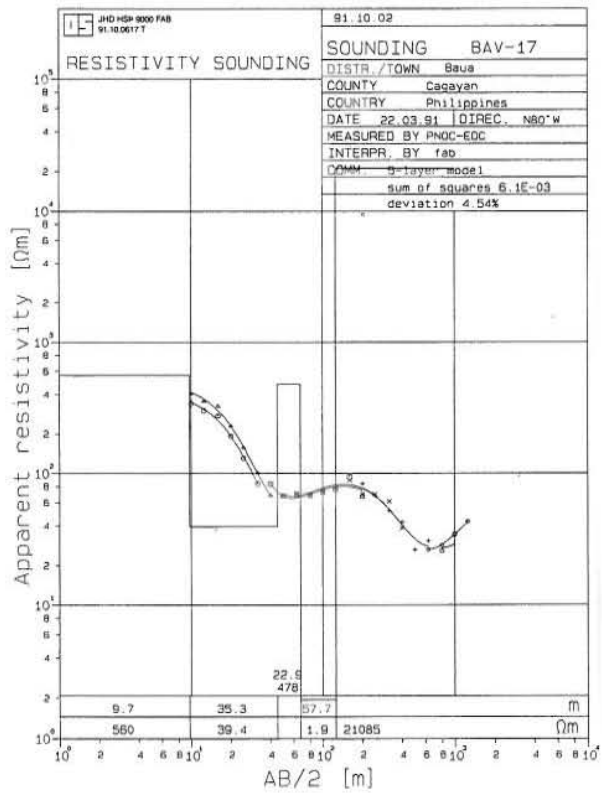
JHD HSP 9000 FAB
91.10.0617 T
91.10.02
RESISTIVITY SOUNDING
SOUNDING BAV-17
DISTR./TOWN Baua
COUNTY Cagayan
COUNTRY Philippines
DATE 22.03.91 | DIREC. N80°W
MEASURED BY PNOC-EDC
INTERPR. BY fab
COMM. 5-layer model
sum of squares 6.1E-03
deviation 4.54%
Apparent resistivity [Ωm]
22.6
478
9.7 35.3 57.7 m
560 39.4 1.9 21085 Ωm
AB/2 [m]

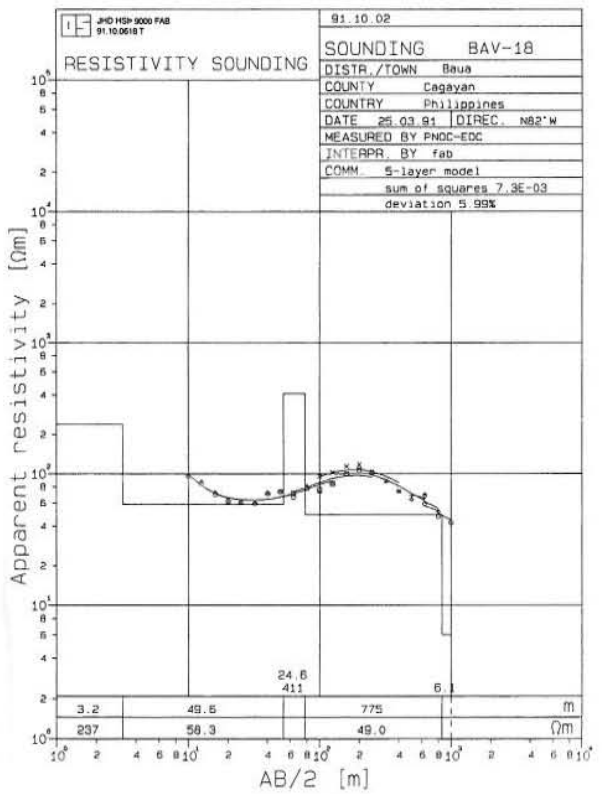
JHD HSP 9000 FAB
91.10.0618 T
91.10.02
RESISTIVITY SOUNDING
SOUNDING BAV-18
DISTR./TOWN Baua
COUNTY Cagayan
COUNTRY Philippines
DATE 25.03.91 | DIREC. N82°W
MEASURED BY PNOC-EDC
INTERPR. BY fab
COMM. 5-layer model
sum of squares 7.3E-03
deviation 5.99%
Apparent resistivity [Ωm]
24.6
411
6.1
3.2 49.6 775 m
237 58.3 49.0 Ωm
AB/2 [m]

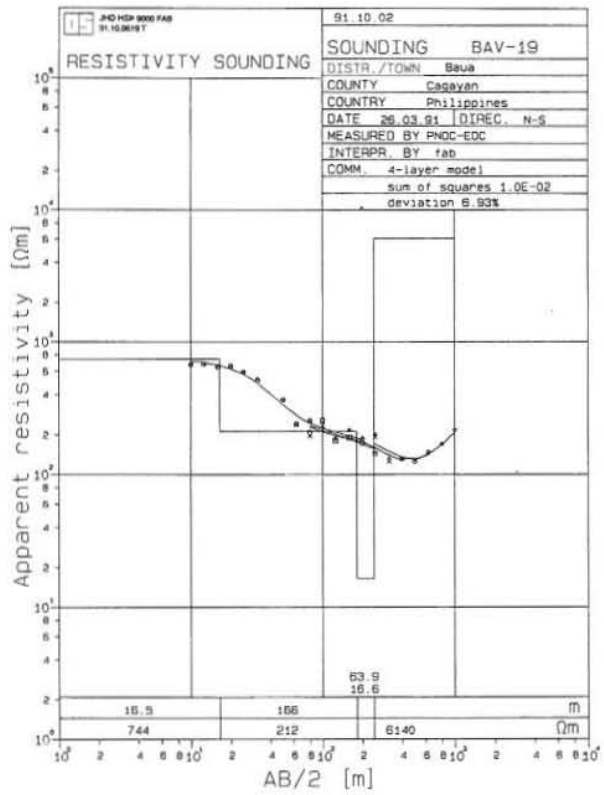
91.10.02
RESISTIVITY SOUNDING
SOUNDING BAV-19
DISTR./TOWN Baua
COUNTY Cagayan
COUNTRY Philippines
DATE 26.03.91 DIREC. N-S
MEASURED BY PNOC-EDC
INTERPR. BY fab
COMM. 4-layer model
sum of squares 1.0E-02
deviation 6.93%
Apparent resistivity [Ωm]
AB/2 [m]
63.9
16.6
15.5 156 m
744 212 6140 Ωm

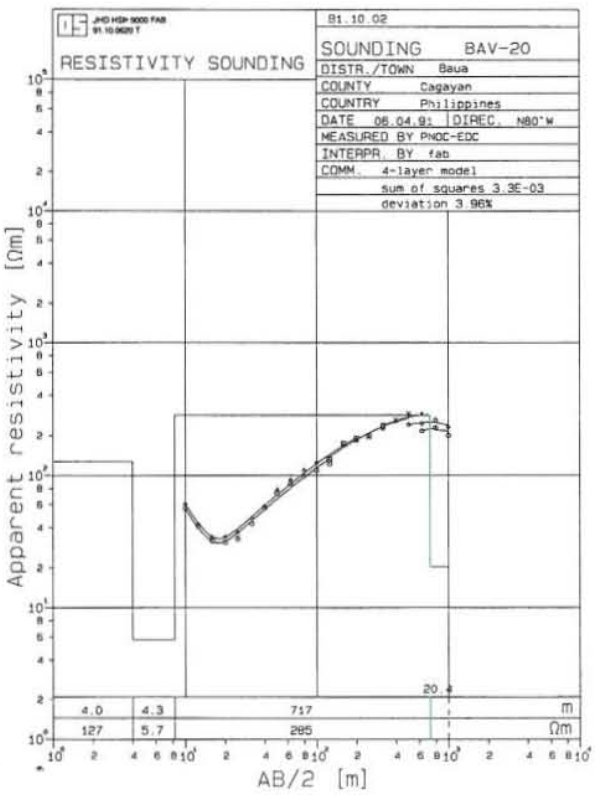
91.10.02
RESISTIVITY SOUNDING
SOUNDING BAV-20
DISTR./TOWN Baua
COUNTY Cagayan
COUNTRY Philippines
DATE 08.04.91 DIREC. N80°W
MEASURED BY PNOC-EDC
INTERPR. BY fab
COMM. 4-layer model
sum of squares 3.3E-03
deviation 3.96%
Apparent resistivity [Ωm]
AB/2 [m]
20.4
4.0 4.3 717 m
127 5.7 285 Ωm

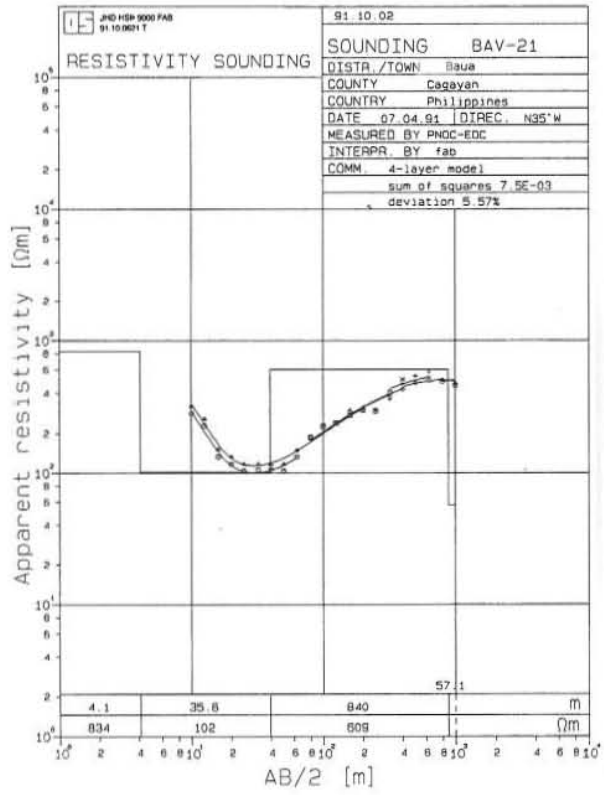
91.10.02
RESISTIVITY SOUNDING
SOUNDING BAV-21
DISTR./TOWN Baua
COUNTY Cagayan
COUNTRY Philippines
DATE 07.04.91 DIREC. N35°W
MEASURED BY PNOC-EDC
INTERPR. BY fab
COMM. 4-layer model
sum of squares 7.5E-03
deviation 5.57%
Apparent resistivity [Ωm]
AB/2 [m]
57.1
4.1 35.6 840 m
834 102 609 Ωm

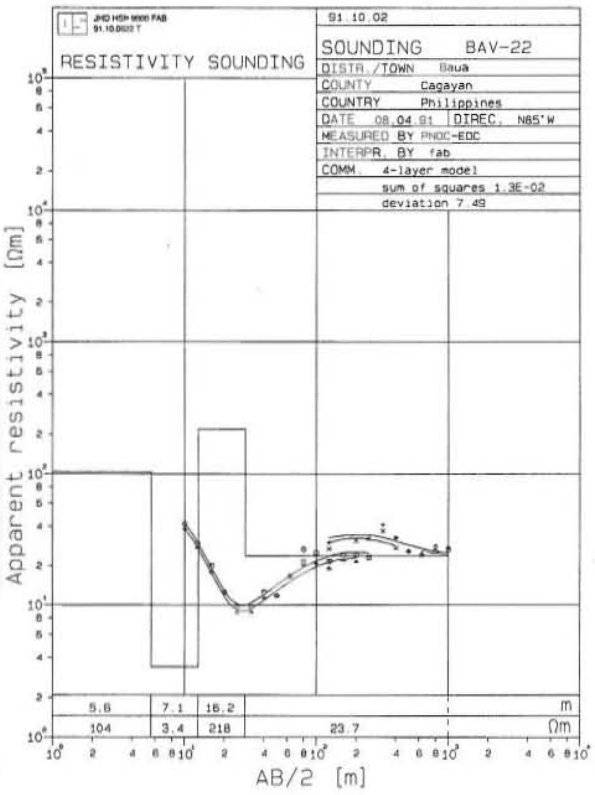
91.10.02
RESISTIVITY SOUNDING
SOUNDING BAV-22
DISTR./TOWN Baua
COUNTY Cagayan
COUNTRY Philippines
DATE 08.04.91 DIREC. N85°W
MEASURED BY PNOC-EDC
INTERPR. BY fab
COMM. 4-layer model
sum of squares 1.3E-02
deviation 7.49
Apparent resistivity [Ωm]
AB/2 [m]
5.6 7.1 16.2 m
104 3.4 218 23.7 Ωm

APPENDIX B

Two dimensional interpretation of Schlumberger soundings along cross-section A-A' using the FELIX program:

Measured apparent resistivity curves are shown as points and the corresponding calculated apparent resistivity from two dimensional modelling are shown as continous curves.

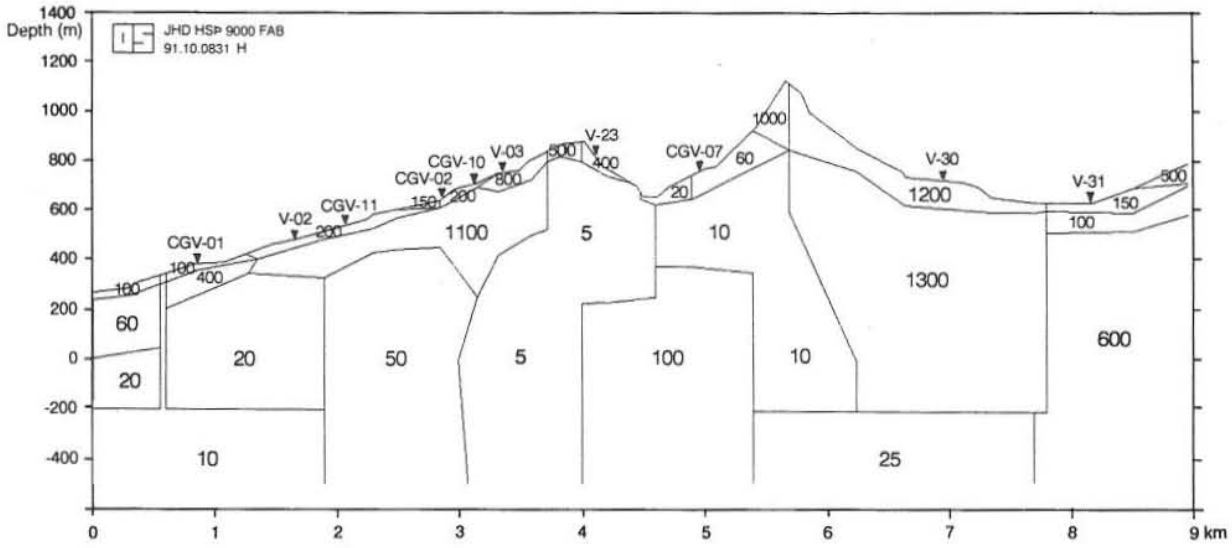

Two-dimensional resistivity model of cross-section A-A'

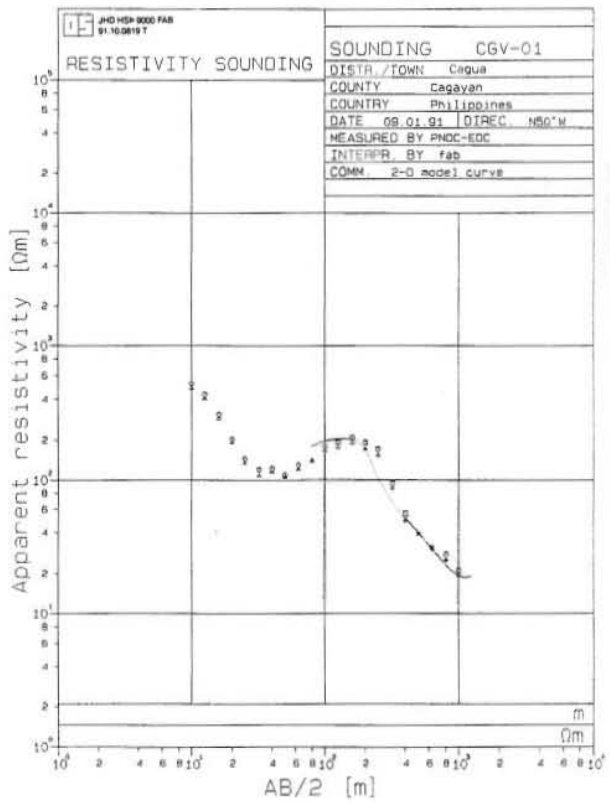

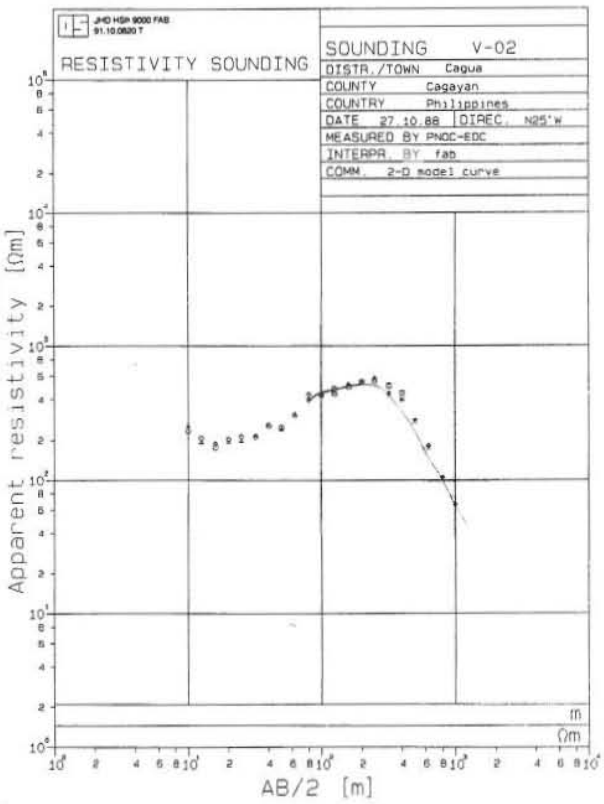

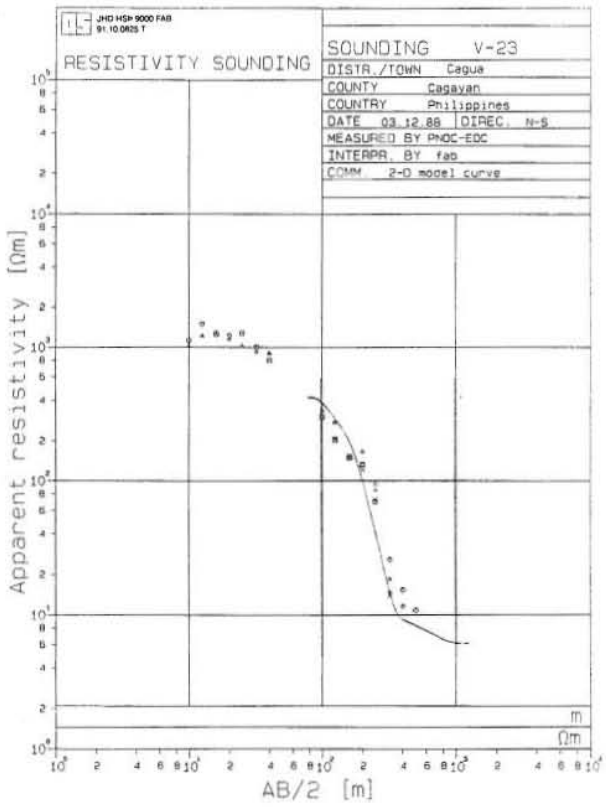
RESISTIVITY SOUNDING
SOUNDING V-23
DISTR./TOWN Cagua
COUNTY Cagayan
COUNTRY Philippines
DATE 03.12.88 DIREC. N-S
MEASURED BY PNOC-EDC
INTERPR. BY fab
COMM. 2-D model curve
Apparent resistivity [Ωm]
AB/2 [m]

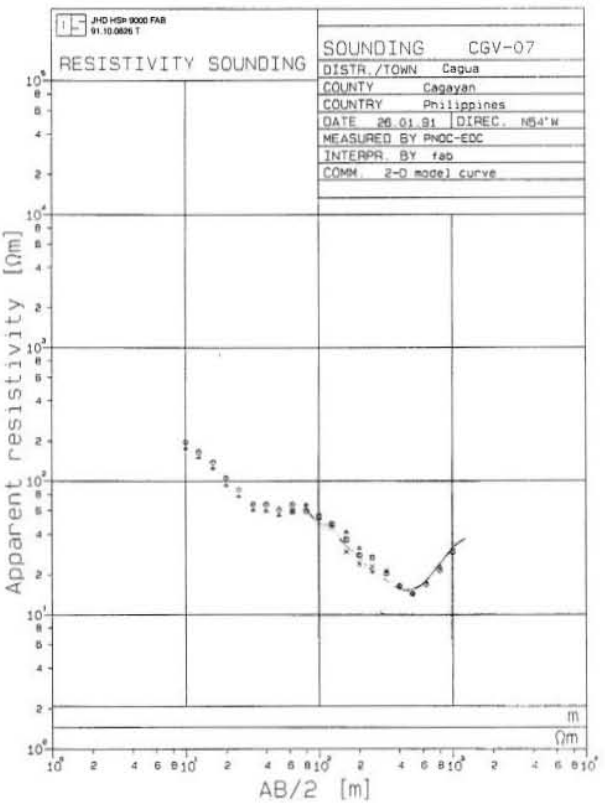
RESISTIVITY SOUNDING
SOUNDING CGV-07
DISTR./TOWN Cagua
COUNTY Cagayan
COUNTRY Philippines
DATE 26.01.91 DIREC. N54°W
MEASURED BY PNOC-EDC
INTERPR. BY fab
COMM. 2-D model curve
Apparent resistivity [Ωm]
AB/2 [m]

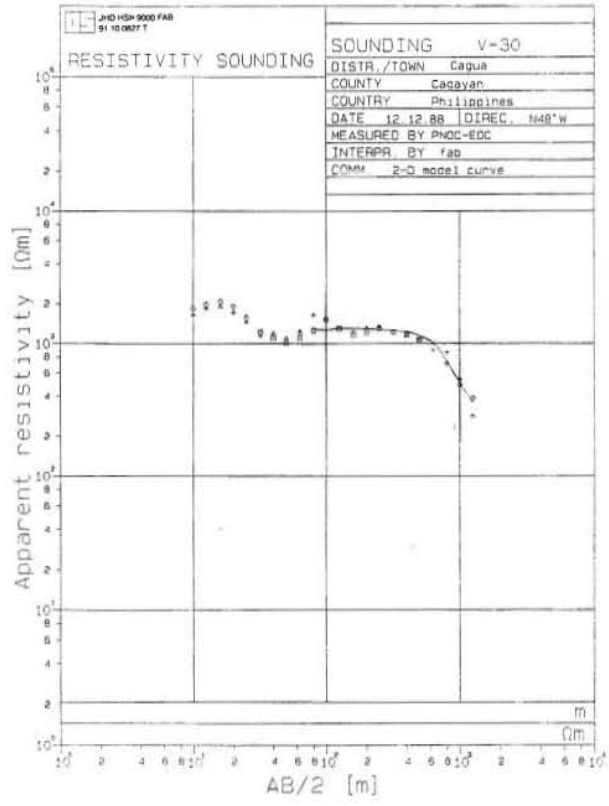
RESISTIVITY SOUNDING
SOUNDING V-30
DISTR./TOWN Cagua
COUNTY Cagayan
COUNTRY Philippines
DATE 12.12.88 DIREC. N48°W
MEASURED BY PNOC-EDC
INTERPR. BY fab
COMM. 2-D model curve
Apparent resistivity [Ωm]
AB/2 [m]

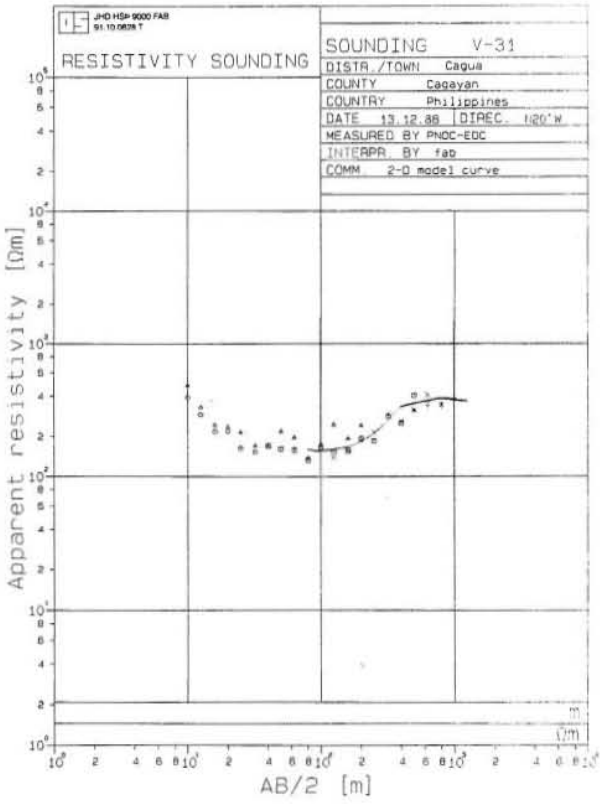
RESISTIVITY SOUNDING
SOUNDING V-31
DISTR./TOWN Cagua
COUNTY Cagayan
COUNTRY Philippines
DATE 13.12.88 DIREC. N20°W
MEASURED BY PNOC-EDC
INTERPR. BY fab
COMM. 2-D model curve
Apparent resistivity [Ωm]
AB/2 [m]

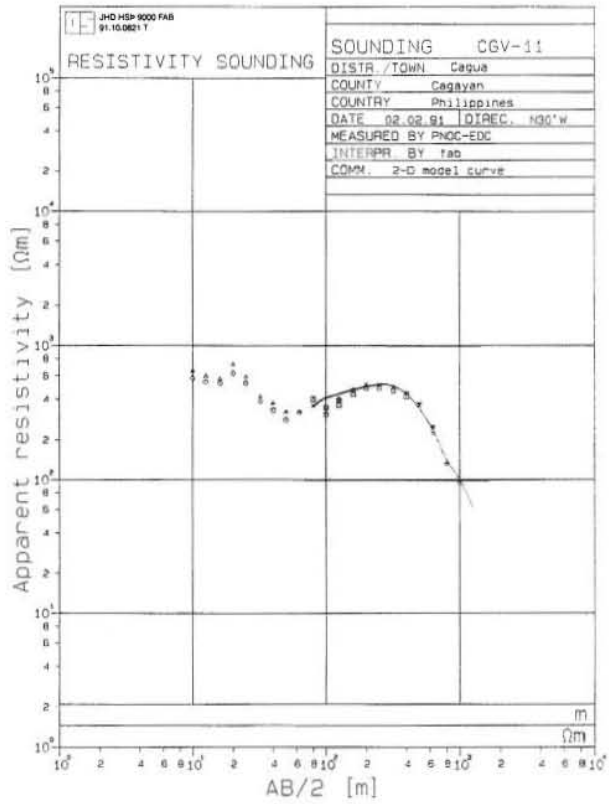
RESISTIVITY SOUNDING
SOUNDING CGV-11
DISTR./TOWN Cagua
COUNTY Cagayan
COUNTRY Philippines
DATE 02.02.91 | DIREC. N30°W
MEASURED BY PNOC-EDC
INTERPR. BY fab
COMM. 2-D model curve
Apparent resistivity [Ωm]
AB/2 [m]
m
Ωm

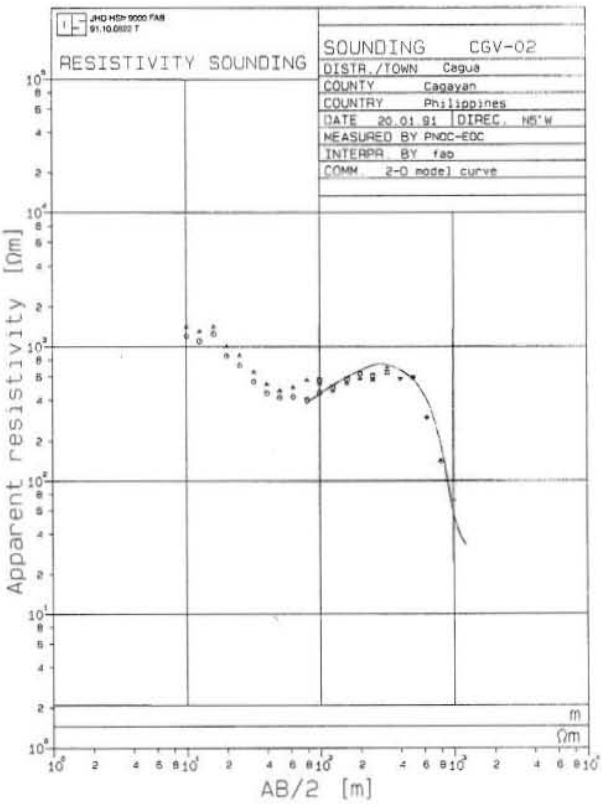
RESISTIVITY SOUNDING
SOUNDING CGV-02
DISTR./TOWN Cagua
COUNTY Cagayan
COUNTRY Philippines
DATE 20.01.91 | DIREC. N5°W
MEASURED BY PNOC-EDC
INTERPR. BY fab
COMM. 2-D model curve
Apparent resistivity [Ωm]
AB/2 [m]
m
Ωm

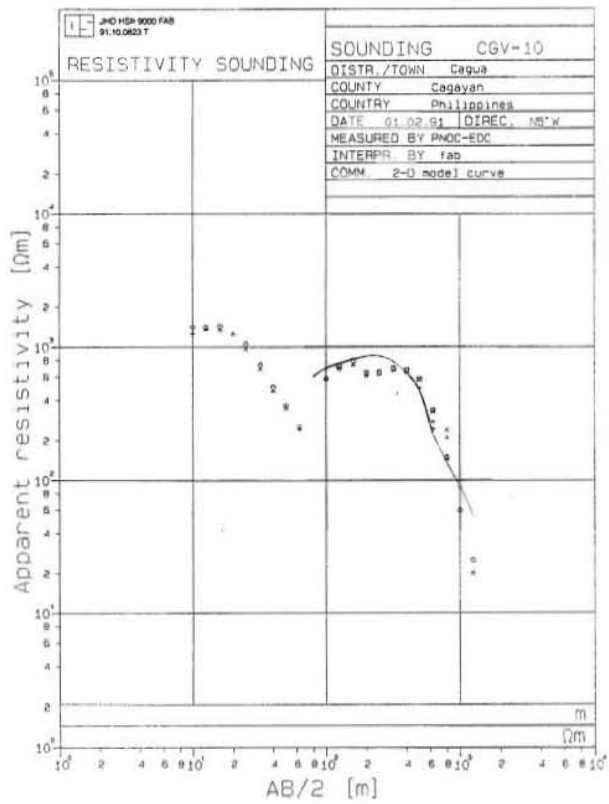
RESISTIVITY SOUNDING
SOUNDING CGV-10
DISTR./TOWN Cagua
COUNTY Cagayan
COUNTRY Philippines
DATE 01.02.91 | DIREC. N5°W
MEASURED BY PNOC-EDC
INTERPR. BY fab
COMM. 2-D model curve
Apparent resistivity [Ωm]
AB/2 [m]
m
Ωm

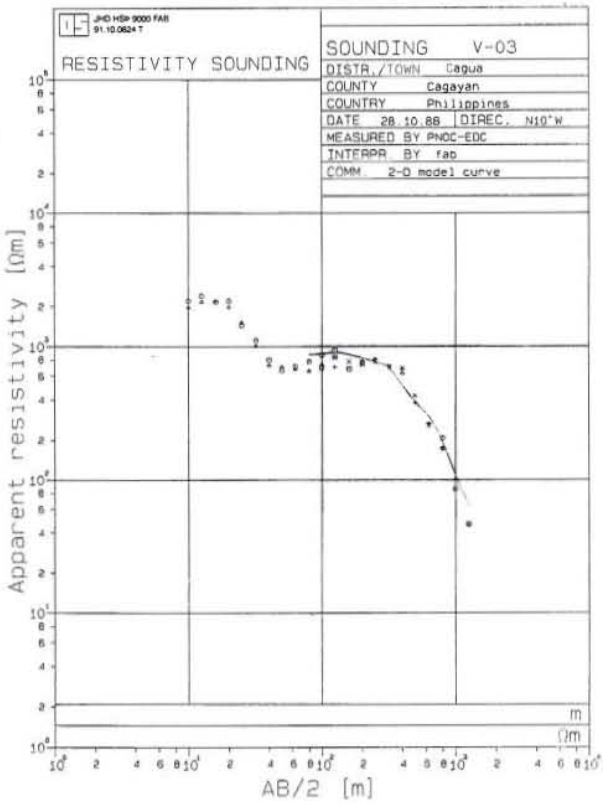
RESISTIVITY SOUNDING
SOUNDING V-03
DISTR./TOWN Cagua
COUNTY Cagayan
COUNTRY Philippines
DATE 28.10.88 | DIREC. N10°W
MEASURED BY PNOC-EDC
INTERPR. BY fab
COMM. 2-D model curve
Apparent resistivity [Ωm]
AB/2 [m]
m
Ωm

APPENDIX C

**One dimensional inversion
of central-loop transient electromagnetic (TEM) soundings
using the TINV program:**

Circles are observed late-time apparent resistivity values, solid lines are fitted curves by the given models (shown both numerically and as a histogram.

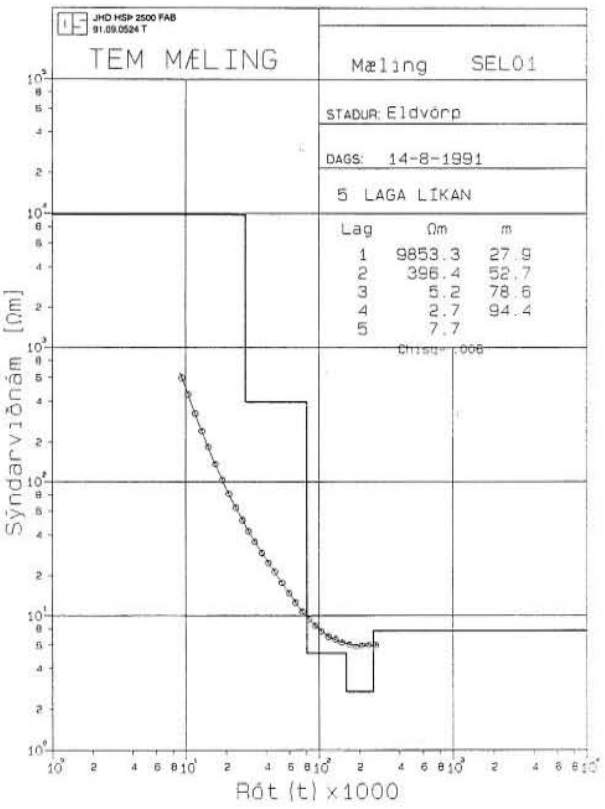
JHD HSÞ 2500 FAB
91.09.0524 T
TEM MÆLING
Mæling SEL01
STAÐUR: Eldvörp
DAGS: 14-8-1991
5 LAGA LÍKAN
Lag Ωm m
1 9853.3 27.9
2 396.4 52.7
3 5.2 78.6
4 2.7 94.4
5 7.7
Chisq= .006
Sýndarviðnám [Ωm]
Rót (t) x1000

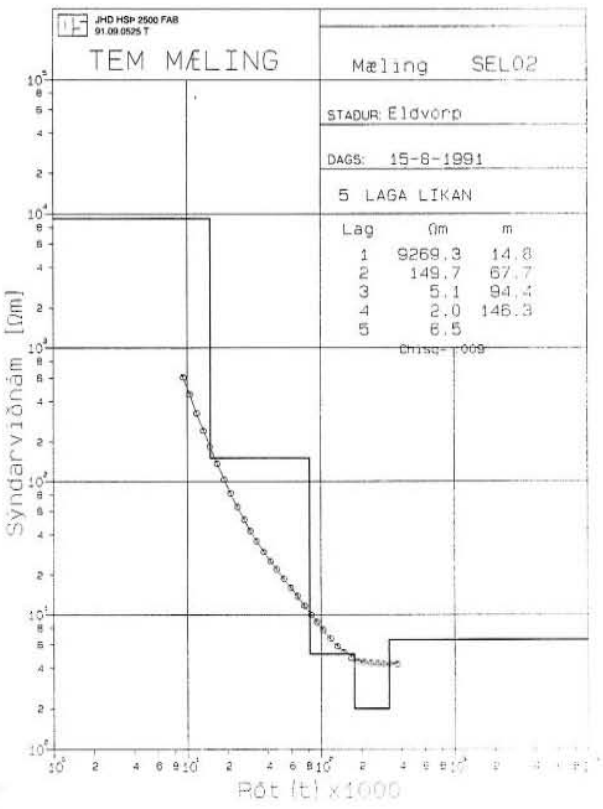
JHD HSÞ 2500 FAB
91.09.0525 T
TEM MÆLING
Mæling SEL02
STAÐUR: Eldvörp
DAGS: 15-8-1991
5 LAGA LÍKAN
Lag Ωm m
1 9269.3 14.8
2 149.7 67.7
3 5.1 94.4
4 2.0 146.3
5 6.5
Chisq= .009
Sýndarviðnám [Ωm]
Rót (t) x1000

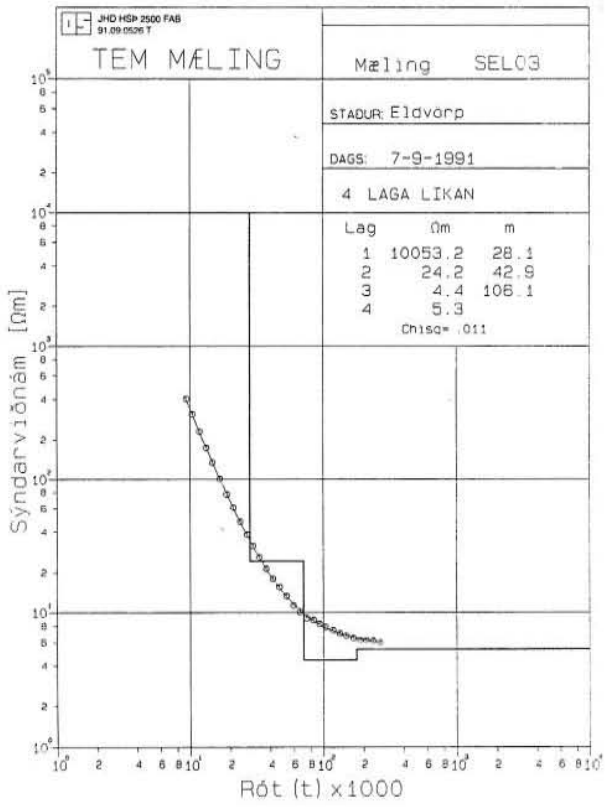
JHD HSÞ 2500 FAB
91.09.0526 T
TEM MÆLING
Mæling SEL03
STAÐUR: Eldvörp
DAGS: 7-9-1991
4 LAGA LÍKAN
Lag Ωm m
1 10053.2 28.1
2 24.2 42.9
3 4.4 106.1
4 5.3
Chisq= .011
Sýndarviðnám [Ωm]
Rót (t) x1000

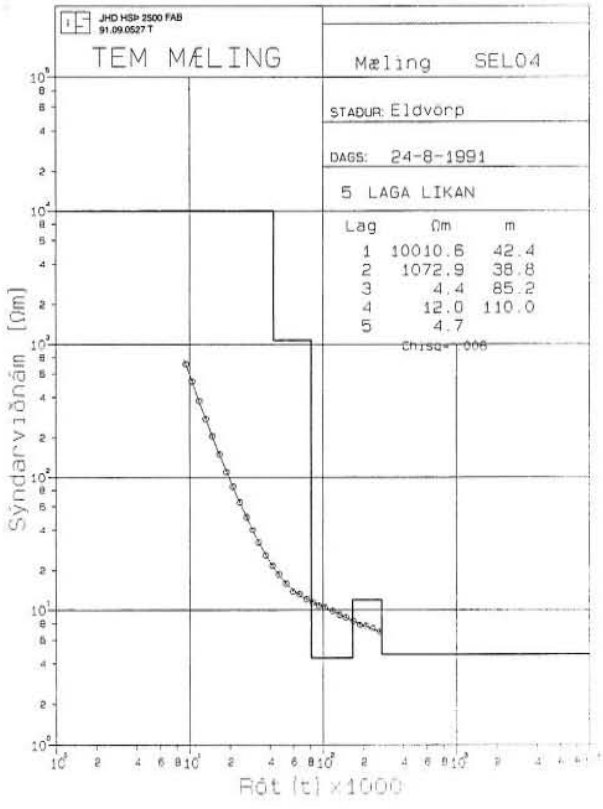
JHD HSÞ 2500 FAB
91.09.0527 T
TEM MÆLING
Mæling SEL04
STAÐUR: Eldvörp
DAGS: 24-8-1991
5 LAGA LÍKAN
Lag Ωm m
1 10010.6 42.4
2 1072.9 38.8
3 4.4 85.2
4 12.0 110.0
5 4.7
Chisq= .006
Sýndarviðnám [Ωm]
Rót (t) x1000

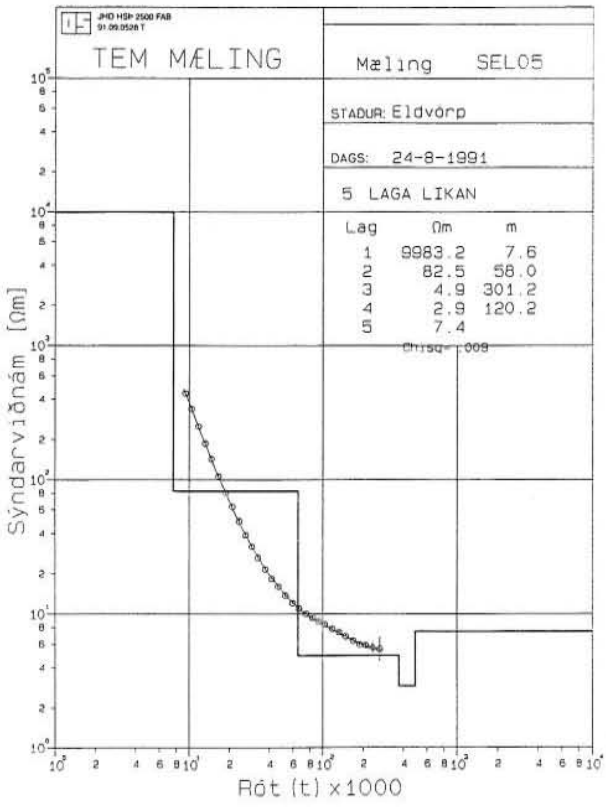
TEM MÆLING
Mæling SEL05
STAÐUR: Eldvörp
DAGS: 24-8-1991
5 LAGA LÍKAN
Lag Ωm m
1 9983.2 7.6
2 82.5 58.0
3 4.9 301.2
4 2.9 120.2
5 7.4
Chisq= .009
Sýndarviðnám [Ωm]
Rót (t) x1000

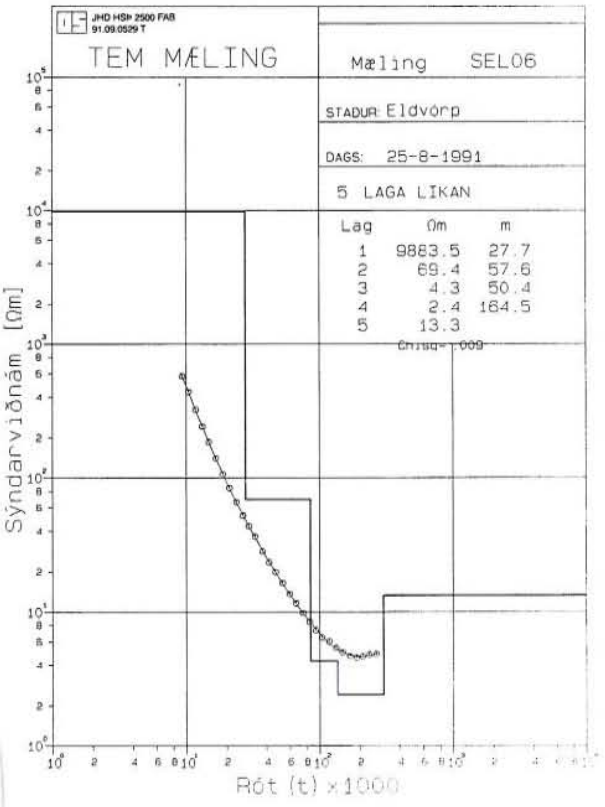
TEM MÆLING
Mæling SEL06
STAÐUR: Eldvörp
DAGS: 25-8-1991
5 LAGA LÍKAN
Lag Ωm m
1 9883.5 27.7
2 69.4 57.6
3 4.3 50.4
4 2.4 184.5
5 13.3
Chisq= .009
Sýndarviðnám [Ωm]
Rót (t) x1000

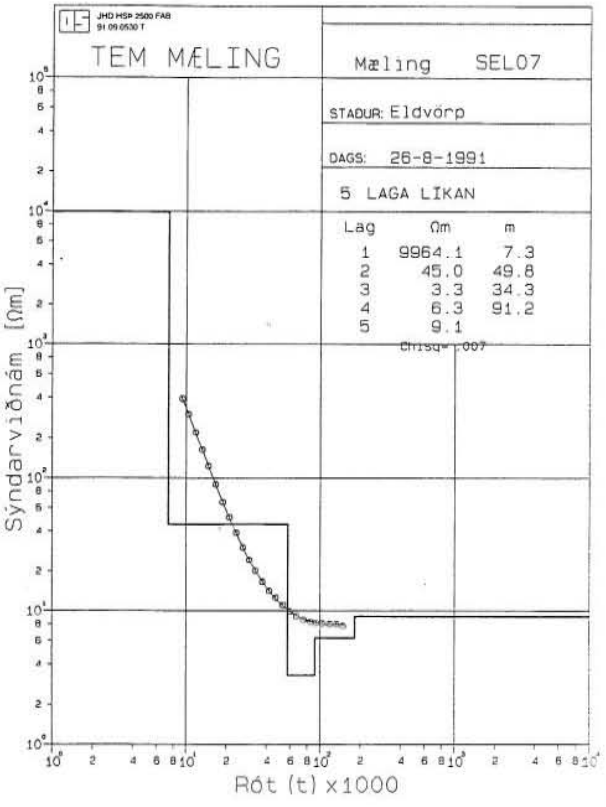
TEM MÆLING
Mæling SEL07
STAÐUR: Eldvörp
DAGS: 26-8-1991
5 LAGA LÍKAN
Lag Ωm m
1 9964.1 7.3
2 45.0 49.8
3 3.3 34.3
4 6.3 91.2
5 9.1
Chisq= .007
Sýndarviðnám [Ωm]
Rót (t) x1000

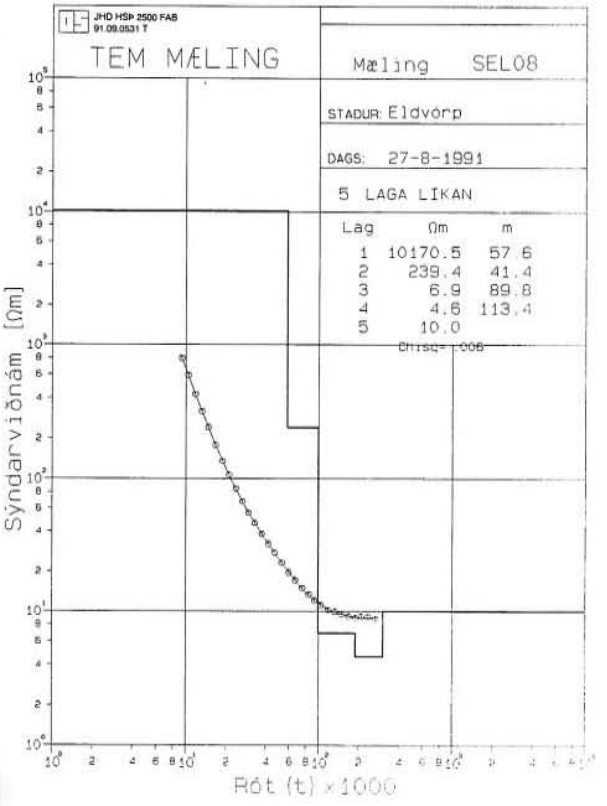
TEM MÆLING
Mæling SEL08
STAÐUR: Eldvörp
DAGS: 27-8-1991
5 LAGA LÍKAN
Lag Ωm m
1 10170.5 57.6
2 239.4 41.4
3 6.9 89.8
4 4.6 113.4
5 10.0
Chisq= .006
Sýndarviðnám [Ωm]
Rót (t) x1000

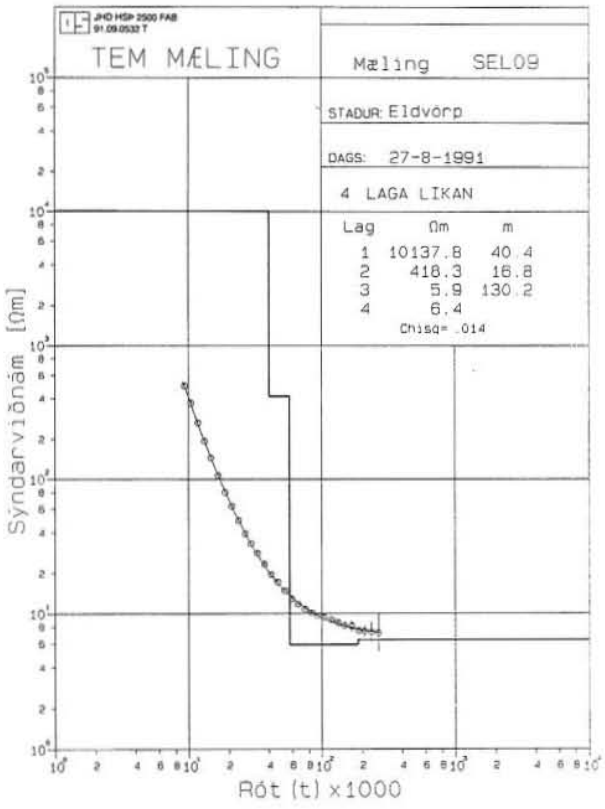
TEM MÆLING
Mæling SEL09
STAÐUR: Eldvörp
DAGS: 27-8-1991
4 LAGA LÍKAN
Lag Ωm m
1 10137.8 40.4
2 418.3 16.8
3 5.9 130.2
4 6.4
Chisq= .014
Sýndarviðnám [Ωm]
Rót (t) x1000

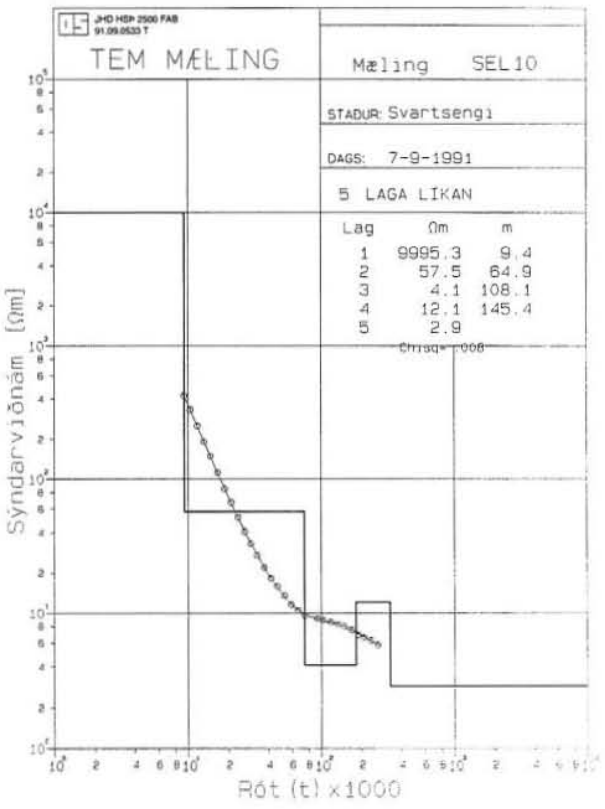
TEM MÆLING
Mæling SEL10
STAÐUR: Svartsengi
DAGS: 7-9-1991
5 LAGA LÍKAN
Lag Ωm m
1 9995.3 9.4
2 57.5 64.9
3 4.1 108.1
4 12.1 145.4
5 2.9
Sýndarviðnám [Ωm]
Rót (t) x1000